MINERALOGY AND PETROLOGY OF METAMORPHOSED IRON-RICH BEDS IN THE LOWER DEVONIAN LITTLETON FORMATION ORANGE AREA, MASSACHUSETTS

BY J. CRAIG HUNTINGTON

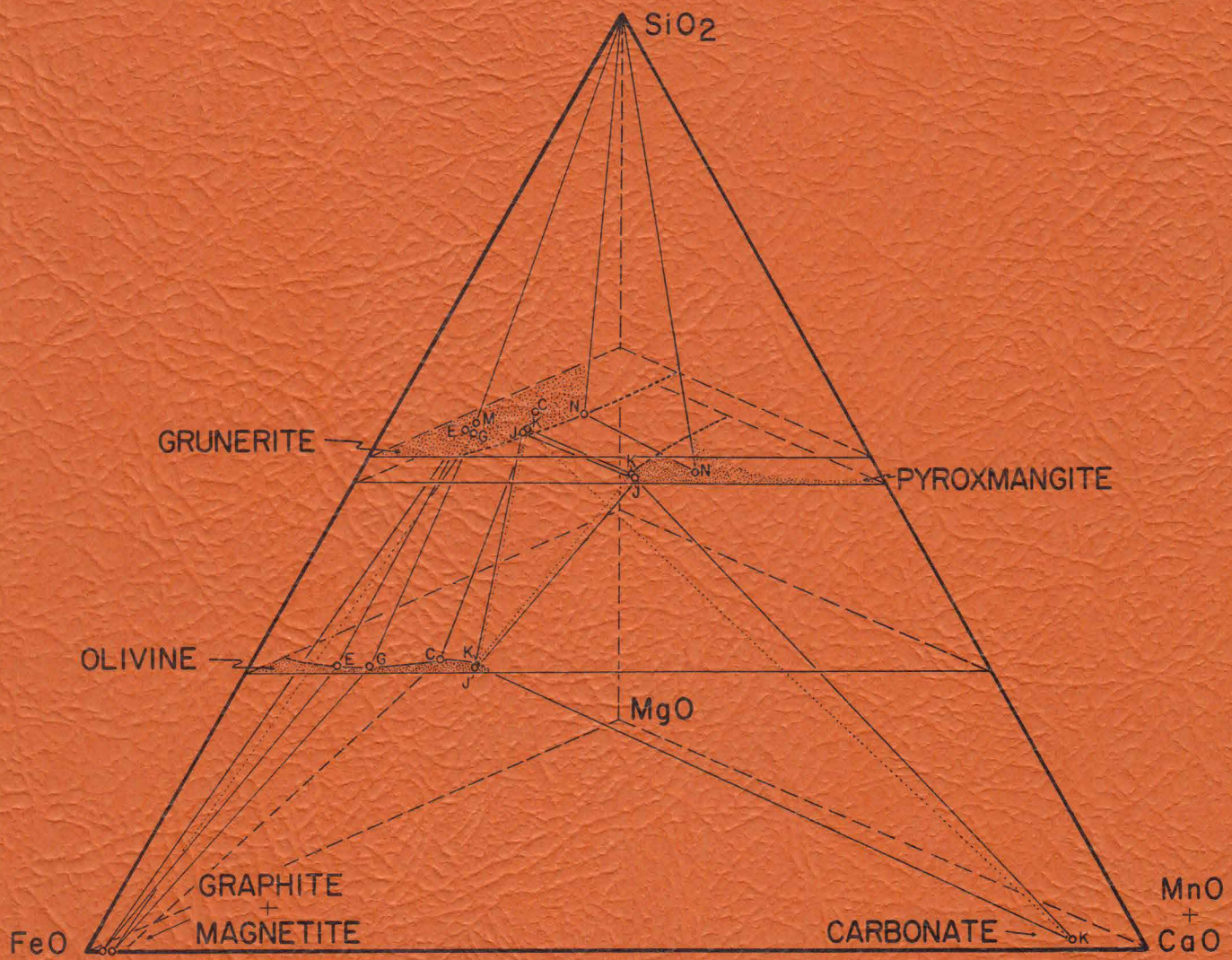

CONTRIBUTION NO. 19
GEOLOGY DEPARTMENT
UNIVERSITY OF MASSACHUSETTS
AMHERST, MASSACHUSETTS

MINERALOGY AND PETROLOGY OF METAMORPHOSED IRON-RICH BEDS IN THE LOWER DEVONIAN LITTLETON FORMATION, ORANGE AREA, MASSACHUSETTS

by

J. Craig Huntington

Contribution No. 19

Department of Geology

University of Massachusetts

Amherst, Massachusetts

March, 1975

TABLE OF CONTENTS

FIGURES

Page

TABLES

PLATES

ABSTRACT

Thin bedded iron-rich boudins up to 3 m thick are situated in graphite-sillimanite-garnet-staurolite-mica schist near the base of the Lower Devonian Littleton Formation, Orange area, Massachusetts. Distribution of kyanite and sillimanite-muscovite assemblages in pelitic schists of the region, which developed during the Acadian orogeny, suggest the iron-rich boudins reached peak metamorphic conditions of 650° C and 6 kbar (Robinson, 1966; Thompson et al., 1968). The mineralogy and petrology of these boudins were studied using transmitted and reflected light microscopy, X-ray powder diffraction and electron probe analysis.

Fe-rich mineral assemblages which developed contemporaneously with those in the pelitic schist include:

olivine-magnetite-graphite-grunerite-garnet

Olivine: $(Fe_{1.70}^{Mn}{}_{.20}^{Mg}{}_{.10})Si_{1.00}O_4$

Grunerite: $(Ca_{.01}^{Mn}{}_{.43}Fe^{2+}_{1.56})(Fe^{2+}_{3.20}Mg_{1.76}Fe^{3+}_{.03}Cr_{.01}Ti_{.01})(Fe^{3+}_{.04}Al_{.01}Si_{7.95})O_{22}(OH)_2$

Garnet: $Alm_{.56}Spess_{.33}Pyr_{.02}Gross_{.09}$

olivine-pyroxmangite-grunerite-carbonate-garnet

Olivine: $(Fe_{1.33}^{Mn}{}_{.57}^{Mg}{}_{.10})Si_{1.00}O_4$

Pyroxmangite: $(Fe_{.88}^{Mn}{}_{.88}^{Mg}{}_{.15}^{Ca}{}_{.09})Si_{2.00}O_6$

Grunerite: $(Ca_{.08}^{Mn}{}_{1.24}Fe^{2+}_{.68})(Fe^{2+}_{3.16}Mg_{1.76}Fe^{3+}_{.08})(Fe^{3+}_{.07}Si_{7.93})O_{22}(OH)_2$

Carbonate: $(Fe_{.05}^{Mn}{}_{.17}^{Mg}{}_{.02}^{Ca}{}_{.75})CO_3$

Garnet: $Alm_{.29}Spess_{.53}Pyr_{.02}Gross_{.17}$

quartz-pyroxmangite-grunerite-graphite-garnet

Pyroxmangite: $(Fe_{.58}Mn_{1.01}Mg_{.17}Ca_{.18})Si_{2.02}O_6$

Grunerite: $Na_{.01}(Ca_{.24}Mn_{1.46}Fe^{2+}_{.30})(Fe^{2+}_{2.29}Mg_{2.69}Si_{.02})Si_{8.00}O_{22}(OH)_2$

Garnet: $Alm_{.22}Spess_{.64}Pyr_{.02}Gross_{.12}$

A fourth assemblage, that occurs only in a cross-cutting vein, is:

olivine-orthopyroxene-grunerite-magnetite-garnet

Olivine: $(Fe_{1.61}Mn_{.32}Mg_{.05})Si_{1.00}O_4$

Orthopyroxene: $(Fe_{1.43}Mn_{.30}Mg_{.24}Ca_{.03})Al_{.01}Si_{1.99}O_6$

Grunerite: $Na_{.01}(Ca_{.09}Mn_{.73}Fe^{2+}_{1.19})(Fe^{2+}_{3.91}Mg_{1.07}Fe^{3+}_{.01}Cr_{.01}Ti_{.01})(Fe^{3+}_{.03}Al_{.02}Si_{7.95})O_{22}(OH)_2$

Garnet: $Alm_{.54}Spess_{.38}Pyr_{.02}Gross_{.06}$

With the exception of garnet, minerals in these assemblages can be represented in the system Fe-C-O-H-MgO-MnO-CaO-SiO_2. Electron probe analyses define fractionation of Mg, Fe, Mn and Ca among coexisting minerals, and indicate that fractionations of Fe and Mn are not seriously affected by relatively minor substitutions of Mg and Ca. Fe/Fe + Mn ratios for coexisting minerals in the observed assemblages are in the order: Magnetite > Grunerite > Olivine > Orthopyroxene > Pyroxmangite > Garnet > Carbonate.

T - $X_{CO_2}/X_{H_2O} + X_{CO_2}$ diagrams developed on the basis of idealized mineral compositions and observed Fe/Mn fractionations in the system Fe-Mn-Si-C-O-H, assuming a graphite buffer, show the following sequence of reactions with increasing temperature:

1) Sid + Qtz + H_2O = Grun + CO_2
2) Sid = Graph + Mt + CO_2
3) Fe-Mn Carb + Grun + Qtz = Pym + H_2O + CO_2

4) Fe-Mn Carb + Grun + Graph + Mt = Ol + H_2O + CO_2

5) Fe-Mn Carb + Grun = Ol + Pym + H_2O + CO_2

These suggest metamorphic reactions for the development of the observed assemblages and textures from Fe-Mn carbonate-quartz parent rocks. The deduced reaction paths suggest that, although many of the equilibria would tend to increase the CO_2 content of the fluid phase, it was in fact probably undergoing progressive dilution by H_2O from pelitic schists in the immediate surroundings at the peak of metamorphism.

Because orthopyroxene is probably not stable in the pure system Fe-C-O-H-MnO-SiO_2 (without MgO) except at very high pressure, it is not included in the reaction sequence above. However, in the presence of modest MgO, orthopyroxene may become stable by the reaction:

Fe-Mg-Mn Grun + Fe-Mn-Mg Ol + Fe-Mn-Mg Pym = Fe-Mn-Mg Opx + H_2O

It appears that the appropriate bulk composition for generation of orthopyroxene as a result of this reaction was attained only by silication of olivine-magnetite-graphite-grunerite-garnet rock.

INTRODUCTION

Location

The iron-rich lenses investigated are exposed east of the Connecticut Valley in the New England Upland, approximately 110 kilometers west-northwest of Boston. Specifically they lie within the Mount Grace 7 1/2 minute quadrangle, about 5 kilometers southeast and east of the village of Warwick, Massachusetts, in the towns of Warwick, Orange, and Royalston.

Geologic Setting

The iron-rich lenses are situated in the Lower Devonian Littleton Formation between the Keene gneiss dome to the north and the main body of Monson gneiss to the south (Figure 1). The Keene dome and the main body of Monson gneiss are two of the mantled gneiss domes of the Bronson Hill anticlinorium, which extends from the Long Island Sound in Connecticut to the Maine-New Hampshire border (Billings, 1956; Thompson et al., 1968). In the center of the Mount Grace quadrangle, the Littleton Formation is present on both sides of a very narrow anticlinal zone of older rocks (Robinson, 1967) that forms the root zone for the Skitchwaug nappe (Figure 1), which is overfolded many miles to the west. The iron-rich lenses are present exclusively in the facies of the Littleton Formation that lies to the east of this root zone and belongs to the upper or upright limb of the nappe.

Sillimanite-muscovite grade regional metamorphism of probable Acadian age produced the various mineral assemblages present in the Littleton Formation. Kyanite and sillimanite-bearing assemblages in muscovite schists and surrounding rocks of the general area (Robinson, 1963) suggest metamorphic conditions of about 650° centigrade and 6 kilobars (Robinson, 1966; Thompson et al., 1968).

FIGURE 1.

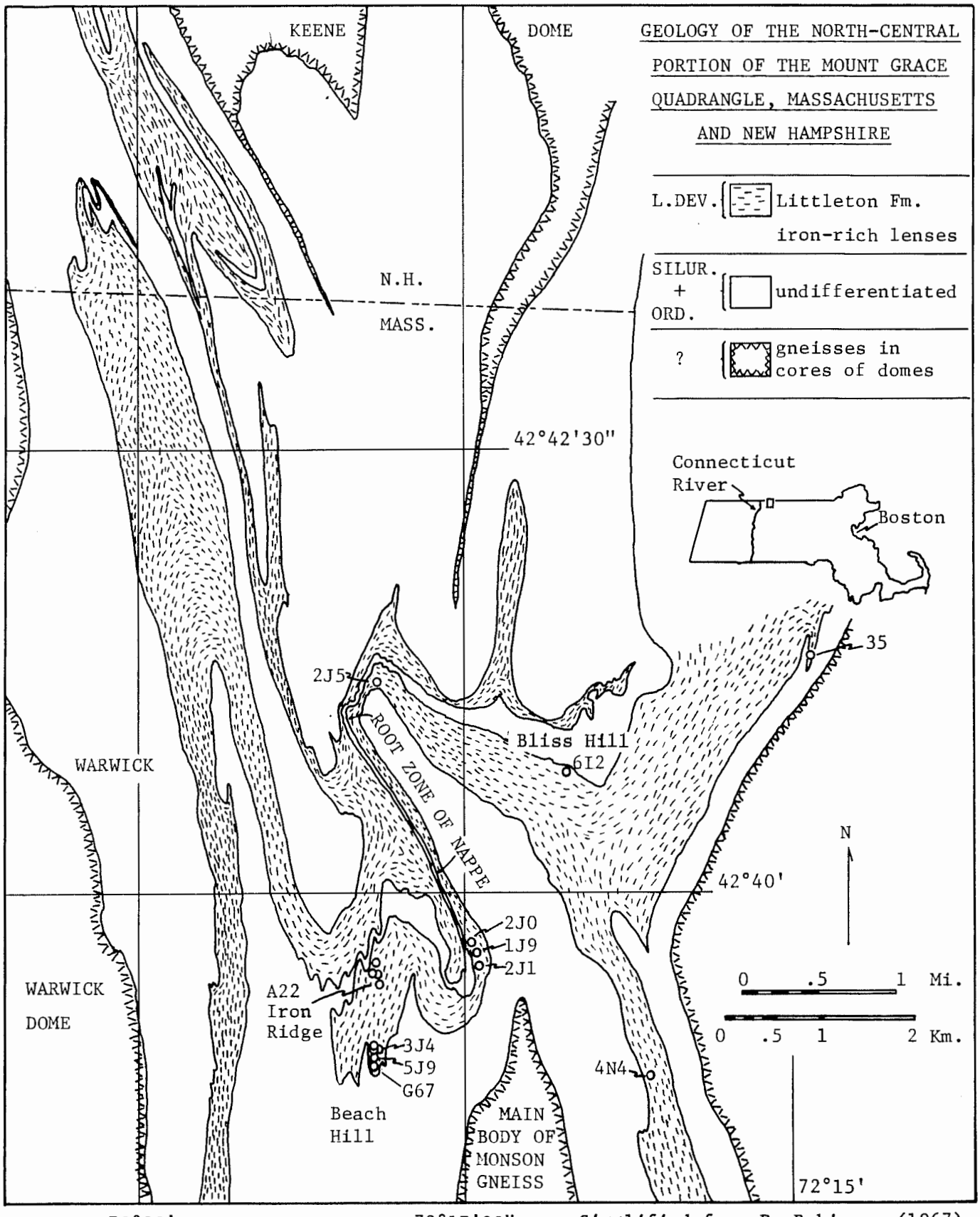
GEOLOGY OF THE NORTH-CENTRAL PORTION OF THE MOUNT GRACE QUADRANGLE, MASSACHUSETTS AND NEW HAMPSHIRE
L.DEV. Littleton Fm.
iron-rich lenses
SILUR. + ORD. undifferentiated
? gneisses in cores of domes
KEENE DOME
N.H.
MASS.
42°42'30"
Connecticut River
Boston
2J5
35
ROOT ZONE OF NAPPE
Bliss Hill
6I2
WARWICK
42°40'
N
2J0
1J9
2J1
WARWICK DOME
A22
Iron Ridge
3J4
5J9
G67
Beach Hill
MAIN BODY OF MONSON GNEISS
4N4
0 .5 1 Mi.
0 .5 1 2 Km.
72°15'
72°20'
72°17'30"
Simplified from P. Robinson (1967)

Previous work

Early in the 19th century, attempts were made to mine the iron ore from several iron-rich lenses in the Littleton Formation. The ore obtained from these lenses was not economically profitable due to impurities (Hitchcock, 1841) and mining operations ceased shortly after they were initiated. A series of open pits from 800 to 1100 meters northeast of the summit of Beach Hill marks the remains of this mining venture. Early topographic maps denote this area as "Iron Ridge." Edward Hitchcock (1841) reported a whole rock chemical analysis of one sample from an iron-rich lens near Warwick. J. B. Hadley (1949) referred to the lenses in his geologic map of the Mount Grace quadrangle. Peter Robinson (1963, 1967) discovered several new iron-rich lenses while mapping the Mount Grace quadrangle in detail. Howard W. Jaffe (Robinson and Jaffe, 1969) noted the presence of orthopyroxene and olivine in a vein in one iron-rich sample during examination in oil immersion and also determined the indices of refraction of these minerals as well as those for grunerite and garnet. This sample was sent to A. E. Bence, who completed preliminary electron microprobe analyses of olivine, orthopyroxene, grunerite and garnet in this magnetite-olivine-orthopyroxene-grunerite garnet assemblage.

Purpose

The purpose of this study was to investigate assemblages of co-existing minerals within the iron-rich lenses of the Littleton Formation in the Mount Grace quadrangle area. Chemical and textural data were obtained from minerals in order to provide insight into metamorphic reactions that took place in the development of the mineral assemblages

under high grade metamorphism. Special attention was given to the construction of a chemical system in which mineral assemblages could be portrayed and which could be used in the future to compare mineralogical data from iron-rich rocks of different metamorphic facies.

Acknowledgments

Professors Peter Robinson and Stephen E. Haggerty suggested this mineralogical study and gave continuing guidance during the research, which was done in partial fulfillment of the requirements for the M. S. degree at the University of Massachusetts, Amherst. Professor Howard W. Jaffe made available his optical data and specimens of the orthopyroxene vein discovered by him. Robert J. Tracy of the University of Massachusetts and A. E. Bence of the State University of New York at Stony Brook performed the microprobe analyses. Hope M. Davies assisted with preparation of tables and captions. Field, laboratory and analytical work, and publication were supported by National Science Foundation Grant GA-31989 to Howard W. Jaffe and Peter Robinson. A grant-in-aid of research from Sigma Xi to Craig Huntington provided support for additional microprobe analyses. To each of these persons and institutions I express my sincere thanks.

GENERAL GEOLOGY OF THE LITTLETON FORMATION, MOUNT GRACE QUADRANGLE

The stratigraphic sequence within the Mount Grace quadrangle consists of basement gneisses of uncertain age overlain by Ammonoosuc Volcanics and Partridge Formation of Middle Ordovician age, Clough Quartzite and Fitch Formation of Silurian age, and Littleton Formation of Lower Devonian age. An unconformity exists between the Partridge Formation and the Clough Quartzite. Due to erosion and extensive structural thinning, the entire stratigraphy from Middle Ordovician through Lower Devonian is rarely preserved in the Mount Grace quadrangle. Consequently, the Littleton Formation may rest directly above any of the five older formations mentioned above.

The Littleton Formation of the Mount Grace quadrangle consists predominantly of gray-weathering graphite-sillimanite-garnet-biotite-muscovite schist with or without staurolite (Robinson, 1963, 1967). It commonly contains thin quartzite beds or beds of quartz-plagioclase-mica granulite, and it is resistant to weathering so that it usually underlies high ground. Minor rock types include calc-silicate rocks and very rare marble (Robinson, pers. comm., 1974). Locally within the facies of Littleton Formation which lies east of the root zone of the Skitchewaug nappe (Figure 1), there is a series of iron-rich lenses that range in thickness from a few centimeters to approximately three meters. These lenses lie close to the base of the Littleton and in some places may actually be in contact with the underlying Clough or Partridge Formations.

The structural deformation of the Littleton and associated formations within the Mount Grace quadrangle during the Devonian Acadian Orogeny was intense and consisted of three distinct phases. The first

stage of deformation led to the development of regional nappe structures with east over west overfolding involving the Partridge, Clough, Fitch and Littleton Formations. The second stage of deformation initiated dome formation with cross folding and overturning of the ends of some domes. The third stage of Acadian deformation involved the main phase of gneiss dome formation and intense isoclinal folding about north-south axes (Robinson, 1967). The Littleton Formation within the western part of the Mount Grace quadrangle contains the synclinal axial surface below the Skitchewaug nappe, which developed during the first stage of deformation. This surface can be traced from the southwest corner of the quadrangle through a series of later folds to Bliss Hill (Figure 1) where the Littleton hinges out (Robinson, 1967; Thompson et al., 1968). To the east the anticlinal axial surface of the nappe follows a thin contorted zone of Partridge, Clough and Fitch Formations. The iron-rich units in the Littleton, which are the major lithologic horizons of interest to this study, are in the upper or upright limb of the nappe overlying the anticlinal axial zone.

GENERAL GEOLOGY OF IRON-RICH BEDS, MOUNT GRACE QUADRANGLE

Johnsonian Pond, Outcrop Locality 2J1

The outcrop of iron-rich beds at locality 2J1, the largest, best known and least altered exposure, was mapped in detail (Figure 2). Most of the iron-rich units at 2J1 are thin bedded. Recognition of bedding in a few hand specimens is enhanced by the presence of layers composed dominantly of one mineral. These layers contain apatite, garnet, grunerite, olivine, pyroxmangite or pyrrhotite as the major phase. Many hand specimens, however, do not contain nearly monomineralic layers, and recognition of bedding in these specimens must be based on the observation of minor variations in the relative abundances of minerals present. Locally, hand specimen mineral identification is difficult, because the grain size is small and certain minerals, notably olivine and pyrrhotite, are severely altered by low temperature alteration or weathering.

The iron-rich beds underwent intense deformation during at least two phases of the Devonian Acadian Orogeny (Robinson, 1967). Because they were structurally competent relative to the enclosing Littleton schist in the last phase of deformation, the beds at locality 2J1 exist as two boudins around which the prominent foliation of the less competent schist is wrapped. The two boudins are separated by a nearly east-west trending shear zone that probably coincides with the boudin neck line. In an earlier phase of deformation when the ductility contrast was less, the iron-rich beds underwent intense, nearly isoclinal folding. Figure 3 is a sketch from a photograph of minor folds on the limb of an anticline at locality 2J1. The folds are readily observed on the surface of the outcrop because the apatite-rich beds commonly

are more deeply weathered than the surrounding beds. The fold axes in the iron-rich beds at this locality trend north-south and plunge 35-40° north. By contrast, the abundant folds in the surrounding schist trend north-south and plunge 45-50° south in agreement with characteristic main stage folds in this part of the quadrangle (Robinson, 1963). It appears that the folds in the iron-rich beds predate the main stage isoclinal folding associated with the formation of gneiss domes in the area, and thus could be related to one of the two earlier episodes of isoclinal folding (Robinson, 1967).

The exact stratigraphic relationship between the two boudin blocks at locality 2J1 is not completely understood. However, one unit, an olivine-magnetite granulite, is common to both. The stratigraphic units from lens 2J1 (Figure 2) are described below in order of age from oldest to youngest. The normal sillimanite-muscovite schist (a) of the Littleton Formation borders and grades into a rusty-weathering mica-garnet schist (b). Directly above the rusty-weathering schist is a garnet-grunerite-quartz granulite (c), which weathers rusty-brown to tan. Thin magnetite-bearing beds occur locally.

The garnet-grunerite-quartz granulite is followed by a thin, weakly magnetic, coarse-grained olivine-pyroxmangite granulite (d). On fresh surfaces pyroxmangite, which occurs only in this unit, can be identified in hand specimen by its prismatic habit and pink color. The olivine-pyroxmangite granulite weathers dull black to rusty-brown. The next younger unit, olivine-magnetite granulite (e), is strongly magnetic, very dense and fine-grained in comparison to the olivine-pyroxmangite granulite (d), but both of these units weather dull-black or rusty-brown. The olivine-magnetite granulite (e) is well bedded relative to the

Figure 2. Geologic map of beds at outcrop locality 2J1.

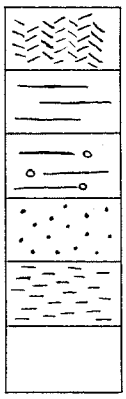

(f) Grunerite-garnet-pyrrhotite granulite

(e) Olivine-magnetite granulite

(d) Olivine-pyroxmangite granulite

(c) Garnet-grunerite-quartz granulite

(b) Mica-garnet schist

(a) Sillimanite-muscovite schist

⊗ Sample location

Strike and dip of foliation

Trend and plunge of fold axis

Trace of axial surface of syncline

Trace of axial surface of anticline

Offset sense of fault in boudin neck zone

Fault

Known contact

Inferred contact

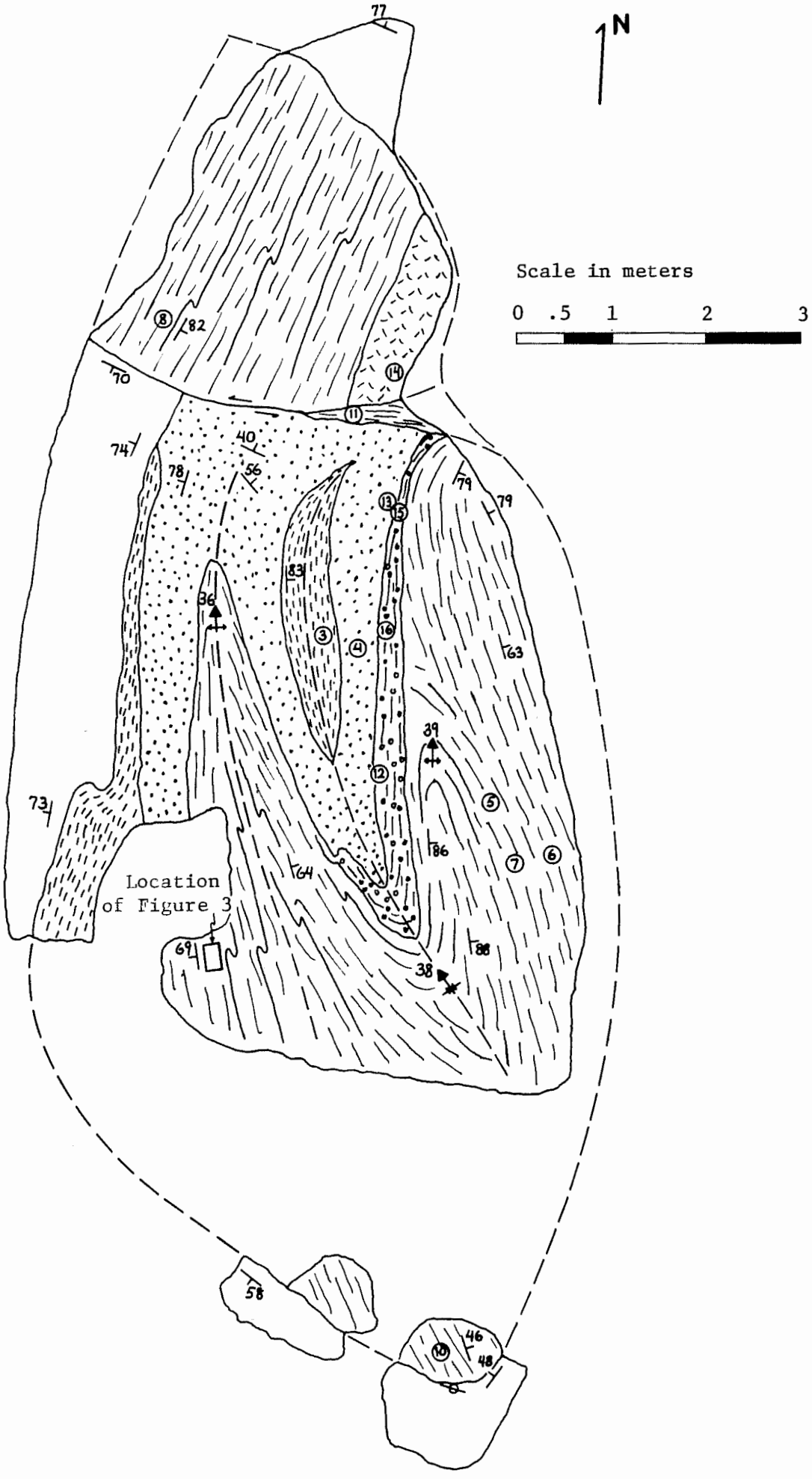
N
Scale in meters
0 .5 1 2 3
Location of Figure 3

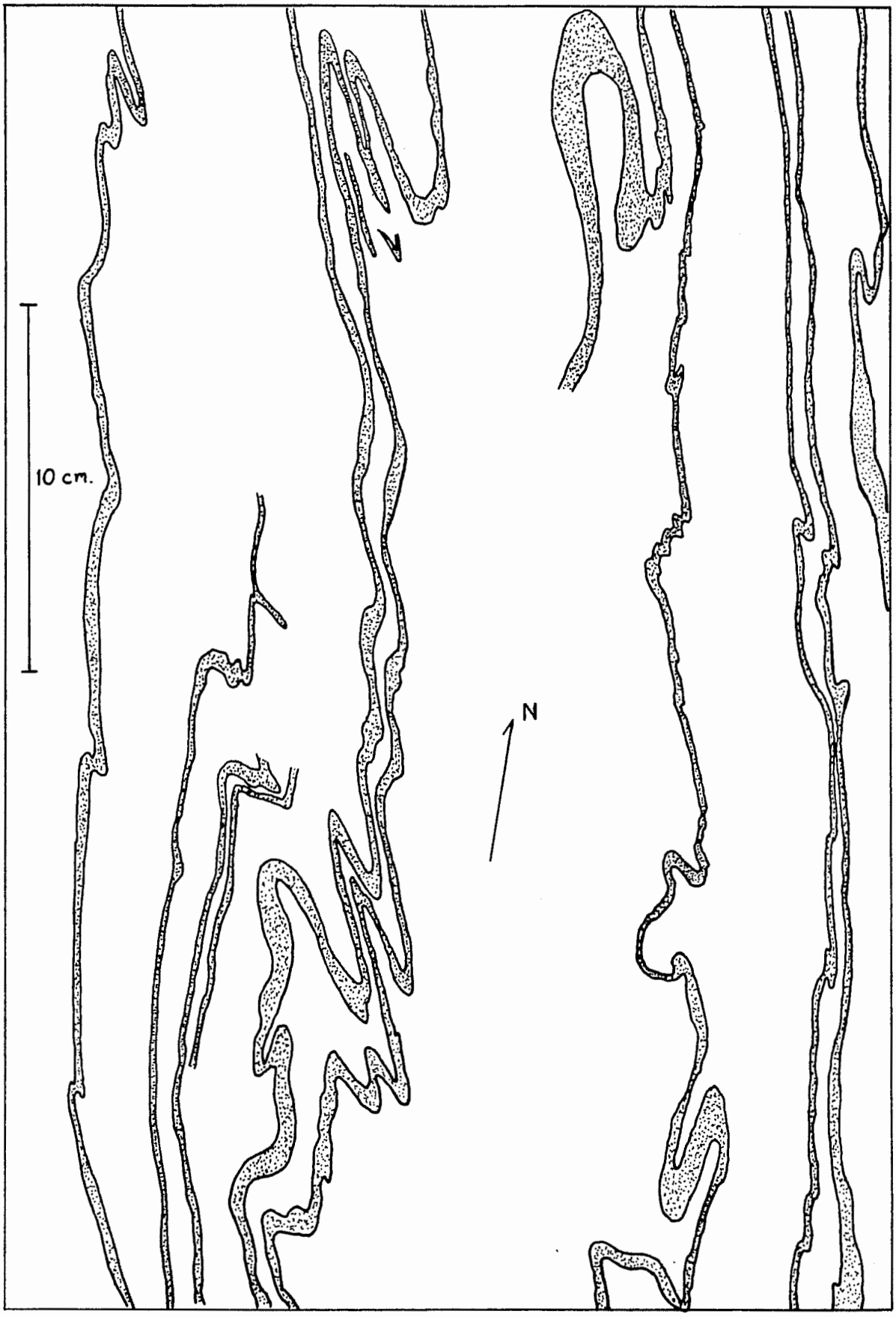

Figure 3. Locality 2J1, minor folds in apatite-rich beds on the limb of an anticline in the olivine-magnetite granulite.

olivine-pyroxmangite granulite (d) and on fresh surfaces thin pale yellow apatite-rich beds (Figure 3) show good contrast against intervening steel-gray beds containing graphite, magnetite, olivine, grunerite and garnet. The olivine-magnetite granulite is the thickest unit in this outcrop and is present in both northern and southern boudins. Most other localities of iron-rich beds in the Littleton Formation contain this olivine-magnetite granulite, and it is therefore of major interest in the development of a chemical model for the iron-rich lenses.

The youngest lithic unit, grunerite-garnet-pyrrhotite granulite (f), occurs at the eastern edge of the northern block of locality 2J1. It has a sharp contact with the underlying olivine-magnetite granulite (e). Hand specimen examination of this unit indicates that the garnet is euhedral and is poikilitically enclosed in large prismatic grunerite grains. These two phases compose most of the unit, but rare 1 mm thick sulfide-rich beds also exist. The eastern edge of this unit is coated with a coarse-grained grunerite vein. Grunerite veins are a common feature in most of the iron-rich lenses, and because they usually occur on what is now the outer surfaces of the iron-rich lenses, they may represent zones of structural weakness through which solutions passed during metamorphism.

Specimens collected at several other outcrops indicate that the rock types present in the lens at 2J1 include most of the types present at other localities. For this reason detailed mineralogical and chemical information obtained on fresh material from locality 2J1 is probably representative of the material from iron-rich lenses of the Littleton Formation within the sillimanite-muscovite zone.

"Iron Ridge," Outcrop Localities A22a, b, c

During the early part of the 19th century, iron ore was taken from three localities on "Iron Ridge," but the process stopped shortly after it was begun, due to impurities in the ore (Hitchcock, 1841). The three iron-rich lenses on "Iron Ridge" were observed briefly by the author during a reconnaissance visit of the known iron-rich localities within the Mount Grace quadrangle. Several grab samples collected by Peter Robinson and H. W. Jaffe were used for petrographic analysis. The three lenses, now exposed in open pits, contain three lithic types: 1) olivine-magnetite granulite, 2) grunerite-garnet-pyrrhotite granulite and 3) garnet-biotite-quartz granulite. The dominant type, olivine-magnetite granulite, closely resembles the analogous unit (e) in locality 2J1. The olivine-magnetite granulites at "Iron Ridge" are strongly magnetic, fine-grained and very dense. They weather dull black to rusty-brown and contain thin apatite-rich beds. A thin orthopyroxene-bearing vein was found in one grab sample of olivine-magnetite granulite from the southernmost pit. Orthopyroxene is not known to occur elsewhere in the Littleton Formation. The second unit at "Iron Ridge," grunerite-garnet-pyrrhotite granulite, is fine- to medium-grained and exhibits a sharp contact with the olivine-magnetite granulite. It is moderately friable and is rusty on weathered surfaces. Grunerite and garnet compose most of the unit, pyrrhotite being locally situated in tiny patches. By comparison, the pyrrhotite in the grunerite-garnet-pyrrhotite granulite of 2J1 is situated in a thin bed. Moreover, the poikilitic texture of garnet within coarse grunerite noted in the granulite at locality 2J1 was not observed in the unit at "Iron Ridge." Despite these differences the two grunerite-garnet-pyrrhotite granulites may be similar with respect to their initial

sedimentary chemistry. Robinson (1963) also reports garnet-biotite-quartz granulite at the "Iron Ridge" outcrop localities, where it forms a distinct zone between magnetite-rich granulite and enclosing schist.

Beach Hill, Outcrop Localities G67, 5J9, 3J4

Three iron-rich lenses are visible on Beach Hill (Figure 1). At locality G67 there is a small pit about 1 meter in width which was probably opened contemporaneously with the three pits on "Iron Ridge." From observation of the two grab samples collected at this locality, the most common rock type is a fine-grained olivine-magnetite granulite. A coarse-grained grunerite-garnet granulite is also present.

Just to the north of locality G67 there is an extremely small iron-rich outcrop approximately 1 meter in length and 0.5 meters in width which lies at the base of the Littleton Formation and is in contact with conglomerate of the underlying Clough Quartzite. No samples were obtained from this unit, but it appears to be rich in garnet and grunerite.

The largest outcrop of iron-rich rock on Beach Hill, locality 3J4, lies about 200 meters to the NNE of G67. Detailed mapping of the beds at locality 3J4 proved to be difficult and results were unsatisfactory due to lack of stratigraphic control. Extreme alteration and weathering have destroyed the one characteristic lithologies. Several samples were obtained by drilling with the help of Professor S. E. Haggerty. A few of these were sufficiently fresh to produce thin sections, but none were fresh enough to warrant microprobe analysis. The basic stratigraphy was partially unravelled with the use of these thin sections and associated grain mounts. The known stratigraphy, listed below, will be discussed from oldest to youngest:

Youngest

Sillimanite-muscovite schist
Garnet-biotite-quartz granulite
Olivine-magnetite granulite
Grunerite-garnet granulite
Mica-garnet schist
Biotite gneiss with garnet-rich boudins

Oldest

The biotite gneiss, consisting of quartz, plagioclase and biotite, contains small garnet-rich boudins. These fine-grained, granular boudins contain the assemblage garnet-biotite-quartz also observed in the youngest granulite at 3J4. Rusty-weathering mica-garnet schist, similar to the mica-garnet schist (b) at locality 2J1, lies above the biotite gneiss. The rusty-weathering schist grades into fine-grained, poorly bedded, weakly magnetic grunerite-garnet granulite with minor apatite, ilmenite and magnetite. This unit is tan-weathering in contrast to the rusty schist. Directly above this is fine-grained, well bedded, dense olivine-magnetite granulite, which where relatively fresh, looks very much like the olivine-magnetite granulite (e) of locality 2J1 and of the "Iron Ridge" pits. Olivine, magnetite, grunerite, garnet and apatite compose most of the rock, but pyrrhotite and marcasite are locally abundant. The youngest unit is a medium-grained garnet-biotite-quartz granulite which weathers reddish-brown. The dominant mineral is euhedral garnet, which is approximately 1 mm in diameter and set in a matrix of biotite and quartz.

Grunerite veins are abundant throughout the iron-rich units at locality 3J4 and have severely altered nearby surrounding beds to the

extent that many of the characteristic lithologic features described above are only locally recognizable. Thus the stratigraphy for locality 3J4 is not completely determined.

The fold axes in the iron-rich units at 3J4 trend about N70E and plunge about 10° to the NE. This attitude is distinctly different from the north-south trend of late folds in the surrounding schists and indicates that these folds, like those at 2J1, are early and have probably been rotated to their present position. The discordant orientation of the lens at locality 3J4 may have facilitated the extensive alteration which penetrated all rock types.

Bliss Hill, Outcrop Locality 6I2

The outcrop at locality 6I2 (Figure 1) forms a small ledge close to the base of the Littleton Formation. The rock consists of a massive, medium- to coarse-grained quartz-pyroxmangite-garnet gneiss. Because the gneiss is rich in manganese as well as iron, the weathered surface is covered with a silver-gray manganese oxide stain. The rock is also very dark because of abundant graphite. The silicates present here differ significantly from other iron-rich silicates observed in this study by having higher Mn/Fe+Mn ratios.

Temple Hill, Outcrop Locality 4N4

About 275 meters southeast of the summit of Temple Hill at the 1015 foot contour interval is a small, well-weathered outcrop of garnet-grunerite granulite.

East of Mayo Corner, Outcrop Locality 2J5

Approximately 60 meters north of the junction of Chase and Royalston roads is a series of iron-rich beds which, from hand specimen examination, contain the assemblages garnet-grunerite-quartz and olivine-pyroxmangite. In hand specimen these granulites are similar to granulites designated (c) and (d) (Figure 2) from locality 2J1. The garnet-grunerite-quartz granulite weathers tan and the olivine-pyroxmangite granulite weathers dull black.

West Royalston, Royalston Quadrangle, Outcrop Locality 35

The Royalston Quadrangle lies directly to the east of the Mount Grace Quadrangle in north-central Massachusetts. South-southwest of the town of West Royalston there is a power line which runs in a general SE-NW direction. Approximately 200 meters further south-southwest of the power line there is a small knob at the 850 foot contour interval; just to the north of the small knob there is a small outcrop of iron-rich beds. This iron-rich unit is a fine-grained olivine-magnetite granulite about 0.5 m thick, which like other strongly magnetic granulites in the Littleton Formation is well bedded, dense and weathered dull black or rusty-brown. It contains 5-10 mm dull white weathering beds rich in apatite.

DETAILED PETROGRAPHY

Polished thin sections were made from iron-rich samples in order to examine mineral phases in transmitted and reflected light simultaneously. The importance of using polished thin sections with both transmitted and reflected light cannot be overemphasized because, for determination of equilibrium assemblages, it is essential to know which mineral phases are in grain to grain contact. This information cannot be readily obtained by using covered thin sections in conjunction with polished chips or grain mounts of opaque phases. Furthermore, the fine-grained, thinly-bedded nature of units such as the olivine-magnetite granulite necessitates the use of polished thin sections with transmitted and reflected light for accurate modal analysis of individual beds. Estimated modes for some of the rocks appear in Table 1. Rock names have been developed so that the most characteristic mineral appears first.

Descriptive petrography is divided into two parts: 1) rocks at locality 2J1, and 2) rocks distinctly different from those at locality 2J1.

Petrography, Locality 2J1

Mica-garnet schist (b). The lowest iron-rich unit at locality 2J1, a rusty-weathering schist (Table 1, 2J1-3), lies directly above the normal sillimanite-muscovite schist of the Littleton Formation. Biotite and muscovite together are responsible for a strong schistosity that is especially noticeable in thin section. Garnet is approximately 1 mm in diameter. Quartz, which is absent in most of the iron-rich rocks studied, is abundant in this unit. The rusty-weathering schist has a gradational contact with the normal sillimanite-muscovite schist of the

Table 1. Estimated modes of iron-rich samples.

Locality	2J1													A22H2			6I2
Sample	3	4	12	16	6-1	6-2	6-3	5	11-1	11-2	11-3	11-4	11-5	host	vein	vein + wall rock	A
Horizon	(b)	(c)	(d)	(d)	(e)			(e)	(e)								
Grunerite		21	17	19	15	2	18	10	20	17	30	12	8	13	43	18	1
Garnet	16	67	11	7	29	5	35	27	25	69	29	9	45	21	7	46	9
Olivine			67	56	25	10	9	30	46	6	29	5	6	61	23	16	
Quartz	33	11															63
Pyroxmangite			tr	16													25
Orthopyroxene															20	14	
Carbonate				2													
Graphite					1	tr	tr		tr	tr	1			tr		tr	2
Magnetite			2		21	2	16	29	6	7	8	8	38	5	tr	tr	
Ilmenite		1	1	tr	7		tr	4			2	1		tr		tr	tr
Apatite			2		1	81	22	tr	3	1	1	65	3	tr	7	6	tr
Pyrrhotite		tr			1												tr
Zircon		tr															
Biotite	39																
Muscovite	12																

Underlined numbers indicate that probe data were obtained. Modes for individual beds in samples 2J1-6 and 2J1-11 are designated by hyphenated numbers after the sample number.

Description of Iron-rich Samples in Table 1.

The location of all samples from locality 2J1 is noted on Figure 2.

2J1-3; Fine-grained, rusty-weathering mica-garnet schist stratigraphically above the normal sillimanite-muscovite schist of the Littleton Formation.

2J1-4; Fine-grained, tan-weathering, thin-bedded garnet-grunerite-quartz granulite (Figures 4 and 5). This sample lies stratigraphically above the rusty-weathering mica-garnet schist.

2J1-12; Coarse-grained, dark gray-weathering olivine granulite. Bedding is only poorly developed in contrast to units stratigraphically above and below it.

2J1-16: Coarse-grained, black-weathering olivine-pyroxmangite granulite (Figures 6 and 7). On fresh surfaces pyroxmangite may be identified by its distinctive pink color and prismatic habit.

2J1-6; Well-bedded, fine-grained, rusty-weathering oliving-magnetite granulite (Figure 8). Thin pale yellow apatite-rich beds visible on fresh surfaces.

2J1-5; Fine-grained, black-weathering, dense olivine-magnetite granulite. No apatite-rich beds present in this sample.

2J1-11; Well-bedded, fine-grained, rusty-weathering olivine-magnetite granulite similar to sample 2J1-6. This sample occurs near the shear zone between northern and southern structural boudins.

A22H2; This sample collected by Peter Robinson and H. W. Jaffe from the southernmost pit on "Iron Ridge" (Figure 1). The host granulite is poorly-bedded, fine-grained and rusty-weathering. It contains a 2 mm thick orthopyroxene-bearing vein. In Table 1, host refers to the olivine-magnetite granulite. Vein refers to vein mineral assemblages inside the garnet wall rock. Vein and wall rock refers to mineral assemblages in both the vein and in the garnet-rich wall rock. See text for microscopic description of this sample (Figure 13) and for discussion of mineral assemblages.

6I2A: Medium- to coarse-grained massive quartz-pyroxmangite-garnet gneiss (Figure 14). Distinctive steel-gray manganese oxide weathering stain. Outcrop forms ledge near the base of the Littleton Formation above Clough Quartzite.

Littleton Formation and marks the beginning of the chemical transition from normal pelitic compositions to those which are rich in iron and manganese.

Garnet-gruneríte-quartz granulite (c). Stratigraphically above the rusty-weathering schist is garnet-gruneríte-quartz granulite (Table 1, 2J1-4). The thin-bedded, heterogeneous nature of this unit is shown in Figure 4; beds consist of garnet-quartz, garnet-gruneríte, or garnet-gruneríte-quartz. Some beds contain interstitial ilmenite, and ilmenite also occurs as inclusions in garnet. Elongate ilmenite plates in garnet are aligned in a subparallel arrangement within separate garnet grains, in what is interpreted as a relict older metamorphic foliation. The garnets have zoning of inclusions in some beds, as is illustrated near the bottom of Figure 4, but microprobe analyses (Table 7, analyses L) indicate that these zoned garnets are homogeneous with respect to major element chemistry. Therefore the inclusions are probably fluid or very fine carbonaceous material, concentrated in the cores of garnets.

The garnet-gruneríte-quartz granulite marks the lowest stratigraphic appearance of gruneríte in the lens at locality 2J1. Large prismatic crystals of gruneríte enclosing small anhedral garnets form a poikilitic texture as is shown in Figure 5. This texture is common at the other localities investigated within the Littleton Formation. The gruneríte is polysynthetically twinned on (100), as in all other gruneríte-bearing beds at locality 2J1. Many gruneríte crystals in the garnet-gruneríte-quartz granulite contain small grains of a radioactive mineral, tentatively identified as zircon, which are not observed in gruneríte from other units at 2J1. These small grains produce brown pleochroic haloes in the gruneríte host that distinguish the gruneríte in the garnet-

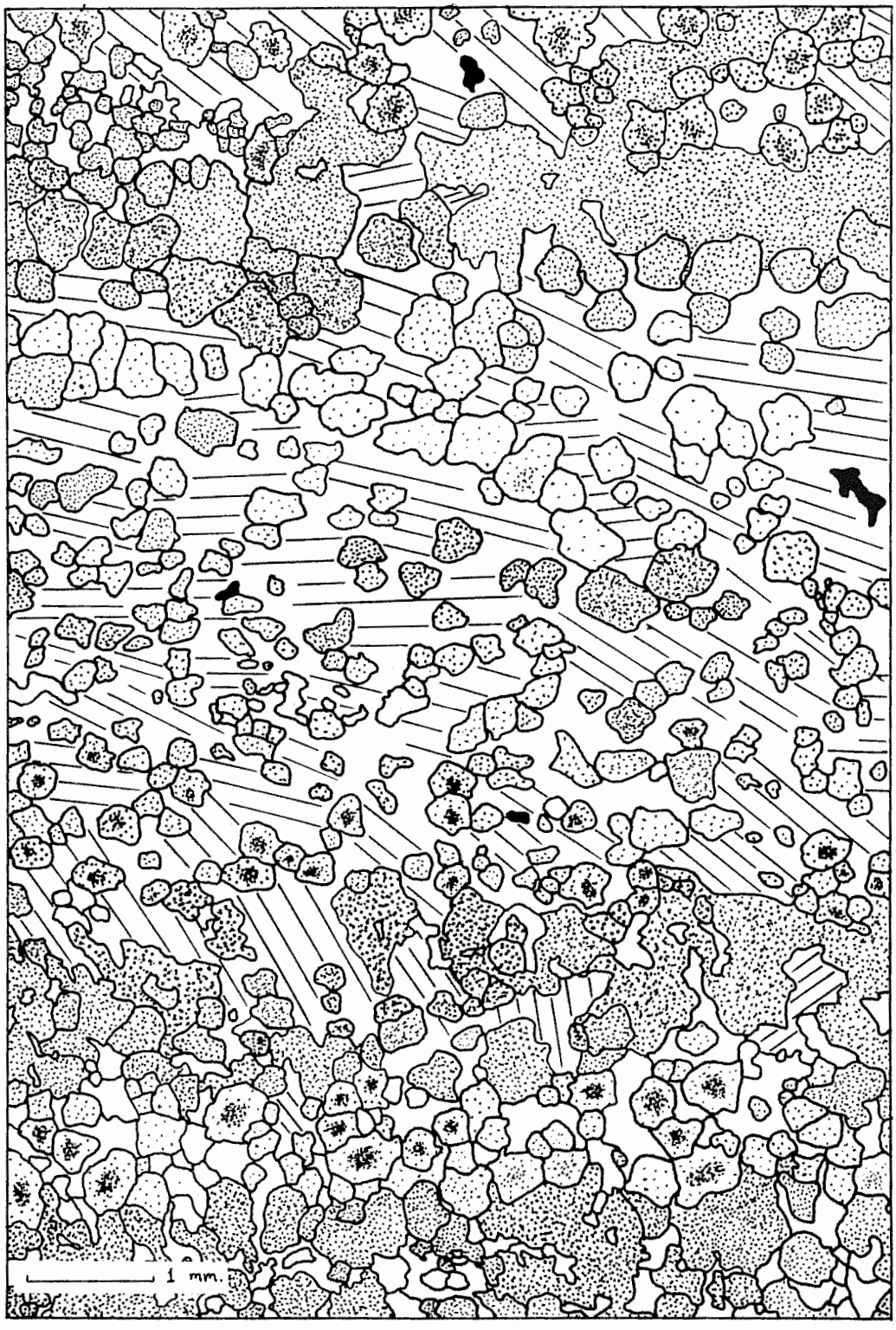

Figure 4. Bedded garnet-grunerite-quartz granulite, 2J1-4.

Garnet Grunerite Quartz Ilmenite

grunerite-quartz granulite from grunerite in overlying beds. The presence of the radioactive mineral presumably reflects a difference in the source of sediment input at the time of deposition.

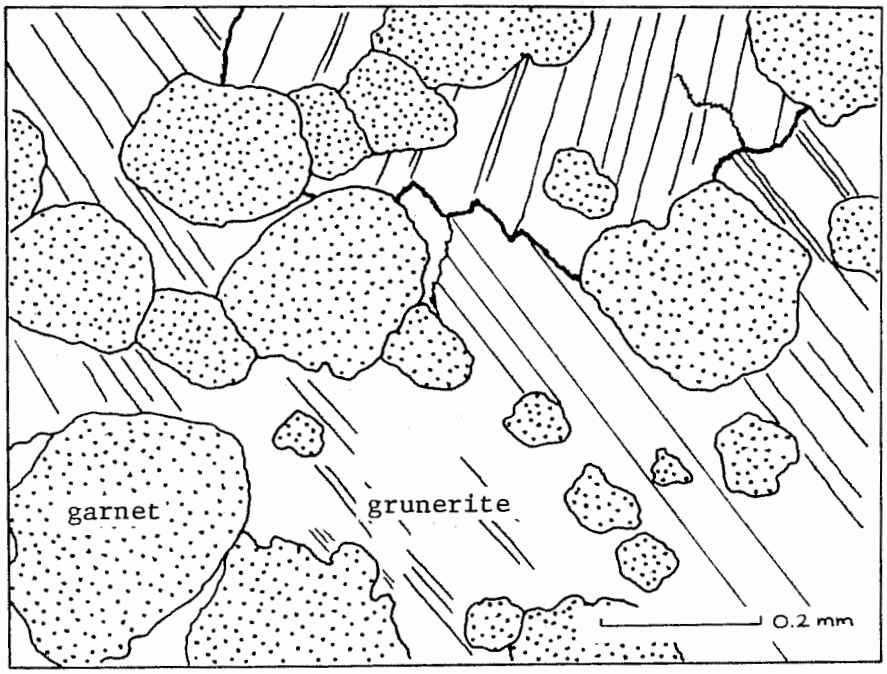

Figure 5. Poikilitic texture with anhedral garnet in prismatic grunerite, 2J1-4.

Olivine-pyroxmangite granulite (d). Above garnet-grunerite-quartz granulite at 2J1 is olivine-pyroxmangite granulite (Table 1, 2J1-12 and 2J1-16). Important textural relationships in this granulite are illustrated in Figures 6 and 7. In Figure 6, optically continuous crystals of olivine and pyroxmangite are intergrown. This texture suggests a slow simultaneous growth of the two phases. Grunerite, on the other hand, is situated at various orientations within Figure 6, suggesting that it developed independently of olivine and pyroxmangite. A metamorphic reaction, discussed in a later section, that might produce the

observed assemblage is:

carbonate + grunerite = olivine + pyroxmangite + H_2O + CO_2.

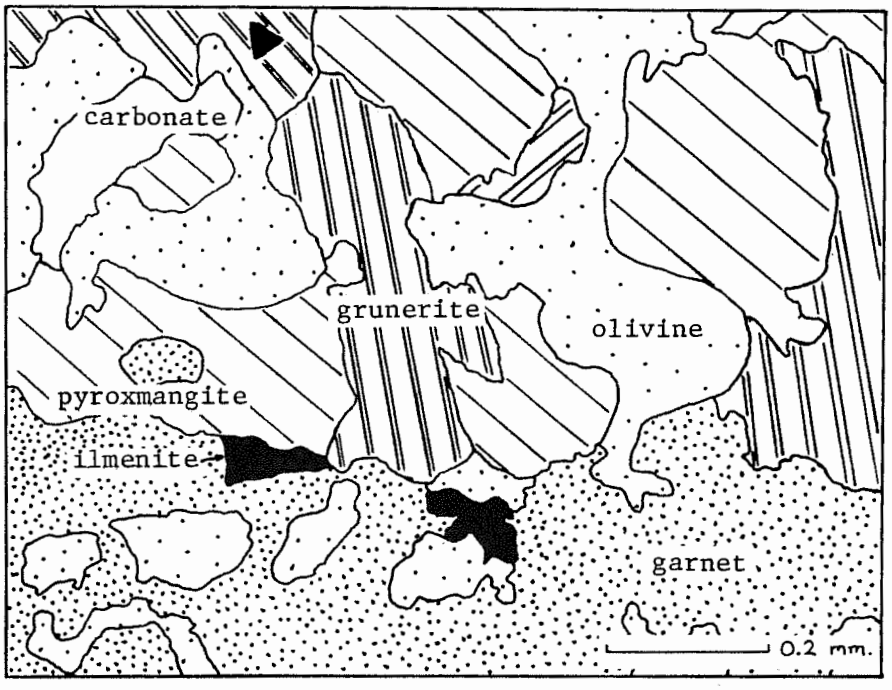

Figure 6. Olivine-pyroxmangite granulite, 2J1-16. Optical continuity preserved in olivine and pyroxmangite within field of view.

Ilmenite occurs interstitially, as is observed in the garnet-grunerite-quartz granulite, but it does not occur as inclusion in garnet. Locally, magnetite forms bladed intergrowths with grunerite.

The garnet is medium pink in color and appears free of fine inclusions, in contrast to the garnet in the underlying garnet-grunerite-quartz granulite.

The chemistry of the carbonate which occurs in one of the two specimens (Table 4, analysis K) suggests that it is primary. Its composition lies approximately halfway between calcite and kutnahorite on

the $CaCO_3$-$MnCO_3$ join, $FeCO_3$ and $MgCO_3$ being relatively minor. It is commonly twinned and is colorless even in relatively thick microprobe sections.

Olivine in the pyroxmangite-bearing granulite specimens examined is weathered along grain boundaries and fractures, whereas other phases present appear fresh.

Locally, grunerite occurs as small grains within large crystals of pyroxmangite (Figure 7). This texture may indicate that grunerite was being consumed by the olivine-pyroxmangite forming reaction noted above.

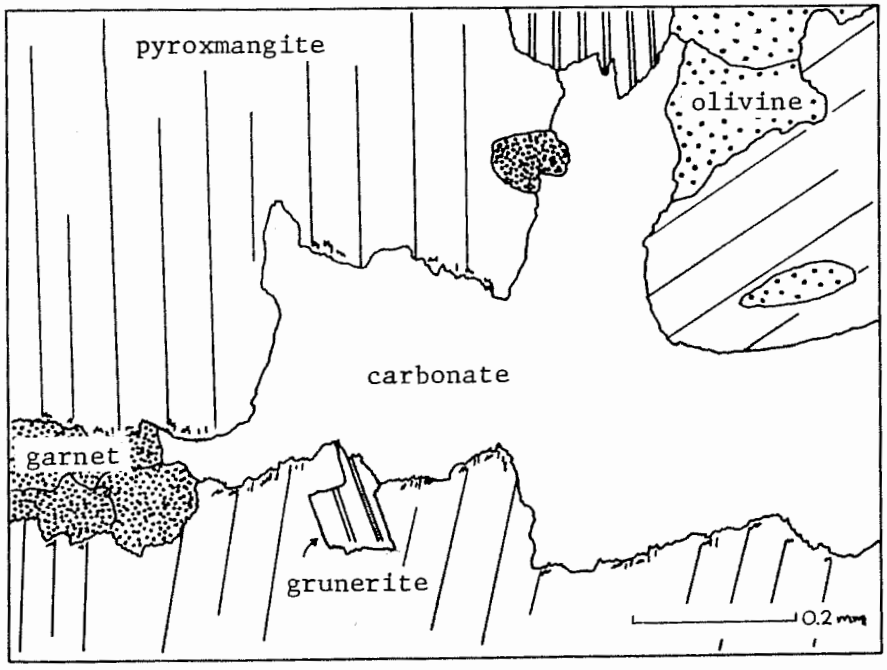

Figure 7. Olivine-pyroxmangite granulite, 2J1-16.

Bedding, if present at all in the olivine-pyroxmangite granulite, is only poorly developed on a local scale, but rare pyroxmangite-rich beds do exist in sample 2J1-15.

Olivine-magnetite granulite (e). Olivine-magnetite granulite (Table 1, 2J1-5, 6, 11) overlies olivine-pyroxmangite granulite. In contrast to the latter, this strongly magnetic granulite is well-bedded and fine-grained. The bedding is readily apparent in thin section (Figure 8), where beds rich in olivine, grunerite, garnet and magnetite alternate with beds rich in apatite and olivine. Large variations exist in the modal percentages of phases present in silicate-rich beds, but the beds rarely approach a monomineralic state. Other minerals in this granulite include graphite, ilmenite, pyrrhotite and marcasite.

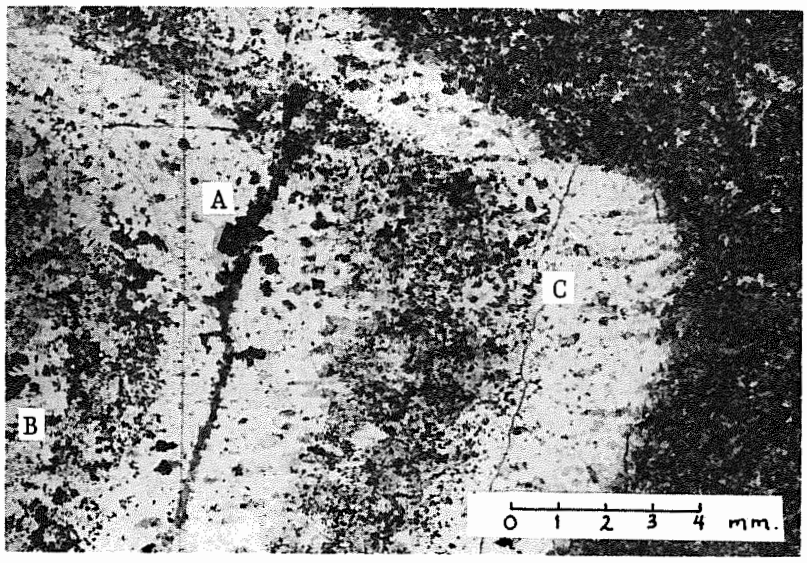

Figure 8. Olivine-magnetite granulite, 2J1-6. Interbedded mafic and apatite-rich units. A) Secondary vein containing fibrous grunerite and rod-shaped graphite. B) Intergrowths of prismatic grunerite and magnetite. C) Elongate olivine growth parallel to the axial plane of the fold.

Graphite, although common in the sillimanite-muscovite schist of the Littleton Formation, is restricted in occurrence at locality 2J1 to the olivine-magnetite granulite. Two textural types of graphite occur

in the granulite: 1) subrounded radial aggregates and 2) elongate rods. Subrounded radial aggregates of graphite are the most common. Each radial aggregate is composed of many individual laths of graphite which radiate from a central core. The rod-shaped variety is rare by comparison, except where intergrown with fibrous grunerite in secondary veins as illustrated in Figure 8. The factors governing the growth of one form of graphite in preference to the other are not understood. Graphite is not present in all beds within this unit; however, where present it is considered an important factor in controlling the gas phase composition during metamorphism.

Magnetite is ubiquitous in this strongly magnetic granulite and comprises the bulk of all opaque grains. It occurs in four different textural forms:

(1) intergrowths of prismatic grunerite and bladed magnetite, Figure 8.

(2) symplectic intergrowths of grunerite and magnetite, Figure 9.

(3) patchy networks of magnetite and garnet, Figure 10.

(4) interstitial magnetite.

Intergrowths of prismatic grunerite and bladed magnetite (1) are far more common than symplectic intergrowths (2) of the two phases. Both types of intergrowths may occur in the same assemblage, and in one area of sample 2J1-6 both types occur in different parts of a single crystal, suggesting that intergrowth types (1) and (2) are genetically related.

Patchy networks (3) of garnet and magnetite as well as garnet with numerous magnetite inclusions are common features of mafic beds in the granulite (Figure 10).

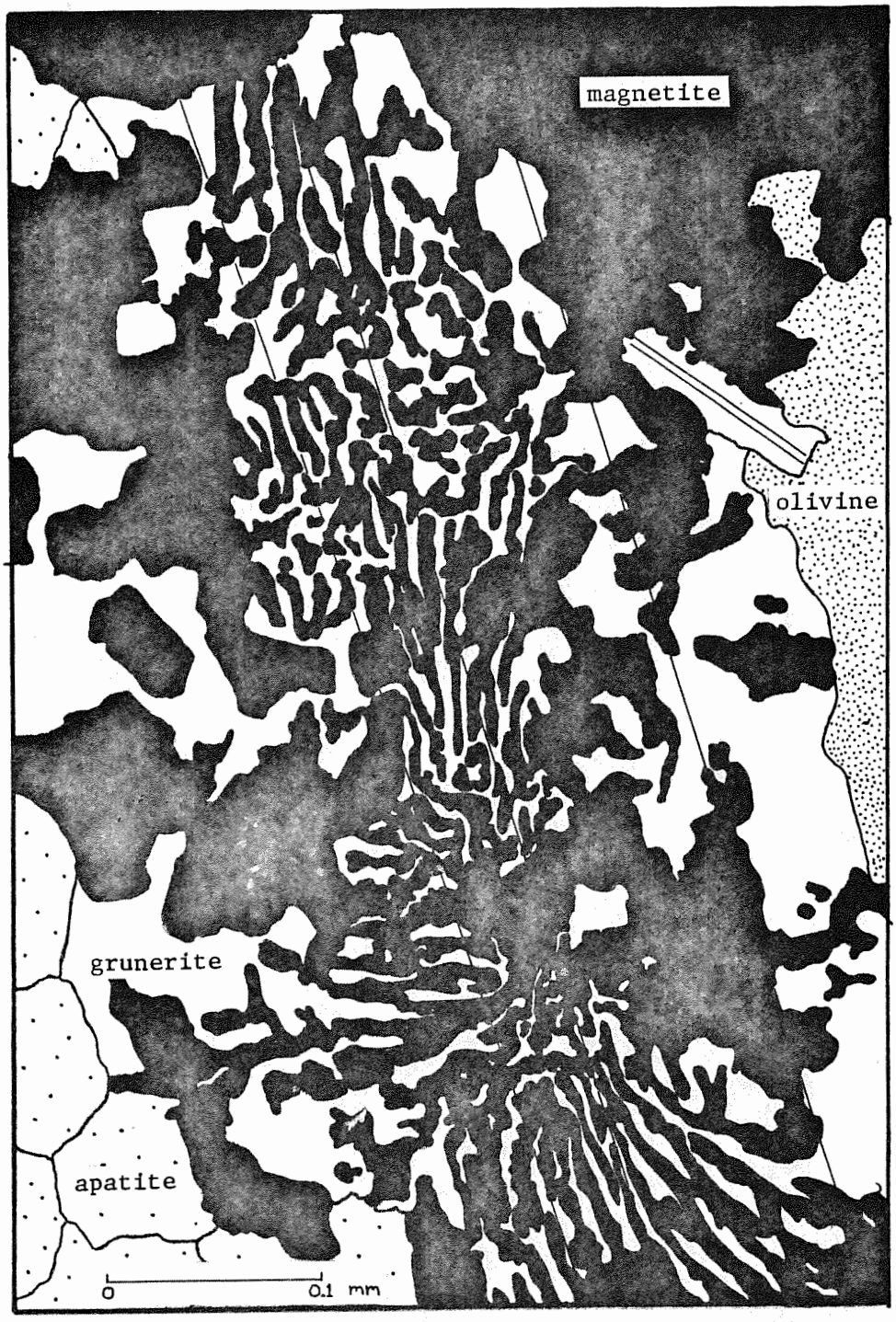

Figure 9. Grunerite-magnetite symplectic intergrowth, 2J1-6. Two individual grunerite crystals are present in the field of view. Both grunerites are twinned on (100).

Figure 10. Patchy network of magnetite and garnet with minor olivine and grunerite, 2J1-10.

Interstitial magnetite (4) is common throughout the granulite. Magnetite generally tends to be optically homogeneous and chemically close to the ideal Fe_3O_4 end member as indicated by microprobe analyses in Table 9. Rare ilmenite oxy-exsolution lamellae do occur, but more commonly magnetite and ilmenite exist as composite grains. Magnetite may also contain small spherical inclusions of pyrrhotite.

Olivine, which composes as much as 67% of the underlying olivine-pyroxmangite granulite, is less abundant in the strongly magnetic granulite. Locally, it has been recrystallized as indicated by well developed triple junctions. However, in most samples there is no evidence of recrystallization. The olivine is anhedral and commonly shows reddish-brown weathering alteration on grain boundaries and fractures. Figure 8 illustrates a particularly unusual growth of olivine within apatite-rich beds, in which olivine has grown parallel to the axial plane of the fold. Some crystals can be shown to be elongate parallel to the c-axis of olivine. These elongate crystals probably formed during early isoclinal fold development. Olivine-rich beds are rare, but do occur in one sample, 2J1-6. These 1 to 2 mm beds are structurally conformable with apatite-rich beds in the same hand-specimen. By comparison, apatite-rich beds are present in most olivine-magnetite granulite samples collected at locality 2J1.

Grunerite, like magnetite, is ubiquitous in the olivine-magnetite granulite. Grunerite-rich beds with magnetite, olivine and garnet are common and within these beds no preferred orientation of prismatic grunerite is developed. In sample 2J1-5, acicular grunerite appears to replace olivine (Figure 11). Grunerite in secondary veinlets is generally fibrous.

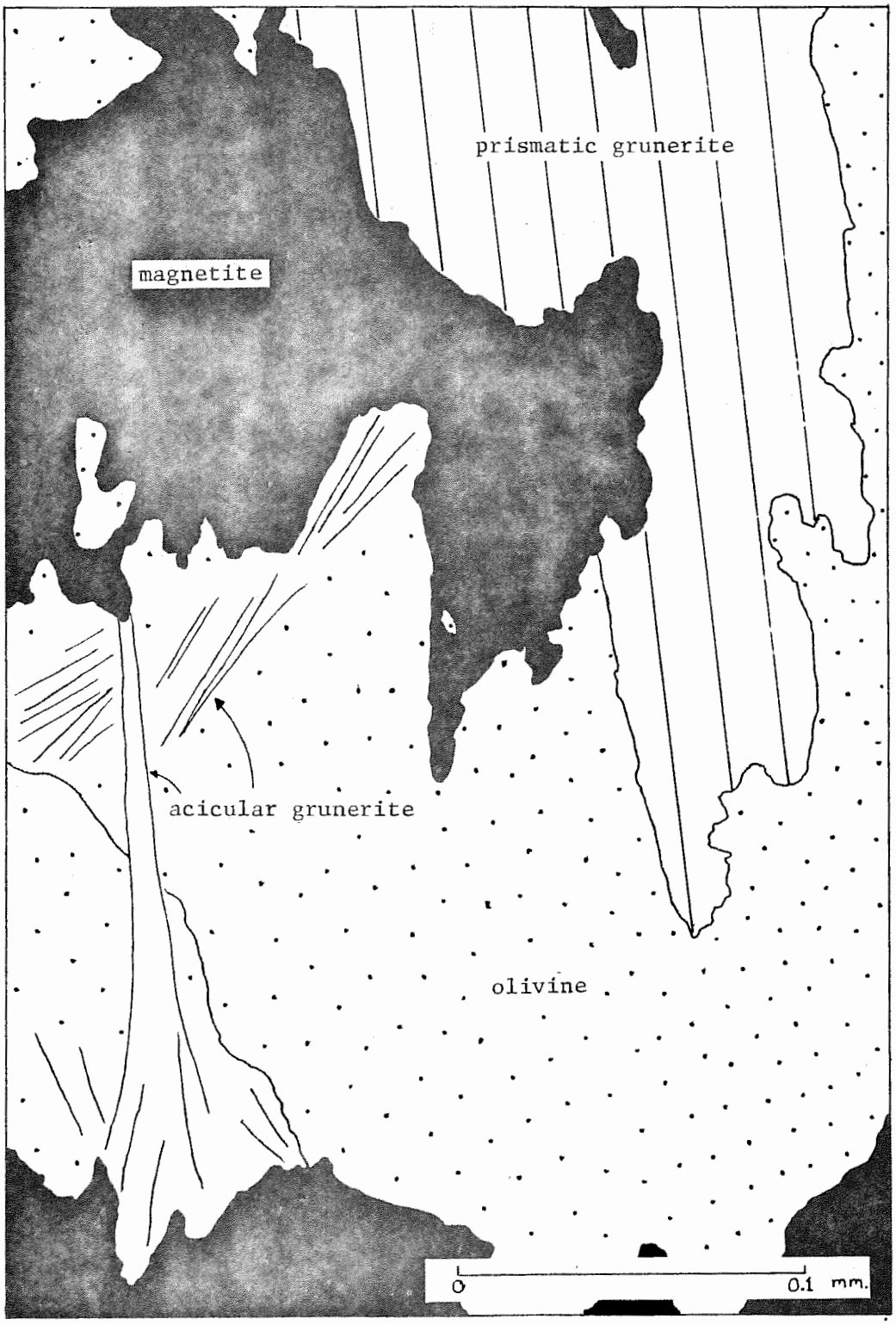

Figure 11. Acicular grunerite in olivine-magnetite granulite, 2J1-5.

Garnet, within the strongly magnetic granulite, is anhedral in all occurrences. Inclusions are present in garnet except in the small 20-40 micron garnet grains that lie in the apatite-rich beds. These inclusions are dominantly magnetite by vary from bed to bed depending on the minerals with which garnet is associated. Graphite, magnetite, ilmenite, olivine, grunerite, apatite or pyrrhotite may exist as inclusions in garnet. The garnet is colorless and is both optically and chemically unzoned. Inclusions, where present, are uniformly scattered within the grain. Rare garnet and magnetite-rich beds occur locally (Figure 10).

Apatite-rich beds in the strongly magnetic granulite are composed dominantly of numerous equidimensional apatite grains approximately 100 microns in diameter. These grains always exhibit an annealed texture as indicated by well developed triple junctions. Trace amounts of apatite occur in mafic beds.

Sulfides are interspersed among some mafic beds. Pyrrhotite is partially or completely weathered to marcasite in most occurrences. "Birds eye" textures are present in these sulfide grains in which cores of pyrrhotite are surrounded by spongy concentric layers of marcasite. Sulfide inclusions within other phases such as garnet tend to be fresher than interstitial sulfides. Trace amounts of chalcopyrite are present.

Grunerite-garnet-pyrrhotite granulite (f). The youngest iron-rich unit at locality 2J1 is grunerite-garnet-pyrrhotite granulite. Figure 12 illustrates the bedded nature of the granulite on a sawed surface. Bed (a) lies within the core of the fold and consists of prismatic grunerite that contains euhedral garnets about 0.5 mm in diameter. The texture is similar to that in the garnet-grunerite-quartz granulite (Figure 5).

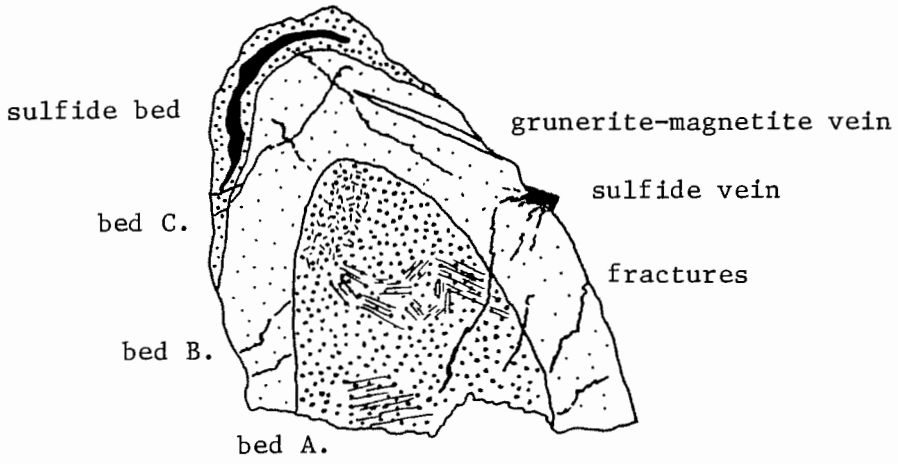

Figure 12. Sawed section of grunerite-garnet-pyrrhotite granulite, 2J1-14. Scale 1:1.

Bed (A) has a razor-sharp contact with a fine-grained garnet granulite bed (B), which in turn has a sharp contact with a grunerite-garnet bed (C). Beds (A) and (C) both have garnet poikilitically enclosed in large prismatic grunerite grains, but a 1 mm thick sulfide bed is present in bed (C). This sulfide bed is folded conformably with the structure and thus may reasonably be interpreted as a bed, rather than a vein. However, a sulfide vein is present on the right limb of bed (B), from which small fractures in beds (A) and (B) radiate. These fractures may have served as conduits for sulfides mobilized during vein formation. A secondary vein containing grunerite and magnetite cuts across bed (B). As might be expected from extensive fracture and vein development, the grunerite-garnet-pyrrhotite granulite is extremely altered.

Petrography of Rocks Distinctly Different from those at Locality 2J1

Orthopyroxene vein in olivine-magnetite granulite. Sample A22H2, a grab sample, collected by Peter Robinson and H. W. Jaffe from the

southern pit on "Iron Ridge," contains an important mineral assemblage not observed in the iron-rich units of the Littleton Formation. This sample is essentially similar to the olivine-magnetite granulite of 2J1, but it contains an orthopyroxene-bearing vein that cuts across bedding. The host granulite of A22H2 (Figure 13) is armoured from the vein by a garnet-rich wall rock. Estimated modes of the host rock, vein, and vein plus wall rock in sample A22H2 are presented in Table 1. The mineral assemblage present within the vein is olivine-orthopyroxene-grunerite-magnetite-garnet-apatite. The mineral assemblage in the host granulite is olivine-magnetite-graphite-grunerite-garnet-apatite. Graphite is present interstitially in the host granulite, but in the vein it occurs only as inclusions within garnet. Therefore, contrary to what was originally stated by Huntington et al. (1974), graphite may not be in chemical equilibrium with other minerals in the vein.

The garnet wall rock (Figure 13) consists dominantly of pink anhedral garnet. In contrast to the garnet in the wall rock, the garnet in the granulite host is fine-grained and colorless. Garnet in the host is depleted in FeO and enriched in MnO and CaO (refer to Table 7) relative to the garnet in the wall rock. Locally, garnet in the wall rock is intergrown with neighboring silicate phases from both the vein and the host granulite. The vein silicate phases involved in the intergrowth are olivine, orthopyroxene and grunerite. Optical continuity is only rarely maintained between trapped grains in the garnet-rich wall rock and in the associated parent grains on either side of the wall rock. Of the three silicate phases that may be intergrown with garnet, only olivine exhibits a tendency toward crystallographic continuity in both the garnet wall rock and the vein.

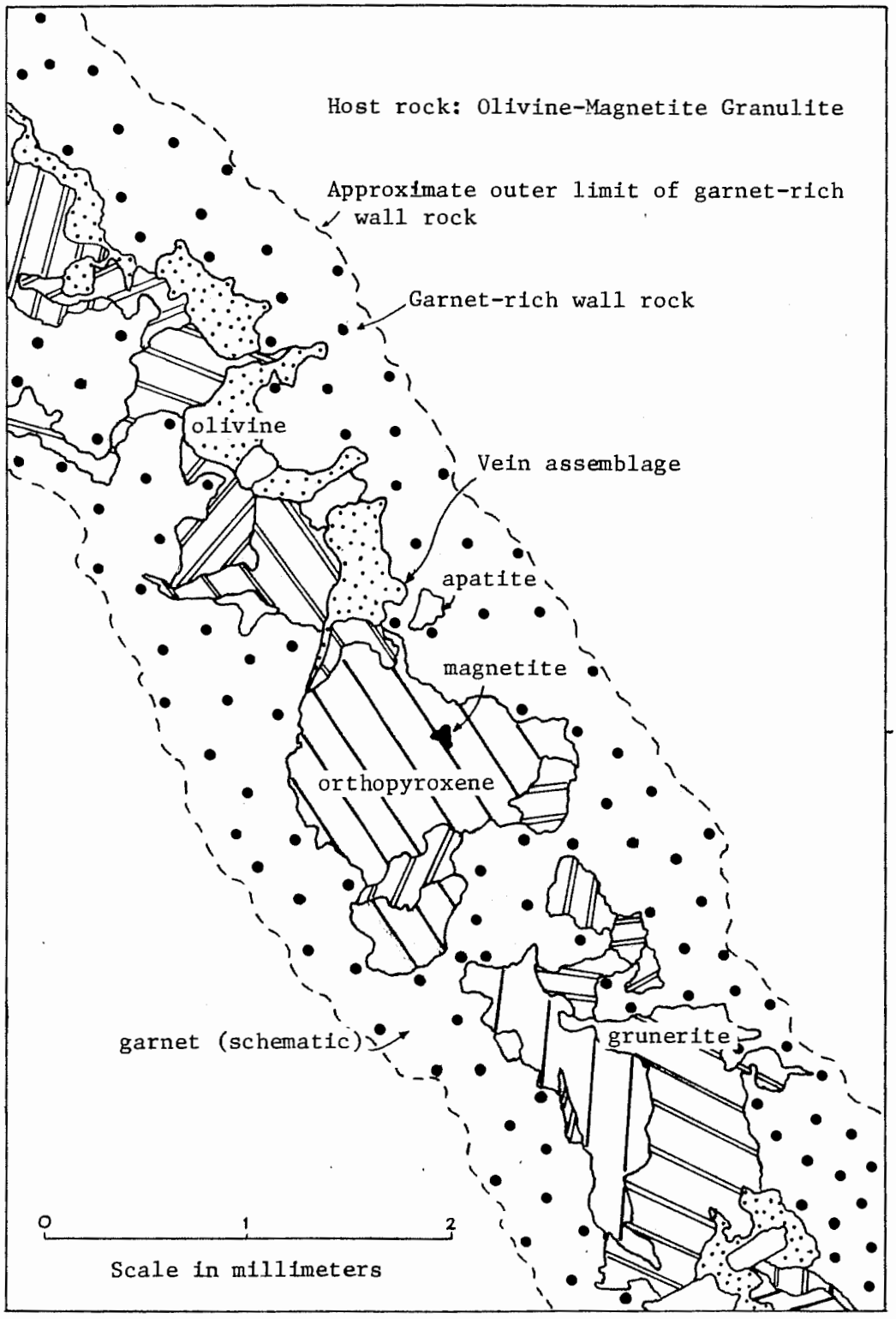

Figure 13. Schematic diagram of orthopyroxene-bearing vein in olivine-magnetite granulite, A22H2.

Olivine in the vein is commonly embayed by orthopyroxene and grunerite (Figure 13). Traces of olivine occur on grain boundaries of some crystals in the vein. By comparison, olivine in the host granulite exhibits a well developed annealed texture with equidimensional olivine grains forming good triple junctions. No replacement of olivine in the host is observed.

Orthopyroxene in the vein is tan, non-pleochroic and prismatic. Locally, in the vein, it appears to be replaced by grunerite. It does not occur in the host granulite.

Grunerite in the vein is not commonly associated with magnetite, whereas grunerite in the host granulite is always intergrown with bladed magnetite.

Apatite in the vein is abundant relative to the host granulite in sample A22H2. Within the vein, apatite occurs locally as euhedral crystals. No other euhedral apatite was observed in the iron-rich units of the Littleton Formation.

The orthopyroxene-bearing vein assemblage is both mineralogically and texturally interesting. A possible paragenetic scheme for its development is discussed below.

Quartz-pyroxmangite-garnet gneiss. The quartz-pyroxmangite-garnet gneiss on Bliss Hill lies close to the base of the Littleton Formation. Modal analysis of sample 6I2A (Table 1) demonstrates that it is highly siliceous. This characteristic, as well as the abundance of graphite, distinguishes it from other iron-rich lithologies in the Littleton Formation. The limiting mineral assemblage is graphite-garnet-pyroxmangite-grunerite-quartz (Figure 14). Grunerite occurs only as small grains associated with pyroxmangite. Graphite is abundant

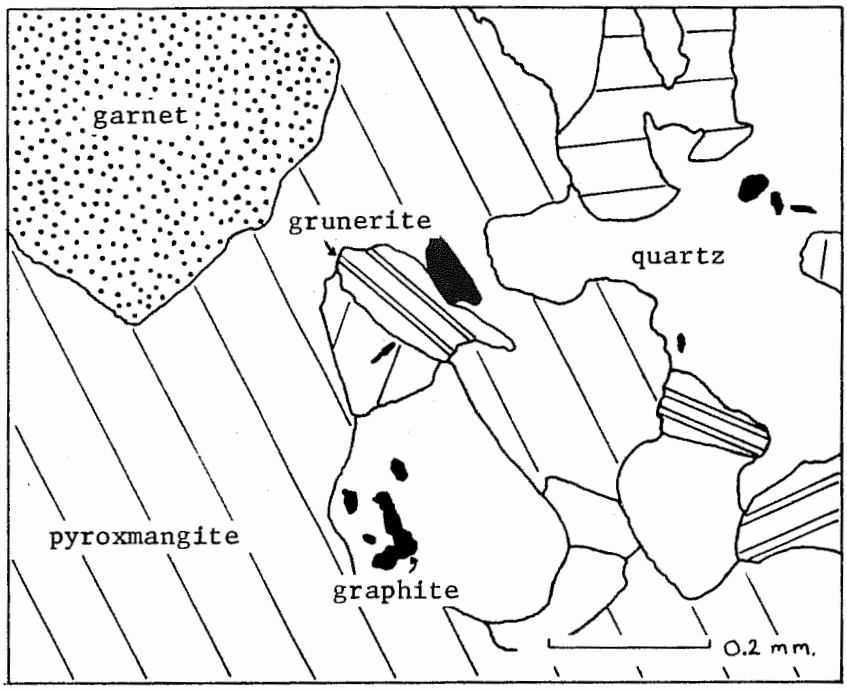

Figure 14. Quartz-pyroxmangite-garnet gneiss, 6I2.

(2 volume %) in comparison to other units investigated in the Littleton Formation and it is associated with all mineral phases. Garnet is either subhedral or euhedral and is cluttered with inclusions of quartz and graphite. Pyroxmangite is prismatic and contains some graphite inclusions. Traces of ilmenite and pyrrhotite occur locally.

Microprobe analyses of pyroxmangite, grunerite and garnet from sample 6I2A (Tables 4, 6 and 7) indicate the manganiferous character of these phases relative to those in the iron-rich units of 2J1.

MINERALOGY

The mineralogical study of iron-rich units presented below is based primarily on detailed petrographic examination of polished thin sections. Oil immersion mounts and X-ray powder photographs were used to identify unknown minerals observed during petrographic examination. The chemical composition of phases in carefully selected mineral assemblages was determined by electron microprobe analysis. The electron microprobe was ideally suited for the determination of mineral chemistry in this study for two reasons.

1) The chemistry of minerals in thinly bedded iron-rich units differs to a large extent in adjacent beds of any sample; hence, a mineral separate used for compositional determination by wet chemical or oil immersion techniques would be of variable composition unless it was derived from a single bed. Many problems are encountered in obtaining such separates.

2) Few optical determinative graphs are accurate for minerals that contain moderate amounts of manganese, such as are present in the iron-rich silicates of the Littleton Formation. Therefore, mineral compositions of Mn-bearing silicates determined by oil immersion techniques in conjunction with Mg-Fe mineral solution graphs will be inaccurate.

The use of the electron microprobe for compositional determinations eliminates both of these problems and provides accurate chemical analyses of coexisting minerals. These analyses permit detailed determination of chemographic relationships in mineral assemblages at sillimanite-muscovite grade metamorphic conditions.

Specific mineral assemblages for which microprobe analyses are available (Table 2) are denoted by capital letters. Microprobe analyses of minerals that bear the same letter belong to the same mineral assemblage. For assemblages in which more than one analysis of a mineral was obtained either an average value or a selection of one analysis from the group of analyses is presented. The number of analyses for each phase

Table 2. Mineral assemblages analyzed by electron microprobe.

A	2J1-6	olivine	grunerite				magnetite				
B	2J1-5	olivine	grunerite	garnet			magnetite				
C	2J1-5	olivine	grunerite	garnet			magnetite				
D	2J1-6	olivine	grunerite	garnet			magnetite	graph.			apatite
E	2J1-6	olivine	grunerite	garnet			magnetite	graph.		pyrrhotite	apatite
F	2J1-11						magnetite	graph.	ilmenite		apatite
G	A22H2	olivine	grunerite	garnet			magnetite	graph.	ilmenite		
H	A22H2	olivine	grunerite	garnet			magnetite	graph.	ilmenite		
I	A22H2	olivine	grunerite	garnet	opx.		magnetite				apatite
J	2J1-12	olivine	grunerite	garnet	pym.				ilmenite		apatite
K	2J1-16b	olivine	grunerite	garnet	pym.	kutnahorite			ilmenite		
L	2J1-4	quartz	grunerite	garnet							
M	2J1-4	quartz	grunerite	garnet					ilmenite		
N	6I2	quartz	grunerite	garnet	pym.			graph.			

Analyzed phases are underlined. opx. = orthopyroxene, pym. = pyroxmangite, graph. = graphite

in the assemblage is listed at the base of the chemical analysis. For example, Av. 2 indicates that 2 analyses were made of the phase and that the average of the two is listed. 1:3 indicates that the best of three analyses of the phase is listed.

Olivine

Diagnostic optical properties used to identify iron-rich olivine in polished thin sections included:

$2V_X$: 45-60° (-)
dispersion r > v
colorless
secondary weathering: orange brown on fractures and grain boundaries

Olivine has high optical relief relative to grunerite. Although the optical relief of Fe-Mn rich olivine is similar to that of garnet in thin section, the common presence of secondary alteration in olivine and the isotropic nature of garnet make them easy to distinguish. Olivine microprobe analyses for various mineral assemblages are listed in Table 3 in order of decreasing Fe/Fe+Mn mole ratio. The olivine analyses are plotted in Figure 15 on the basis of mole fraction MgO, FeO and MnO. Olivine analyses in Figure 15 lie near the fayalite-knebelite solid solution series.

Table 3. Electron probe analyses of olivine.

Assemblage letter	E	A	H	G	I*	I	D	C	B	K	J
Sample	2J1-6	2J1-6	A22H2	A22H2	A22H2	A22H2	2J1-6	2J1-5	2J1-5	2J1-16b	2J1-12
Notes			wall rock	host gran.	vein	vein					
SiO_2	30.03	29.37	29.44	29.58	30.57	29.41	29.60	30.21	30.02	29.63	29.78
TiO_2	.04	.02	.16	.10	.00	.10	.00	.00	.00	.00	.00
Al_2O_3	.05	.00	.05	.07	.02	.09	.03	.03	.00	.00	.05
Cr_2O_3	.05	.02	.13	.17	.03	.13	.00	.00	.00	.05	.00
FeO	61.07	60.55	58.03	57.60	58.20	56.70	56.91	49.34	48.20	47.18	47.13
MnO	7.16	7.22	9.62	10.08	11.33	11.26	11.41	15.53	17.68	20.06	21.44
MgO	2.00	2.18	1.44	1.42	1.17	1.02	1.14	3.64	2.99	1.99	1.31
CaO	.04	.00	.06	.07	.06	.06	.02	.03	.03	.00	.05
Na_2O	.04	.00	.15	.06	.00	.02	.00	.17	.05	.04	.00
K_2O	.01	.00	.02	.01	.00	.03	.00	.00	.00	.00	.00
Total	100.49	99.36	99.10	99.16	101.38	98.82	99.11	98.95	98.97	98.95	99.76
	av. of best 3 of 4	1:1	av. 2	av. 2	av. 3	av. 2	av. 2	1:2	1:1	1:5	1:2

Formulas calculated on the basis of 4 oxygens.

	E	A	H	G	I*	I	D	C	B	K	J
Si	.997	.989	.994	.998	1.000	.998	1.000	1.000	1.000	.997	.999
Al	.002		.002								.001
Ti	.001		.004	.002		.002					
Cr										.001	
Fe		.011								.002	
Total	1.000	1.000	1.000	1.000	1.000	1.000	1.000	1.000	1.000	1.000	1.000
Si					.008			.001	.001		
Al				.003	.001	.004	.001				.001
Ti				.001		.001					
Cr	.001		.003	.005	.001	.003					
Mg	.099	.108	.072	.071	.058	.052	.056	.180	.148	.100	.065
Fe	1.696	1.694	1.639	1.625	1.605	1.609	1.610	1.369	1.344	1.325	1.322
Mn	.201	.205	.275	.288	.317	.324	.326	.436	.499	.572	.609
Ca	.001		.002	.003	.002	.002					.002
Na	.004		.010	.004		.001		.010	.003	.002	
K			.001			.001					
Total	2.002	2.007	2.002	2.000	1.992	1.997	1.993	1.996	1.995	1.999	1.999
$\frac{Fe}{Fe+Mn}$	.894	.892	.857	.849	.835	.832	.831	.758	.729	.699	.685
$\frac{Fe}{Mg+Fe}$	.944	.940	.958	.958	.965	.969	.967	.883	.901	.930	.953
$\frac{Fe}{Mg+Fe+Mn+Ca}$	.848	.844	.825	.817	.810	.810	.808	.689	.675	.664	.661

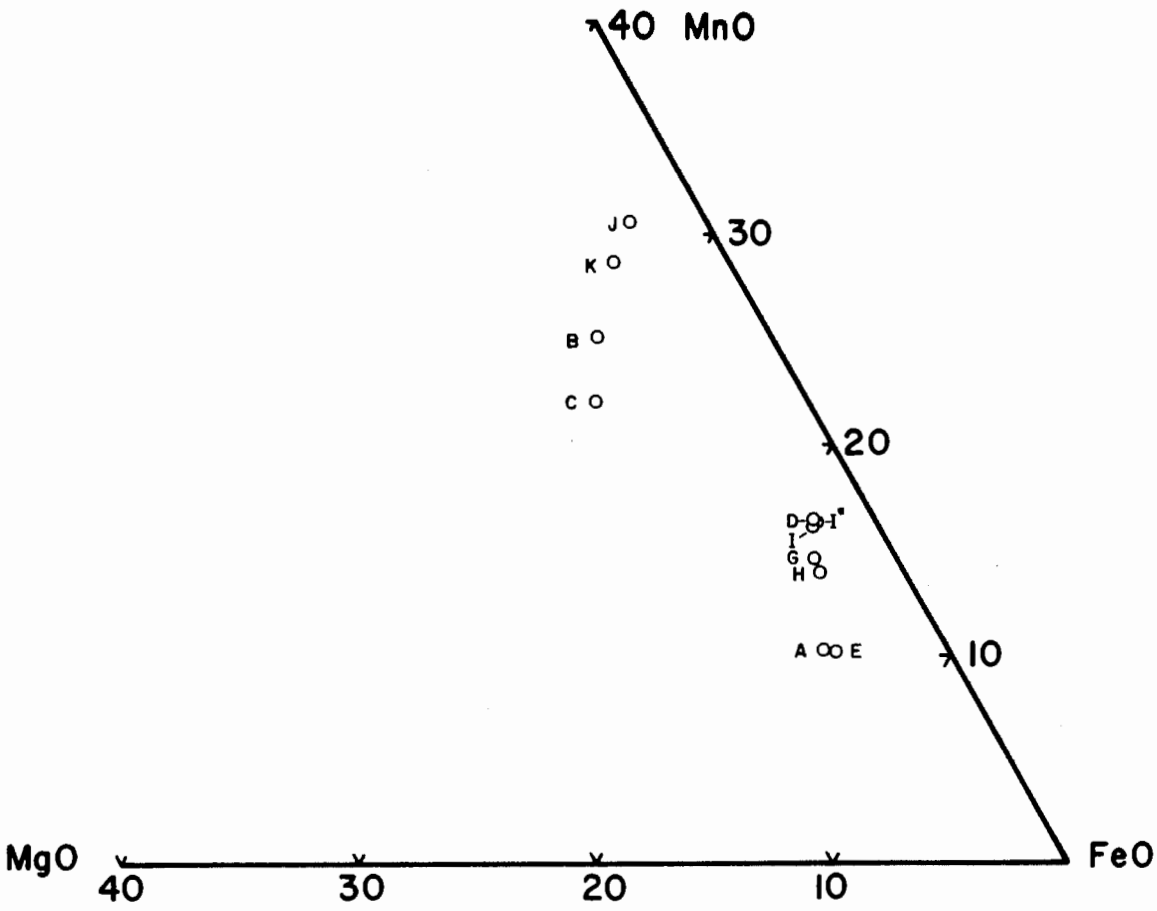

Figure 15. Olivine analyses plotted in terms of mole fraction MgO, FeO and MnO. Assemblage letters refer to analyses in Table 3.

Orthopyroxene

Indices of refraction for orthopyroxene from the vein in sample A22H2 were determined by H. W. Jaffe and are listed below along with other distinguishing optical properties.

γ : 1.770 ± 0.001	$2V_Z$ by visual estimate: 80-85° (+)
β : 1.759 ± 0.001	$2V_Z$ calculated with Mertie chart: 85° (+)
α : 1.750 ± 0.001	dispersion r > v
0.020 ± 0.002	color: tan
	cleavage: prismatic, well developed

Orthopyroxene microprobe analyses completed by A. E. Bence and R. J. Tracy are listed in Table 4 and are illustrated in Figures 16 and 17 in terms of MgO, FeO, MnO and CaO. The large $MnSiO_3$ component in

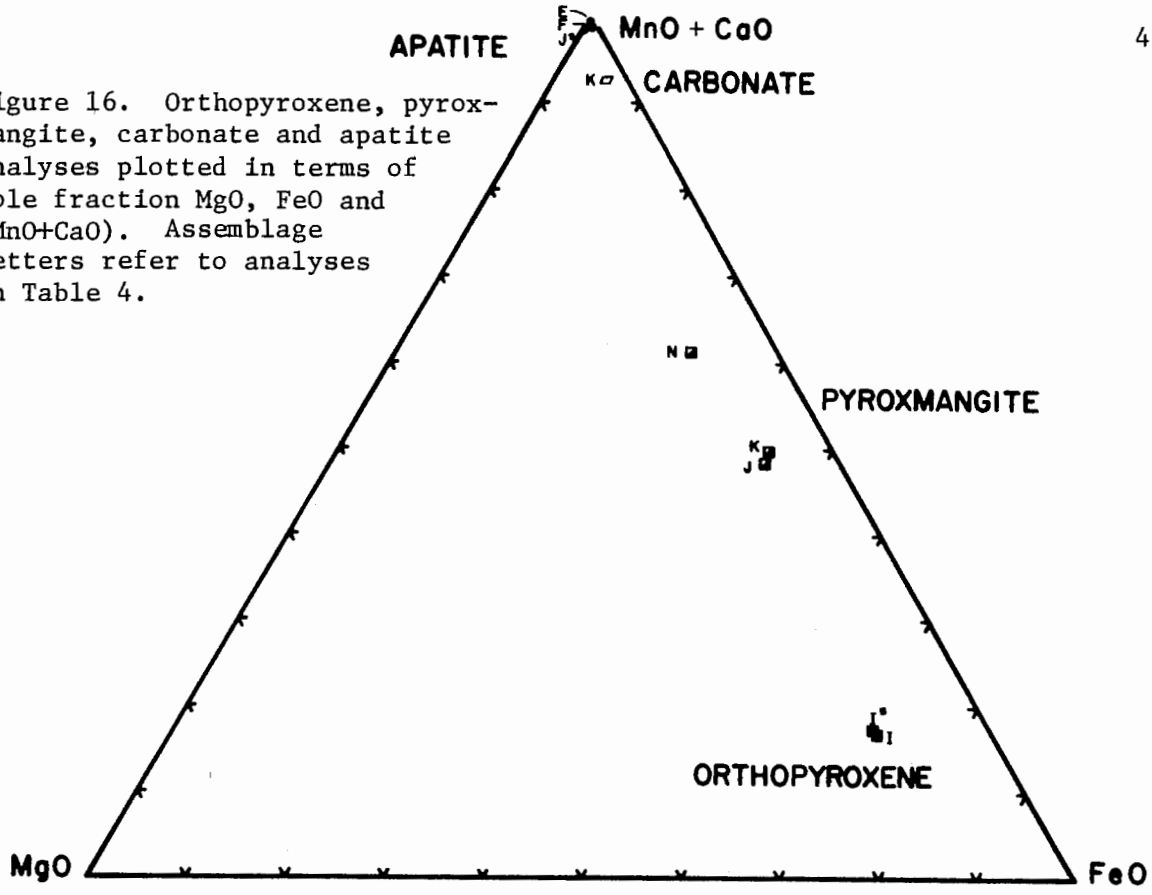

Figure 16. Orthopyroxene, pyroxmangite, carbonate and apatite analyses plotted in terms of mole fraction MgO, FeO and (MnO+CaO). Assemblage letters refer to analyses in Table 4.

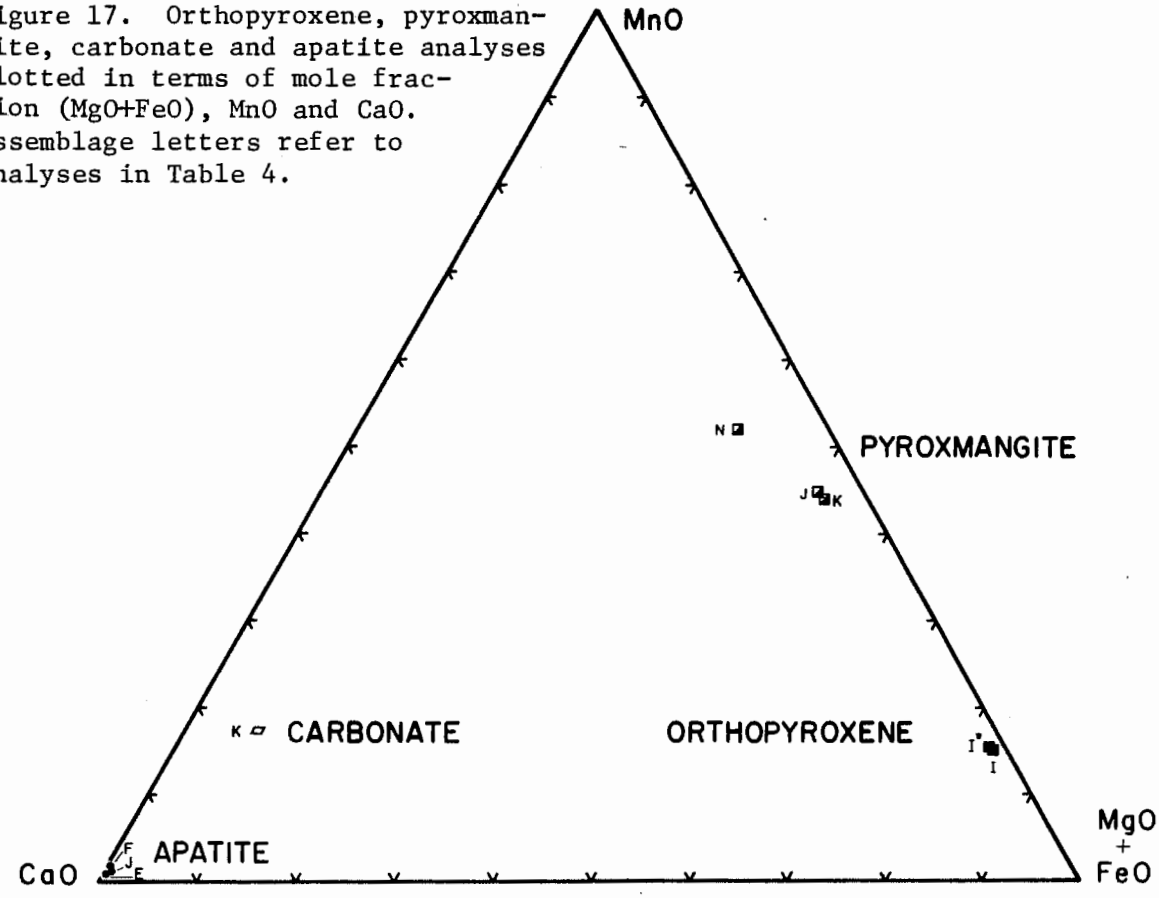

Figure 17. Orthopyroxene, pyroxmangite, carbonate and apatite analyses plotted in terms of mole fraction (MgO+FeO), MnO and CaO. Assemblage letters refer to analyses in Table 4.

Table 4. Electron probe analyses of orthopyroxene, pyroxmangite, carbonate and apatite.

	Orthopyroxene		Pyroxmangite		
Assemblage letter	I	I*	K	J	N
Sample	A22H2	A22H2	2J1-16b	2J1-12	6I2
SiO_2	46.44	47.70	45.90	46.77	47.89
TiO_2	.11	.07	.00	.00	.00
Al_2O_3	.11	.00	.04	.04	.02
Cr_2O_3	.06	.01	.00	.01	.05
FeO	39.68	39.65	24.10	24.17	16.33
MnO	8.27	8.56	23.88	24.49	28.35
MgO	3.69	3.79	2.30	2.07	2.76
CaO	.61	.72	1.94	2.09	4.02
Na_2O	.07	.00	.02	.01	.05
K_2O	.01	.00	.00	.00	.00
Total	99.05	100.50	98.18	99.65	99.47
	av. 2	av. 2	av. 5	av. 3	av. 3

* Analysts R. J. Tracy and A. E. Bence.

	Carbonate	Apatite			
	K	D	J	F	#
	2J1-16b	2J1-6	2J1-12	2J1-11	
FeO	3.73	.07	.59	.18	.32
MnO	12.13	.71	.80	1.20	.02
MgO	.89	.02	.02	.06	.05
CaO	41.85	53.50	55.24	53.11	55.08
Subtotal	58.60	54.30	56.65	54.55	55.47
P_2O_5	nd	nd	nd	nd	42.40
(OH,F,Cl)	nd	nd	nd	nd	2.81
CO_2¢	43	nd	nd	nd	nd
Total	101.60	54.30	56.65	54.55	100.68
	av. 4	1:1	1:1	1:1	

\# hydroxy-fluor-apatite (Deer, Howie and Zussman, 1971, p. 506).

¢ wt. % CO_2 calculated from mole fraction carbonate species.

nd not determined.

Formulas calculated on the basis of 6 oxygens.

	Orthopyroxene		Pyroxmangite		
	I	I*	K	J	N
Si	1.994	2.011	1.998	2.006	2.024
Al	.006		.002		
Total	2.000	2.011	2.000	2.006	2.024
Al				.002	
Ti	.004	.002			
Cr	.002				.002
Mg	.236	.238	.150	.132	.174
Fe	1.425	1.398	.878	.866	.578
Mn	.301	.306	.880	.890	1.014
Ca	.028	.033	.090	.096	.182
Na	.006		.002		.004
K	.001				
Total	2.003	1.977	2.000	1.986	1.954
$\frac{Fe}{Fe+Mn}$	.826	.820	.499	.494	.363
$\frac{Fe}{Mg+Fe}$	.857	.854	.854	.868	.769
$\frac{Ca}{Mg+Fe+Mn+Ca}$	.014	.017	.045	.048	.093

Mole fraction Mg, Fe, Mn and Ca in iron-rich samples based on 1 cation in carbonate and on 5 cations in apatite.

	Carbonate	Apatite			
	K	D	J	F	#
Mg	.022	.002	.002	.007	.006
Fe	.052	.005	.041	.013	.023
Mn	.173	.052	.056	.088	.002
Ca	.753	4.941	4.901	4.892	4.944
Total	1.000	5.000	5.000	5.000	4.975
$\frac{Ca}{Mn+Ca}$	.813	.990	.989	.982	.999
$\frac{Fe}{Fe+Mn}$	.231	.088	.423	.129	.920

\# hydroxy-fluor-apatite (Deer, Howie and Zussman, 1971, p. 506).

orthopyroxene from assemblage I (Figure 17) has a significant effect on the En composition derived from the optical plot of Hess (1952). The En composition derived from the γ index of refraction is 15.4±0.8 mole percent in comparison to 12.0 mole percent determined by microprobe analysis. The difference in En values may be logically explained by crystal-chemical changes in orthopyroxene resulting from substitution of a larger, less dense cation, Mn^{+2}, for a smaller more dense cation, Fe^{+2}. The effect of this substitution is to lower both the density and, by the rule of Gladstone and Dale, the index of refraction. As a result, En values derived from the γ index of refraction and the optical plot of Hess (1952) are high.

Pyroxmangite

Pyroxmangite was tentatively identified in thin section in samples 2J1-15 and 6I2. It was subsequently confirmed using powder X-ray photographs. Diagnostic properties observed in thin section include:

$2V_Z$: 40° (+)
dispersion r > v, weak
colorless
cleavage: prismatic, excellent
relief: greater than grunerite, less than olivine and garnet

Results of Debye-Scherrer X-ray data used to confirm the identity of pyroxmangite in samples 2J1-15 and 6I2 are listed in Table 5 with pyroxmangite from Ajiro mine, Japan (Perutz, 1937). All X-ray data were obtained using FeK_α radiation with a Mn filter. Sample 2J1-15 exhibits a strong grunerite d-spacing of 8.18 Å, which results from small grunerite grains in the host pyroxmangite.

Pyroxmangite analyses are listed in Table 4. Pyroxmangite from assemblage N is significantly more Ca- and Mn-rich than pyroxmangite

Table 5. Debye-Scherrer X-ray powder data for pyroxmangite in samples 6I2 and 2J1-15 compared with data from Ajiro Mine, Japan (Perutz, 1937). All data obtained using Mn-filtered Fe K_α radiation.

Sample 6I2		Sample 2J1-15		Ajiro Mine, Japan	
I	d Å	I	d Å	I	d Å
		10	8.18		
				5	6.84
<10	6.52	10	6.59	5	6.56
				2	4.80
10	4.68	10	4.60	10	4.68
<10	4.22			2	4.22
				5	3.68
				5	3.55
10	3.45	<10	3.38	15	3.44
				10	3.34
20	3.31	<10	3.27	5	3.30
				2	3.22
		20	3.14	15	3.18
30	3.10	20	3.08	60	3.12
				15	3.03
10	3.00			15	2.99
100	2.94	100	2.94	100	2.95
				10	2.87
				10	2.82
80	2.67	80	2.66	50	2.67
10	2.62			40	2.63
10	2.58			40	2.60
10	2.50			5	2.51
				15	2.49
10	2.44			15	2.44
<10	2.28			2	2.28
				5	2.22
20	2.19			50	2.21
40	2.17	70	2.17	70	2.18
				2	2.15
<10	2.11	<10	2.09	20	2.12
				15	2.06
20	2.05	10	2.04	20	2.04
<10	1.97	<10	1.95	5	1.98
				5	1.94
<10	1.86	<10	1.85	5	1.87
				5	1.85
<10	1.81	<10	1.80	5	1.81
				5	1.76
20	1.71	30	1.69	15	1.72
20	1.69	30	1.66	10	1.70
10	1.67				
10	1.65				
10	1.57	10	1.56		
10	1.48				
20	1.41				

from assemblages J and K. This chemical relationship is illustrated in Figures 16 and 17, but X-ray data (Table 5) give little indication of this chemical difference.

Carbonate

Carbonate was identified in thin section by its characteristic high birefringence and uniaxial negative interference figure. No estimate of the carbonate chemistry could be made in thin section; however, the common association of carbonate with pyroxmangite suggested that it might contain moderate amounts of manganese. The microprobe analysis in Table 4 indicates that this is true. Carbonate analysis K indicates that the mineral contains 75.3% $CaCO_3$, 17.3% $MnCO_3$, 5.2% $FeCO_3$ and 2.2% $MgCO_3$ (Figure 17). It might be termed kutnahorite or manganoan calcite (Frondel and Bauer, 1955).

Apatite

Diagnostic optical properties of apatite observed in thin section include extremely low birefringence, uniaxial negative interference figure and annealed texture of 50-100 micron apatite grains. Indices of refraction for apatite from an apatite-rich bed in sample 2J1-6 are:

$$\omega = 1.647$$
$$\varepsilon = 1.640$$
$$\text{birefringence} = 0.007$$

These optical properties suggest a formula of $Ca(PO_4)_3(OH_{.9}F_{.1})$ (Deer, Howie and Zussman, 1971, p.507). Partial microprobe analyses of apatite from three different assemblages are listed in Table 4 with a natural hydroxy-fluor-apatite (Deer, Howie and Zussman, 1971) for comparison. Apatite analyses are plotted in Figures 16 and 17 in terms of MgO, FeO,

MnO and CaO. The substitution of FeO and MnO for CaO in the apatite is evident but very modest considering the high FeO and MnO and low CaO content of the rocks.

Cummingtonite-Grunerite

A member of the cummingtonite-grunerite series occurs in virtually all of the iron-rich granulites within the Littleton Formation. Diagnostic properties of the cummingtonite-grunerite series observed in thin section are listed below.

$2V_Z$: 80°(+) - 95°(-)
dispersion r > v
colorless to pale green
cleavage: prismatic, good
pleochroism: colorless to pale green in some samples
twinning: (100) lamellar

Up to this point in the text the mineral name grunerite has been used for members of the cummingtonite-grunerite series, and for the sake of brevity grunerite will continue to be used in this manner. However, Figure 18, a plot of probe analyses (Table 6), shows that six are grunerites in the strict sense (Jaffe et al., 1961; Klein, 1964), five are manganoan grunerites, and one is a manganoan cummingtonite.

Table 6. Electron probe analyses of cummingtonite-grunerite.

Assemblage letter	I	H	G	D	E	A	J	K	M	B	C	N
Sample	A22H2	A22H2	A22H2	2J1-6	2J1-6	2J1-6	2J1-12	2J1-16b	2J1-4	2J1-5	2J1-5	6I2
Notes	vein	wall rock	host gran.									
SiO_2	49.51	49.69	49.53	49.73	51.05	50.04	51.06	49.50	50.88	51.31	51.92	52.84
TiO_2	.06	.12	.05	.00	.05	.00	.00	.00	.00	.00	.00	.00
Al_2O_3	.09	.16	.20	.14	.07	.05	.03	.00	.14	.03	.05	.01
Cr_2O_3	.09	.09	.09	.00	.04	.00	.00	.00	.01	.00	.00	.00
FeO	38.22	37.69	36.86	35.87	37.09	35.95	30.09	29.84	34.58	25.82	25.68	20.45
MnO	5.35	4.54	4.76	4.96	3.27	3.54	9.35	9.15	3.10	6.89	7.21	11.35
MgO	4.45	5.38	6.11	6.28	7.57	7.61	6.45	7.38	9.03	12.12	12.34	11.87
CaO	.51	.43	.38	.10	.07	.06	.50	.44	.17	.16	.19	1.45
Na_2O	.04	.04	.09	.00	.01	.00	.00	.00	.00	.02	.01	.02
K_2O	.00	.00	.00	.00	.01	.00	.00	.00	.00	.00	.00	.00
Total	98.32	98.14	98.07	97.08	99.23	97.25	97.48	96.31	97.91	96.35	97.40	97.99
	av. 2	av. 2	av. 2	av. 2	av. 2	1:1	1:1	1:5	av. 2	1:1	1:1	av. 3

Formulas calculated on the basis of 15 cations exclusive of Na, K.

	I	H	G	D	E	A	J	K	M	B	C	N
Si	7.951	7.940	7.883	7.974	7.947	7.935	8.000	7.926	7.930	7.934	7.933	8.000
Al	.017	.030	.038	.026	.013	.013			.026	.005	.009	
Fe^{+3}	.032	.030	.079		.040	.052		.074	.044	.061	.058	
Total	8.000	8.000	8.000	8.000	8.000	8.000	8.000	8.000	8.000	8.000	8.000	8.000
Si							.119					.023
Al							.006					
Ti	.007	.014	.006		.006							
Cr	.011	.011	.011		.005				.001			
Fe^{+3}	.012	.006	.068	.024	.033	.064		.076	.069	.061	.064	
Mg	1.065	1.281	1.449	1.500	1.756	1.798	1.528	1.761	2.098	2.793	2.811	2.685
Fe^{+2}	3.905	3.688	3.466	3.476	3.200	3.138	3.347	3.163	2.832	2.146	2.125	2.292
Total	5.000	5.000	5.000	5.000	5.000	5.000	5.000	5.000	5.000	5.000	5.000	5.000
Fe^{+2}	1.185	1.311	1.293	1.309	1.557	1.514	.655	.683	1.563	1.070	1.035	.304
Mn	.727	.615	.642	.674	.431	.476	1.260	1.241	.409	.903	.934	1.460
Ca	.088	.074	.065	.017	.012	.010	.085	.076	.028	.027	.031	.236
Total	2.000	2.000	2.000	2.000	2.000	2.000	2.000	2.000	2.000	2.000	2.000	2.000
Na	.012	.012	.028		.003					.006	.003	.006
K					.002							
Total	.012	.012	.028		.005					.006	.003	.006
$\frac{Fe}{Mg+Fe}$	.828	.797	.772	.762	.733	.726	.724	.694	.682	.545	.539	.491
$\frac{Fe}{Fe+Mn}$	.876	.891	.884	.877	.918	.909	.761	.764	.917	.787	.779	.640
$\frac{Ca}{Mg+Fe+Mn+Ca}$	.013	.011	.009	.002	.002	.001	.012	.011	.004	.004	.004	.034

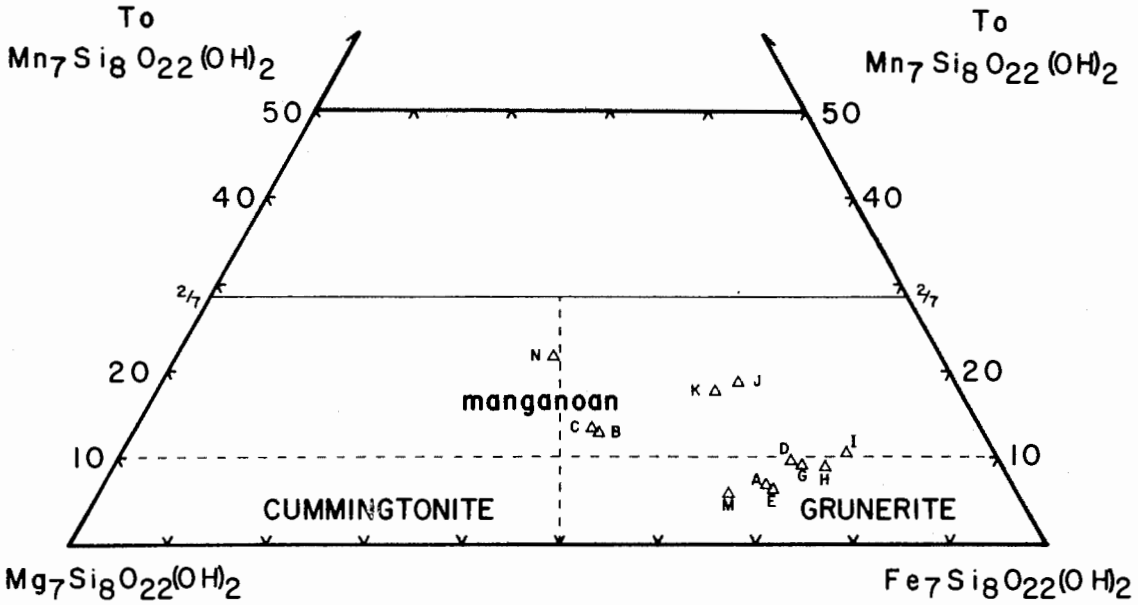

Figure 18. Cummingtonite-grunerite analyses plotted in terms of $Mg_7Si_8O_{22}(OH)_2$, $Fe_7Si_8O_{22}(OH)_2$, and $Mn_7Si_8O_{22}(OH)_2$. Classification suggested by C. Klein (1964). Assemblage letters refer to analyses in Table 6.

Garnet

Garnet occurs in all iron-rich rocks sampled. Diagnostic optical properties used to identify garnet in thin section include the isotropic character of all grains, high optical relief, and common occurrence of inclusions. Garnet may be colorless to medium pink. Microprobe analyses from sample 2J1-4, assemblage L (Table 7) indicate that garnet is unzoned from core to rim with respect to major element chemistry. Garnet microprobe analyses are plotted in Figures 19 and 20 in terms of MgO, FeO, MnO and CaO. The garnets are essentially almandine-spessartine garnets with almandine ranging from 22 to 64% and spessartine from 25 to 64%. Grossular ranges from 4 to 17% and is generally highest in the most spessartine-rich samples. Pyrope ranges from 1 to 7% and is generally highest in the most almandine-rich varieties.

Figure 19. Garnet analyses plotted in terms of mole fraction MgO, FeO and (MnO+CaO). Assemblage letters refer to analyses in Table 7.

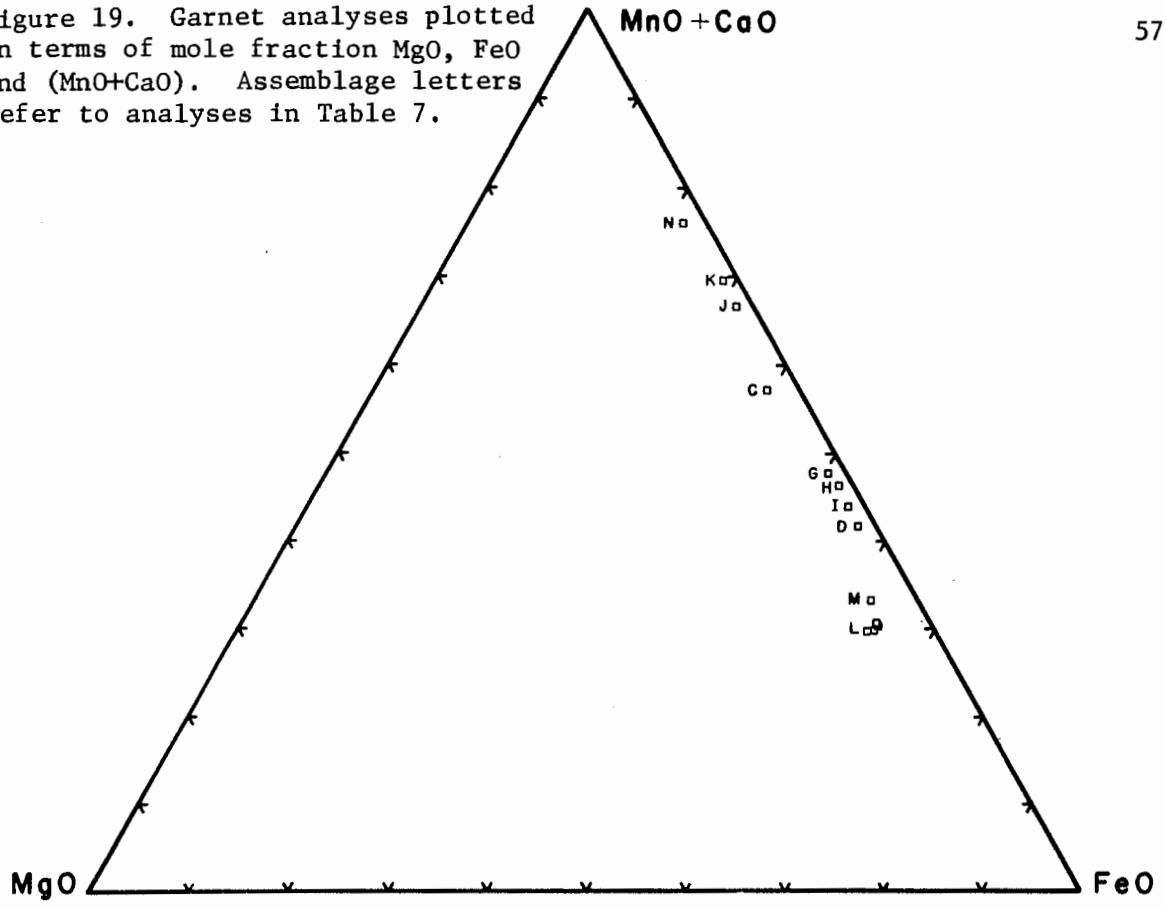

Figure 20. Garnet analyses plotted in terms of mole fraction (MgO+FeO), MnO and CaO. Assemblage letters refer to analyses in Table 7.

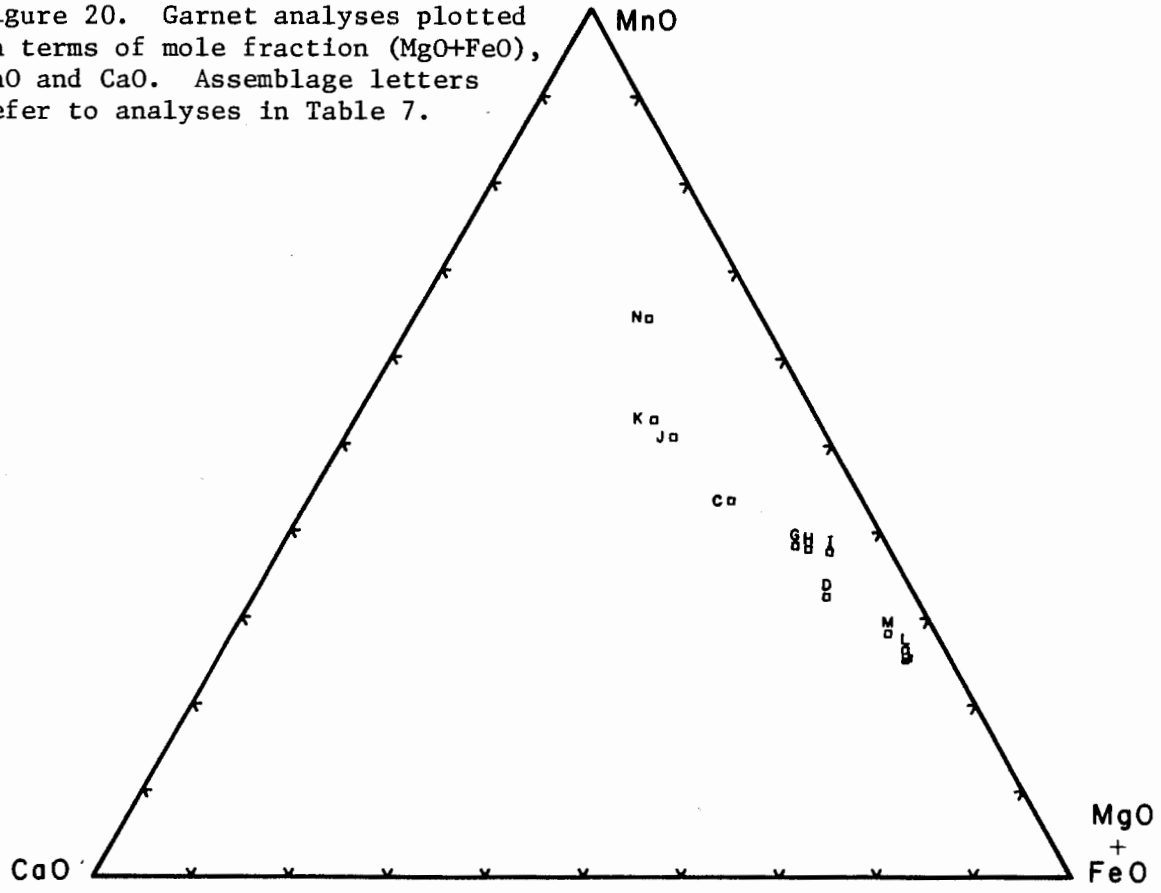

Table 7. Electron probe analyses of garnet.

Assemblage letter	L	L	L	L	M	D	I	H	G	C	J	K	N
Sample	2J1-4	2J1-4	2J1-4	2J1-4	2J1-4	2J1-6	A22H2	A22H2	A22H2	2J1-5	2J1-12	2J1-16b	6I2
Notes	core	inside halo	halo	rim			vein	wall rock	host gran.				
SiO_2	37.38	37.11	36.71	37.31	37.25	36.78	36.38	36.40	36.78	36.61	37.47	36.46	37.94
TiO_2	.00	.03	.03	.00	.02	.00	.11	.06	.07	.00	.00	.00	.05
Al_2O_3	20.05	20.30	20.76	20.63	20.12	19.97	19.53	19.75	19.18	20.74	18.31	20.18	19.59
Cr_2O_3	.00	.01	.00	.03	.02	.00	.08	.08	.09	.00	.00	.00	.05
FeO	28.04	28.17	27.75	28.01	27.12	24.34	23.58	22.55	22.02	17.37	14.18	12.91	9.51
MnO	10.86	11.06	11.05	11.32	12.18	13.87	16.13	16.24	16.60	18.87	22.60	23.41	28.01
MgO	1.50	1.38	1.68	1.39	1.16	.46	.40	.33	.45	.84	.43	.38	.56
CaO	1.63	1.61	1.47	1.46	1.71	3.10	2.17	2.87	3.22	4.69	5.59	5.85	4.01
Na_2O	.02	.12	.11	.04	.00	.00	.05	.02	.03	.05	.00	.00	.02
K_2O	.00	.00	.00	.00	.00	.00	.00	.02	.01	.00	.00	.00	.00
Total	98.48	99.79	99.56	100.19	99.58	98.52	98.43	98.32	98.45	99.17	98.58	99.19	99.74
	1:1	1:1	1:1	1:1	av. 2	av. 2	av. 2	av. 2	av. 2	1:1	1:1	1:5	1:1

Formulas calculated on the basis of 12 oxygens.

	L	L	L	L	M	D	I	H	G	C	J	K	N
Si	3.054	3.029	2.998	3.029	3.047	3.044	3.034	3.031	3.058	2.994	3.102	2.995	3.087
Al			.002							.006		.005	
Total	3.054	3.029	3.000	3.029	3.047	3.044	3.034	3.031	3.058	3.000	3.102	3.000	3.087
Al	1.931	1.954	1.997	1.974	1.940	1.949	1.920	1.939	1.880	1.994	1.787	1.950	1.879
Cr		.001		.002	.001		.005	.005	.006				.001
Ti		.002	.002		.001		.007	.004	.004				.003
Total	1.931	1.957	1.999	1.976	1.942	1.949	1.932	1.948	1.890	1.994	1.787	1.950	1.883
Mg	.183	.168	.204	.168	.141	.057	.050	.041	.056	.102	.053	.047	.068
Fe	1.916	1.923	1.895	1.902	1.855	1.685	1.644	1.570	1.531	1.188	.982	.887	.647
Mn	.752	.765	.764	.778	.844	.972	1.139	1.145	1.169	1.307	1.585	1.629	1.930
Ca	.143	.141	.129	.127	.150	.275	.194	.256	.287	.411	.496	.515	.350
Na	.003	.019	.017	.006			.008	.003	.005	.008			.003
K								.002	.001				
Total	2.997	3.016	3.009	2.981	2.990	2.989	3.035	3.017	3.049	3.016	3.116	3.078	2.998
Alm.	.640	.642	.633	.639	.620	.564	.543	.522	.503	.395	.315	.288	.216
Spes.	.251	.255	.255	.262	.282	.325	.376	.380	.384	.435	.508	.529	.644
Gros.	.048	.047	.044	.043	.051	.092	.064	.084	.095	.136	.160	.168	.117
Pyr.	.061	.056	.068	.056	.047	.019	.017	.014	.018	.034	.017	.015	.023

Biotite and Muscovite

Biotite is present in rusty-weathering schist at localities 2J1, 3J4, and in garnet-biotite granulite at "Iron Ridge." Biotite from the rusty-weathering schist is pale greenish-brown with strong pleochroism from pale greenish-brown to dark brown. $2V_X$ is close to 0°.

Muscovite, which is present with biotite in the rusty-weathering schist, is colorless. No chemical analyses were made of biotite or muscovite.

Opaque Minerals

Optical examination of opaque minerals was made using polished thin sections in conjunction with a reflected light illuminator and oil immersion objectives. Diagnostic optical properties for magnetite, ilmenite, graphite, pyrrhotite, marcasite and chalcopyrite are listed in Table 8 for ease of comparison.

Graphite. Graphite occurs in only very minor amounts in some beds of the iron-rich rocks, but even small quantities of graphite will produce a large buffering effect with respect to changes in the composition of the gas phase during metamorphism (French, 1966). Consequently, careful petrographic work was performed to ascertain which mineral assemblages actually contain graphite. Diagnostic optical properties of graphite include:

birefringence: strong, bronze to dark brown
anisotropy: yellow to dark brown
reflectivity: low, approximately 10%
polishing hardness: low, less than other minerals present.

The optical identification of graphite was confirmed by Debye-Scherrer X-ray powder photographs in sample 2J1-6.

Table 8. Optical properties of opaque phases observed in polished thin section.

	COLOR	BIREFLECTANCE	ANISOTROPY	REFLECTIVITY	POLISHING HARDNESS
Magnetite	gray	none	none	low to intermediate 20%	high > ilmenite
Ilmenite	light to dark brown	distinct: light pinkish brown to dark brown	light to dark gray	low to intermediate 20%	moderate < magnetite
Graphite	bronze	strong: bronze to dark brown	yellow to dark brown	low 10%	low < other minerals present
Pyrrhotite	cream with light brown tint	distinct: cream to pinkish brown cream	cream to grayish blue	intermediate to high 40%	moderate < ilmenite
Marcasite	yellowish white	yellowish white to yellow with greenish tint	blue to light brown	intermediate to high 50%	moderate > pyrrhotite
Chalcopyrite	brassy yellow	none	bluish gray to greenish gray	intermediate 40%	low to moderate < pyrrhotite

Magnetite. Optical properties of magnetite in polished thin section include:

color: gray
bireflectance: none
anisotropy: none
reflectivity: low to intermediate, approximately 20%
polishing hardness: high, greater than ilmenite.

Magnetite is an abundant phase in many of the iron-rich beds and occurs in different textural forms as discussed above, but it exhibits very little variation in chemistry from bed to bed in the iron-rich units as is shown by the microprobe analyses (Table 9). The magnetites analyzed closely approach the ideal Fe_3O_4 end member.

Ilmenite. Ilmenite occurs in minor amounts within some of the iron-rich rocks. Its diagnostic optical properties include:

color: light to dark brown
bireflectance: distinct, light pinkish-brown to dark brown
anisotropy: light to dark gray
reflectivity: low to intermediate, approximately 20%
polishing hardness: moderate, less than magnetite.

Unlike magnetite, ilmenite exhibits a range of chemistry with respect to FeO/FeO+MnO ratio (Table 10, Figure 21). Ilmenite is enriched in MnO relative to coexisting magnetite in the iron-rich beds. D. Rumble (1973) noted a similar MnO enrichment in ilmenite from coexisting magnetite-ilmenite assemblages in regionally metamorphosed quartzites from western New Hampshire.

Because ilmenite is sensitive to iron and manganese chemistry, it may be used to test for complete equilibration of minerals in ilmenite-bearing assemblages. Ilmenite occurs interstitially and as inclusions in garnet and grunerite in sample 2J1-4 (Figure 22). It is questionable

Table 9. Electron probe analyses of magnetite.

Assemblage letter	D	A	E	F	H	G
Sample	2J1-6	2J1-6	2J1-6	2J1-11	A22H2	A22H2
Notes					wall rock	host gran.
SiO_2	.23	1.11	.25	.13	.57	.57
TiO_2	.41	.11	.83	.55	.27	.63
Al_2O_3	.15	.14	.22	.10	.18	.23
Cr_2O_3	.16	.04	.08	.18	.21	.15
Fe_2O_3¢	66.53	65.22	65.88	67.80	65.89	65.43
FeO	30.98	32.02	31.51	31.38	30.95	31.28
MnO	.21	.18	.29	.47	.45	.58
MgO	.06	.02	.05	.02	.13	.12
CaO	.08	.06	.03	.05	.07	.07
Total	98.81	98.90	99.14	100.68	98.72	99.06
	1:1	1:1	av. 3	1:1	1:1	1:2
Formulas calculated on the basis of 3 cations.						
Si	.009	.043	.010	.005	.022	.022
Ti	.012	.003	.024	.016	.008	.018
Al	.007	.006	.010	.005	.008	.010
Cr	.005	.001	.002	.005	.006	.005
Fe^{+3}	1.946	1.900	1.920	1.949	1.925	1.904
Total	1.979	1.953	1.966	1.980	1.969	1.959
Mg	.003	.001	.003	.001	.008	.007
Fe^{+2}	1.007	1.037	1.020	1.002	1.005	1.012
Mn	.007	.006	.010	.015	.015	.019
Ca	.003	.002	.001	.002	.003	.003
Total	1.020	1.046	1.034	1.020	1.031	1.041
$\frac{Fe}{Fe+Mn}$	.993	.992	.990	.985	.985	.982

¢ Ferric correction after L. Finger (1971).

Table 10. Electron probe analyses of ilmenite.

Assemblage letter	H	G	M	M	M	J	F	K	K	K
Sample	A22H2	A22H2	2J1-4	2J1-4	2J1-4	2J1-12	2J1-11	2J1-16b	2J1-16b	2J1-16b
Notes	wall rock	host gran.	in grun.	inter-stitial	in gar.					
SiO_2	.30	.74	.37	.14	.44	.25	.14	.20	.23	.35
TiO_2	51.08	51.23	53.68	52.51	52.96	51.34	51.11	51.45	52.09	51.87
Al_2O_3	.09	.09	.05	.06	.18	.07	.04	.13	.18	.18
Cr_2O_3	.17	.13	.05	.08	.05	.00	.01	.00	.00	.08
Fe_2O_3 ç	2.22	1.42	np	np	np	1.01	.17	1.16	.16	.40
FeO	40.19	40.56	40.72	38.55	38.18	33.07	30.57	28.37	25.66	25.47
MnO	5.77	5.89	6.45	8.39	8.80	13.02	15.09	17.23	21.00	21.04
MgO	.09	.19	.09	.03	.02	.09	.03	.09	.06	.11
CaO	.08	.07	.07	.07	.10	.04	.17	.41	.06	.07
Total	99.99	100.32	101.48	99.83	100.73	98.89	97.33	99.04	99.44	99.57
	1:2	1:1	1:1	1:1	1:1	1:1	1:1	1:1	1:1	1:1

ç Ferric correction after L. Finger (1971).

np No ferric iron predicted from ferric iron correction.

Formulas calculated on the basis of 2 cations.

	H	G	M	M	M	J	F	K	K	K
Si	.008	.019	.009	.004	.011	.006	.004	.005	.006	.009
Ti	.968	.965	1.002	.997	.995	.983	.994	.982	.990	.984
Al	.003	.003	.001	.002	.005	.002	.001	.004	.005	.005
Cr	.003	.003	.001	.002	.001					.002
Fe^{+3}	.042	.027				.019	.003	.022	.003	.008
Total	1.024	1.017	1.013	1.005	1.012	1.010	1.002	1.013	1.004	1.008
Mg	.003	.007	.003	.001	.001	.003	.001	.003	.002	.004
Fe^{+2}	.847	.850	.845	.814	.798	.704	.661	.602	.542	.537
Mn	.123	.125	.136	.179	.186	.281	.331	.370	.450	.449
Ca	.002	.002	.002	.002	.003	.001	.005	.011	.002	.002
Total	.975	.984	.986	.996	.988	.989	.998	.986	.996	.992
$\frac{Fe}{Fe+Mn}$	.873	.872	.861	.820	.811	.715	.666	.619	.546	.545

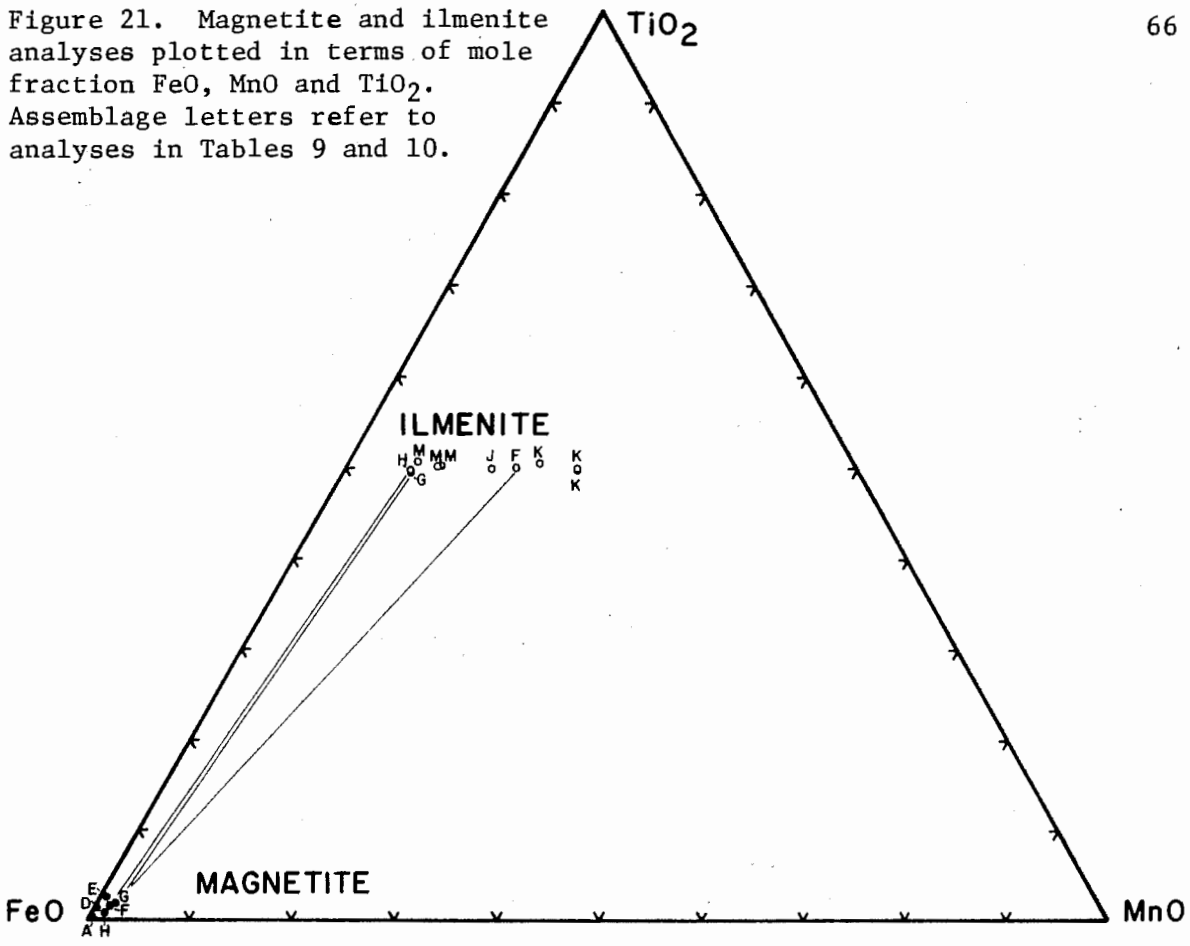

Figure 21. Magnetite and ilmenite analyses plotted in terms of mole fraction FeO, MnO and TiO_2. Assemblage letters refer to analyses in Tables 9 and 10.

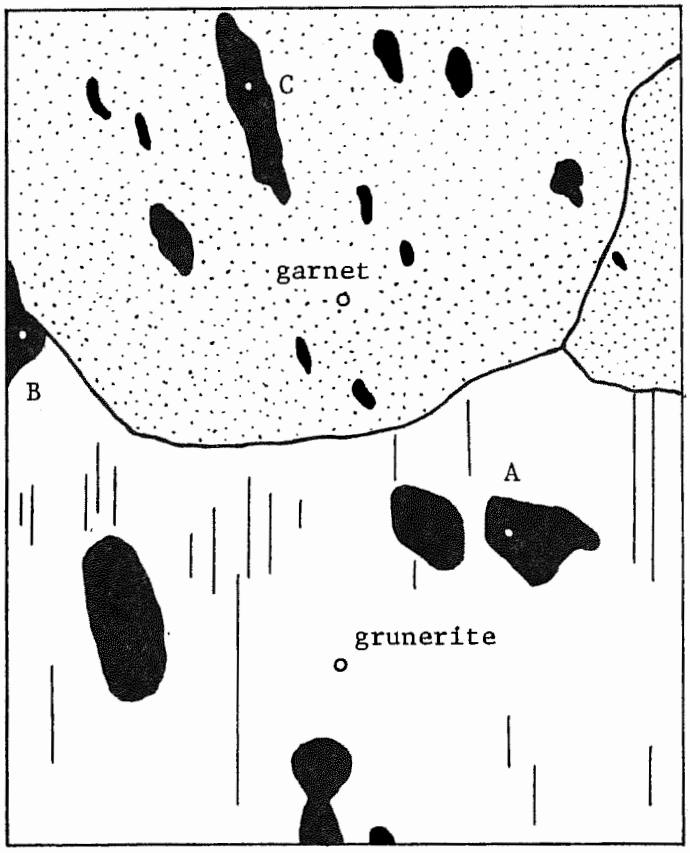

Figure 22. Diagram of mineral assemblage M, sample 2J1-4, quartz (not shown)-garnet-grunerite-ilmenite. Microprobe analysis points for garnet, grunerite and ilmenite grains are shown by small circles.

whether or not ilmenite inclusions are in equilibrium with other minerals in the assemblage beside the host mineral. Microprobe analysis points of ilmenite in assemblage M, sample 2J1-4, are illustrated in Figure 22. Grain A is an inclusion in grunerite. Grain B occurs interstitially and is associated with both grunerite and garnet. Grain C is an inclusion in garnet. Microprobe analyses indicate that grain C is enriched in MnO and depleted in FeO relative to grain A. Grain B has FeO and MnO values intermediate between grains A and C. In this specific example one may cautiously assume that the interstitial grain equilibrated with both garnet and grunerite. Ilmenite grains are generally much smaller than associated silicate phases and thus it is difficult to prove that equilibrium is achieved between any single ilmenite grain and all other associated phases. Similar heterogeneous MnO and FeO values for ilmenite are present in assemblage K, sample 2J1-16. Thus, in these two assemblages, local disequilibrium among small ilmenite grains is apparent.

Pyrrhotite and Marcasite. Pyrrhotite and marcasite are commonly associated with each other in the iron-rich rocks. Their diagnostic optical properties include:

	Pyrrhotite	Marcasite
Color:	cream with light brown tint	yellowish white
Bireflectance:	distinct, cream to pinkish-brown cream	yellowish-white to yellow with greenish tint
Anisotropy:	cream to grayish-blue	blue to light brown
Reflectivity:	intermediate to high, 40%	intermediate to high, 50%
Polishing hardness:	moderate, less than ilmenite	moderate, greater than pyrrhotite.

Color and anisotropy contrast between these two phases is pronounced and it is especially useful for identification purposes.

Chalcopyrite. Chalcopyrite is associated with pyrrhotite and marcasite in the vein of sample 2J1-14. It also occurs rarely as inclusions in magnetite. The diagnostic optical properties of chalcopyrite include:

Color: brassy yellow
Bireflectance: none
Anisotropy: bluish-gray to greenish-gray
Reflectivity: intermediate to high, 40%
Polishing hardness: low to moderate, less than pyrrhotite.

No chemical data were obtained for sulfide phases.

CHEMOGRAPHIC RELATIONS

The graphical analysis of chemical data presented should provide a basic understanding of the mineral chemistry and phase relations in the iron-rich units of the Littleton Formation. The first part of this section deals primarily with the development of a chemical model for many of the important iron-rich minerals observed in the Littleton Formation, using the graphical approach of J. B. Thompson (1972). In conjunction with this, gas phase chemistry in the system C-O-H is discussed briefly, because a C-O-H gas phase is commonly associated with the metamorphism of carbonaceous iron-rich sediments. After the chemical model is presented, ternary diagrams are used to illustrate the chemistry of coexisting mineral phases and to give a general idea of the major element partitioning between iron-manganese rich silicates and oxides under sillimanite-muscovite grade metamorphic conditions.

The components used to model the iron-rich lenses of the Littleton Formation are Fe-C-O-H-MgO-(MnO+CaO)-SiO_2. These permit graphical representation of the minerals olivine, orthopyroxene, pyroxmangite, grunerite, kutnahorite, quartz and magnetite plus graphite in a tetrahedron, assuming the presence of a C-O-H gas phase. Although CaO has been combined with MnO in the list of components above, it forms only a small fraction of the mineral chemistry of olivine, orthopyroxene, pyroxmangite and grunerite. Therefore, the addition of CaO to the MnO apex does not radically alter the topologic relations for these four minerals. By contrast, CaO forms a large part of the chemistry of kutnahorite, and as a result, CaO is critically important to the graphical position of this mineral.

Garnet and ilmenite are common minerals in the iron-rich rocks; but, since they are the only minerals with significant Al_2O_3 and TiO_2 respectively, it is most convenient to omit them at first from the chemical model. Garnet and ilmenite chemistry and its relationship to other coexisting minerals is discussed at the end of this section. Other minerals from Table 2 that have not been included in the chemical model are apatite and pyrrhotite for which the components P_2O_5 and S, respectively, would have to be added.

The Chemical Model

To begin the development of the chemical model in the system Fe-C-O-H-MgO-(MnO+CaO)-SiO_2, consider first the two sub-systems Fe-C-O and Fe-H-O (Figures 23 and 24) plotted in terms of FeO-Fe_2O_3-CO_2 and FeO-Fe_2O_3-H_2O, respectively. These systems can be combined along the (-O)-Fe_2O_3 composition join to produce the four component system Fe-C-O-H (Figure 25) plotted in terms of FeO, Fe_2O_3, H_2O, and CO_2. As interpreted by French (1966) from the data obtained by Dayhoff et al. (1964), the significant gas species in the system C-O-H are CO_2, CO, H_2O, H_2, CH_4 and O_2. French (1966) does not consider complex organic compounds in the C-O-H gas phase because 1) the gas species noted above compose almost the entire gas pressure, and 2) the partial pressure of CH_4 greatly exceeds that of the more complex organic compounds. These petrologically important gas species, which exist as one or possibly two gas phases, are illustrated in the system Fe-C-O-H along with the important minerals graphite, siderite, magnetite, and goethite (Figure 25).

In Figure 25 the C-O-H gas phase compositions lie entirely in the upper left face of the tetrahedron defined by H_2O, CO_2 and (-O). The gas composition field is limited in the corner near C by graphite

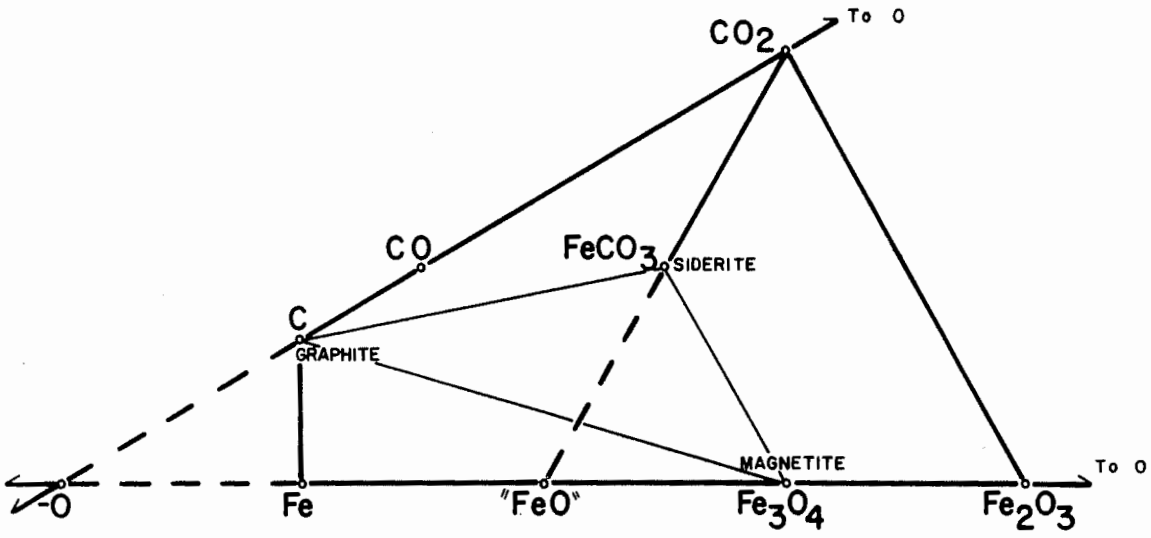

Figure 23. The system Fe-C-O plotted in terms of mole units FeO, Fe_2O_3 and CO_2 after Thompson (1972) with important minerals and gas species illustrated. Tie lines connect graphite-magnetite-siderite for temperatures up to 465° C at 2 kbar pressure (French, 1971).

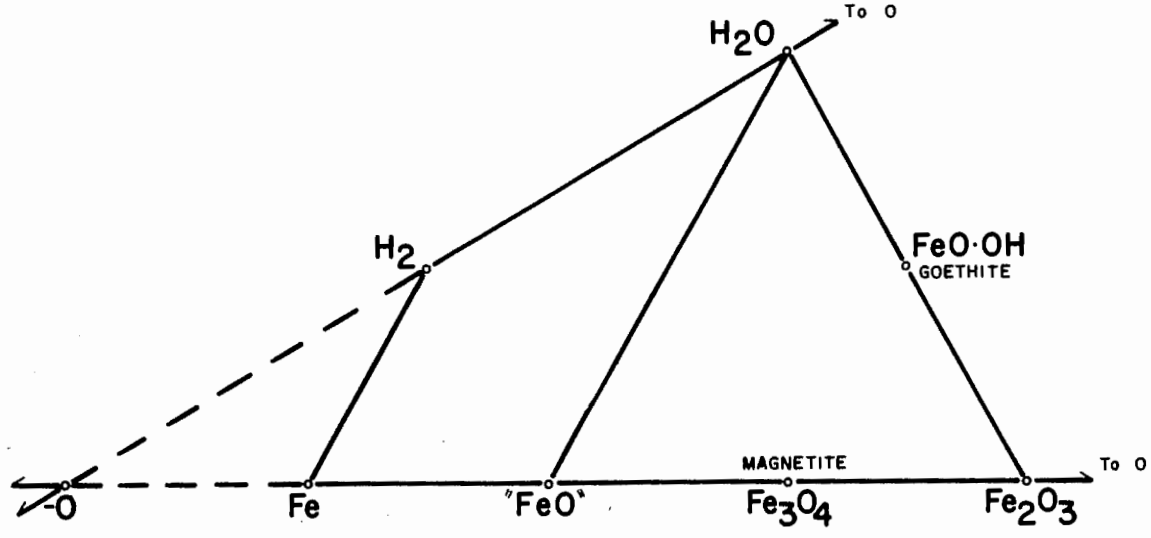

Figure 24. The system Fe-H-O plotted in terms of mole units FeO, Fe_2O_3 and H_2O after Thompson (1972) with important minerals and gas species illustrated.

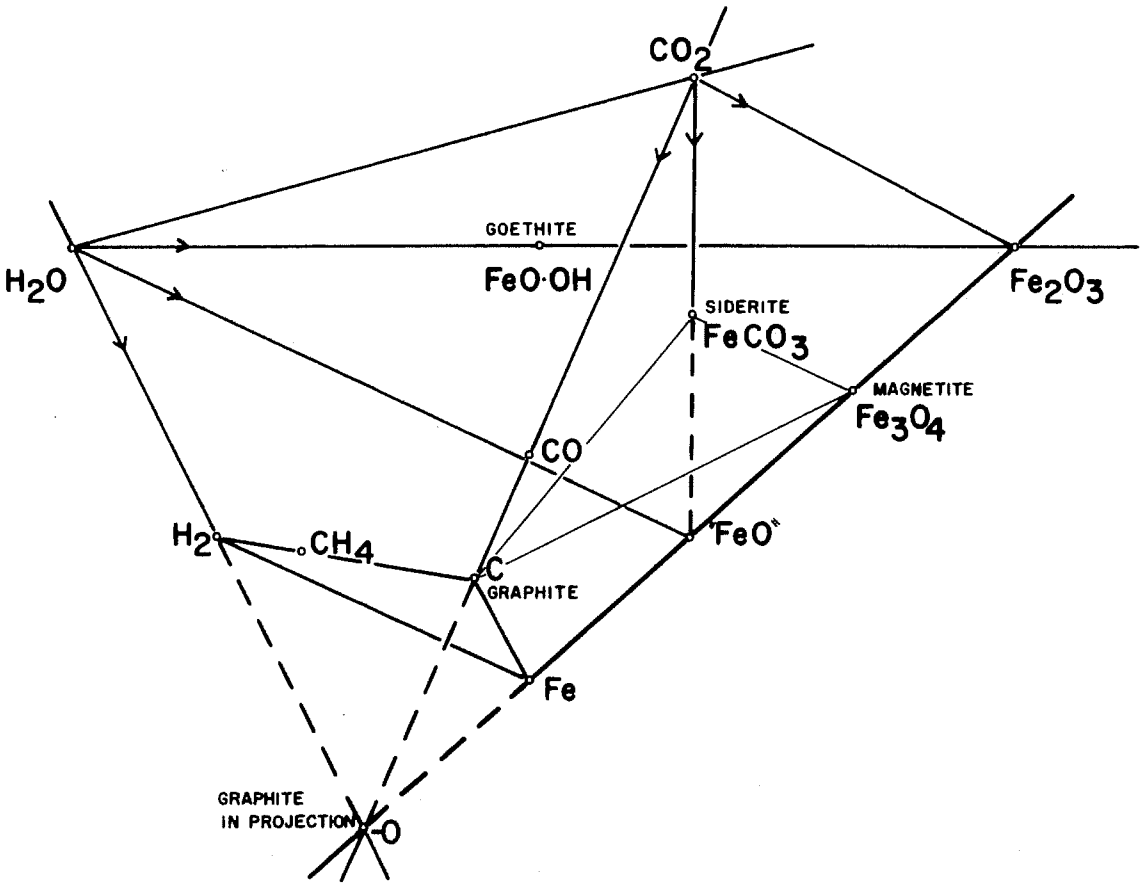

Figure 25. The system Fe-C-O-H after Thompson (1972) with important minerals and gas species illustrated. Heavy black line, the join (-O)-Fe_2O_3, is the composition coordinate for the system Fe-C-O-H as a function of temperature, pressure and activities of CO_2 and H_2O. This plot is in mole units FeO and Fe_2O_3.

saturation. Any C-O-H gas composition can be completely described by the ratio between the components H_2O and CO_2 and the oxygen fugacity. At constant pressure and temperature and arbitrarily chosen C-O-H gas composition, only one solid Fe phase would be expected in the system. If on the other hand, oxygen fugacity is buffered by two coexisting solid Fe phases, then the C-O-H gas composition is entirely a function of the H_2O/CO_2 ratio. This is also true when the gas coexists with graphite. In such cases H_2O and CO_2 may be considered as the only perfectly mobile components, and all other phases are projected onto the extended line through (-O)-Fe_2O_3, as shown in Figure 25.

Because graphite occurs in several of the observed mineral assemblages in the iron-rich lenses it is permissible to project from graphite along the line toward Fe_2O_3 such that all constituents project to a single point labelled "FeO". Three additional components, MgO, (MnO+CaO) and SiO_2, may now be added to the model to form a tetrahedron. It should be emphasized that the FeO apex of this tetrahedron represents the components Fe-C-O-H and the phases graphite, siderite, magnetite and a C-O-H gas.

Due to the presence of graphite in the iron-rich lithologies, Fe_2O_3 (hematite) and Mn_3O_4 (hausmanite) do not exist as stable phases at moderate to high grade metamorphic conditions. Magnetite, a ferric iron-bearing mineral, is stable in the presence of graphite over a moderately large range of geologic conditions; however, fO_2 values for graphite-buffered assemblages lie below the MnO/Mn_3O_4 buffer curve (Figure 26), indicating that trivalent manganese is unstable. Therefore, in the presence of graphite all manganese in the chemical model will exist as Mn^{+2}, whereas iron may exist as Fe^{+2} or Fe^{+3}.

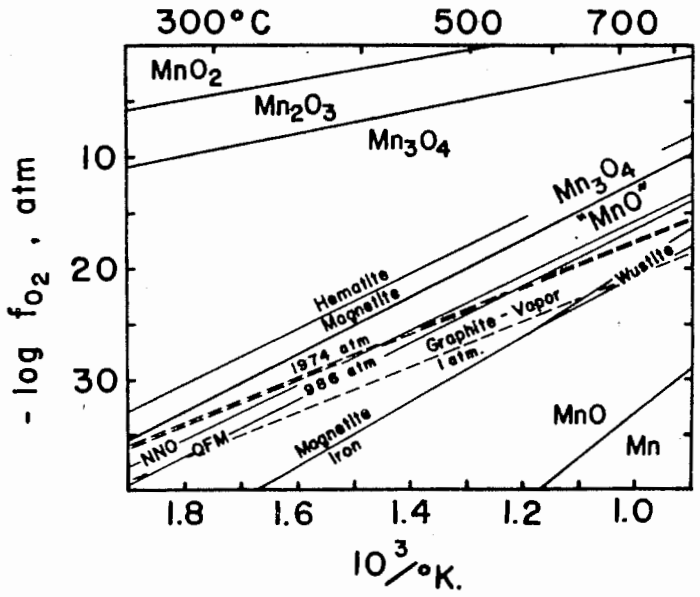

Figure 26. Temperature-Log fO_2 plot illustrating iron oxide, manganese oxide and graphite buffers, Huebner (1969).

Graphical Analysis of Iron-rich Mineral Assemblages

Coexisting mineral assemblages from the iron-rich lenses that fit into the chemical model are illustrated on ternary diagrams below. Chemical analyses of minerals plotted in ternary diagrams throughout this section are listed in the section "Mineralogy" under the appropriate mineral and assemblage letter. In the diagrams that follow, solid tie lines connect coexisting minerals from the same assemblage, except in a few instances where tie lines have been omitted for easier viewing.

MgO-FeO-(MnO+CaO) Ternary. The small tetrahedron (Figure 27) illustrates the chemical model that has been developed for the iron-rich lenses of the Littleton Formation. In this view of the tetrahedron all of the phases have been projected from the SiO_2 apex on to the base containing the components MgO-FeO-(MnO+CaO). Although assemblages M and N

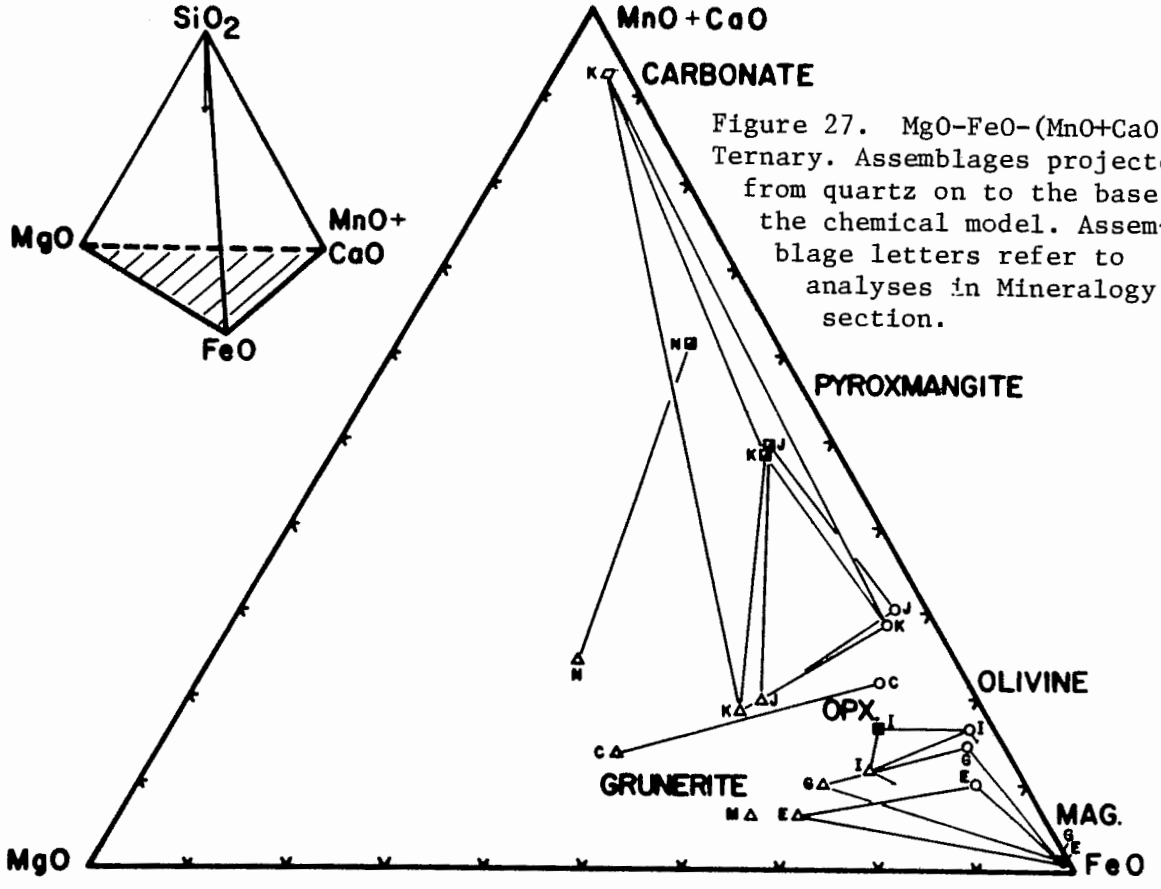

Figure 27. MgO-FeO-(MnO+CaO) Ternary. Assemblages projected from quartz on to the base of the chemical model. Assemblage letters refer to analyses in Mineralogy section.

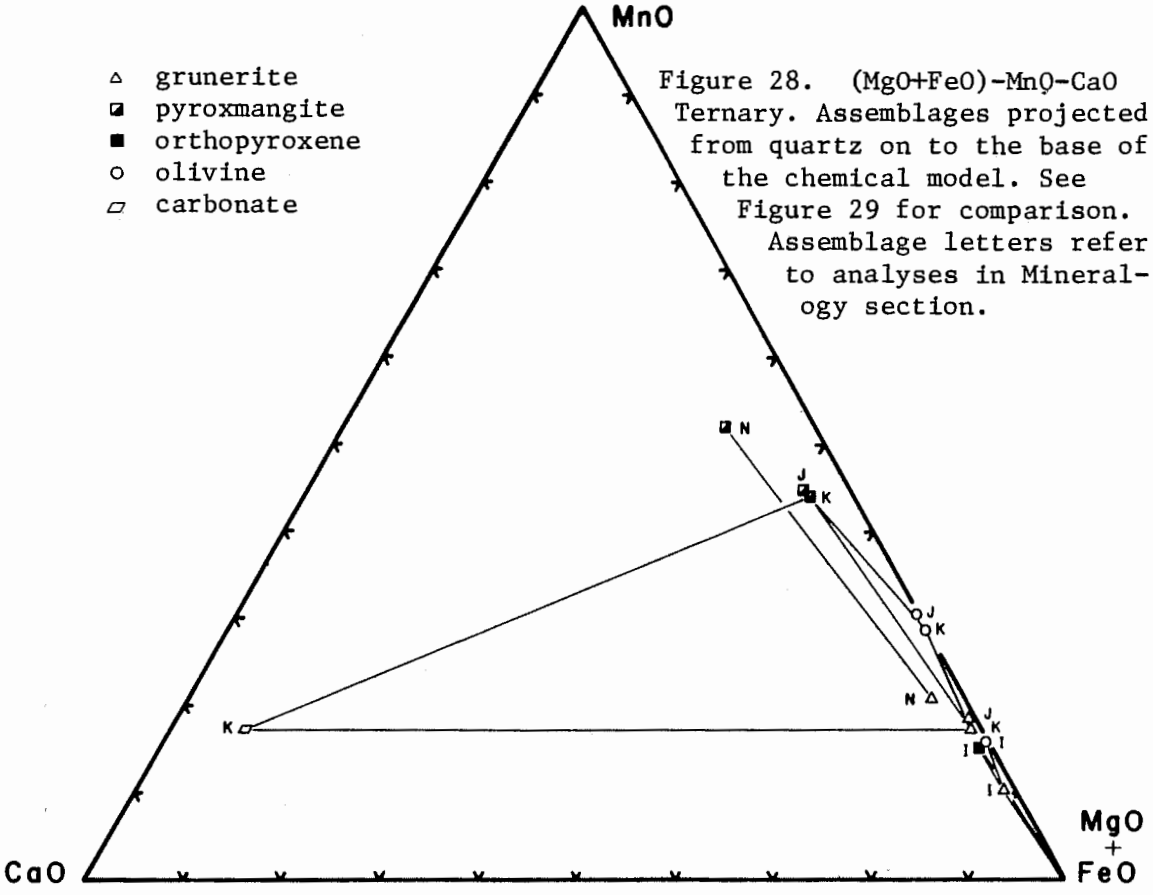

△ grunerite
◪ pyroxmangite
■ orthopyroxene
○ olivine
▱ carbonate

Figure 28. (MgO+FeO)-MnO-CaO Ternary. Assemblages projected from quartz on to the base of the chemical model. See Figure 29 for comparison. Assemblage letters refer to analyses in Mineralogy section.

are the only quartz-bearing assemblages in the system and thus the only ones accessible to SiO_2, it is useful to consider the mineral assemblages present in the system purely on the basis of the divalent cations Mg^{+2}-Fe^{+2}-(Mn^{+2}+Ca^{+2}). The grunerite analyses lie close to the MgO-FeO edge. Olivine and pyroxmangite analyses lie along the FeO-(MnO+CaO) edge. The only orthopyroxene observed in the lenses occurs in the vein assemblage, I, and it plots between the fields of grunerite and olivine. Magnetite analyses are situated very close to the FeO apex with only minor solid solution toward MnO and MgO. Kutnahorite, a carbonate from assemblage K, plots on the base of the tetrahedron. It contains about 75 mole percent calcium carbonate. This diagram gives an overall view of the arrangement of minerals in the chemical model with respect to the components FeO-MgO-(MnO+CaO).

(MgO+FeO)-MnO-CaO Ternary. Figure 28, like Figure 27, is a projection from SiO_2 onto the base of the chemical model. However, the base of the tetrahedron in Figure 28 consists of the components (MgO+FeO)-MnO-CaO so that MgO and FeO are combined at one apex rather than shown separately. By combining MgO and FeO at one apex, partitioning of MnO and CaO in the manganoan and calcic assemblages I, J, K and N is illustrated. Extremely calcium-poor assemblages have been omitted from Figure 28 because they merely cluster along the (MgO+FeO)-MnO edge. Note that all minerals with the exception of kutnahorite are depleted in CaO and also that the olivine-pyroxmangite-grunerite assemblages J and K are richer in MnO than the olivine-orthopyroxene-grunerite assemblage I. It appears unlikely that an olivine-orthopyroxene-grunerite assemblage much more manganese-rich than assemblage I could exist under these metamorphic conditions, due to the close proximity of assemblage I to the

more manganese-rich pyroxmangite-bearing assemblages J and K. It is also possible that the orthopyroxene-bearing vein assemblage developed at different metamorphic conditions than were present in the host rocks.

MgO-(FeO+MnO)-SiO_2 Ternary. Partitioning of MgO and (FeO+MnO) is illustrated in Figure 29 for the calcium-poor assemblages C, E, G and I. Of particular interest in this diagram are the minerals olivine, orthopyroxene, grunerite and magnetite. Because CaO forms a very small portion of these four minerals, it has been omitted from consideration. In comparison with olivine, grunerite exhibits a strong trend toward Mg enrichment; orthopyroxene lies between grunerite and olivine with respect to Mg enrichment, but interestingly lies on the iron-rich side of the most iron-rich grunerite-olivine tie line. Magnetite has only trace amounts of solid solution toward MgO in the presence of the silicates olivine, orthopyroxene and grunerite.

(MgO+FeO)-(MnO+CaO)-SiO_2 Ternary. Mineral assemblages in Figure 30 have been plotted in the plane (MgO+FeO)-(MnO+CaO)-SiO_2, as is illustrated by the small tetrahedron. Two mineral assemblages, N and M, plot in the silica-saturated portion of the diagram. Assemblage N forms a three phase field containing grunerite-pyroxmangite-quartz. For more iron- and magnesium-rich bulk compositions than N, the two phase assemblage grunerite-quartz, M, is stable.

In the silica-undersaturated region of the diagram, close to the (MgO+FeO)-SiO_2 join, there are two three-phase assemblages E and G (counting graphite + magnetite as one phase) that contain graphite-magnetite-olivine-grunerite. The vein assemblage, I, contains orthopyroxene in addition to magnetite, olivine and grunerite. Assemblage C consists of magnetite-olivine-grunerite but does not contain graphite.

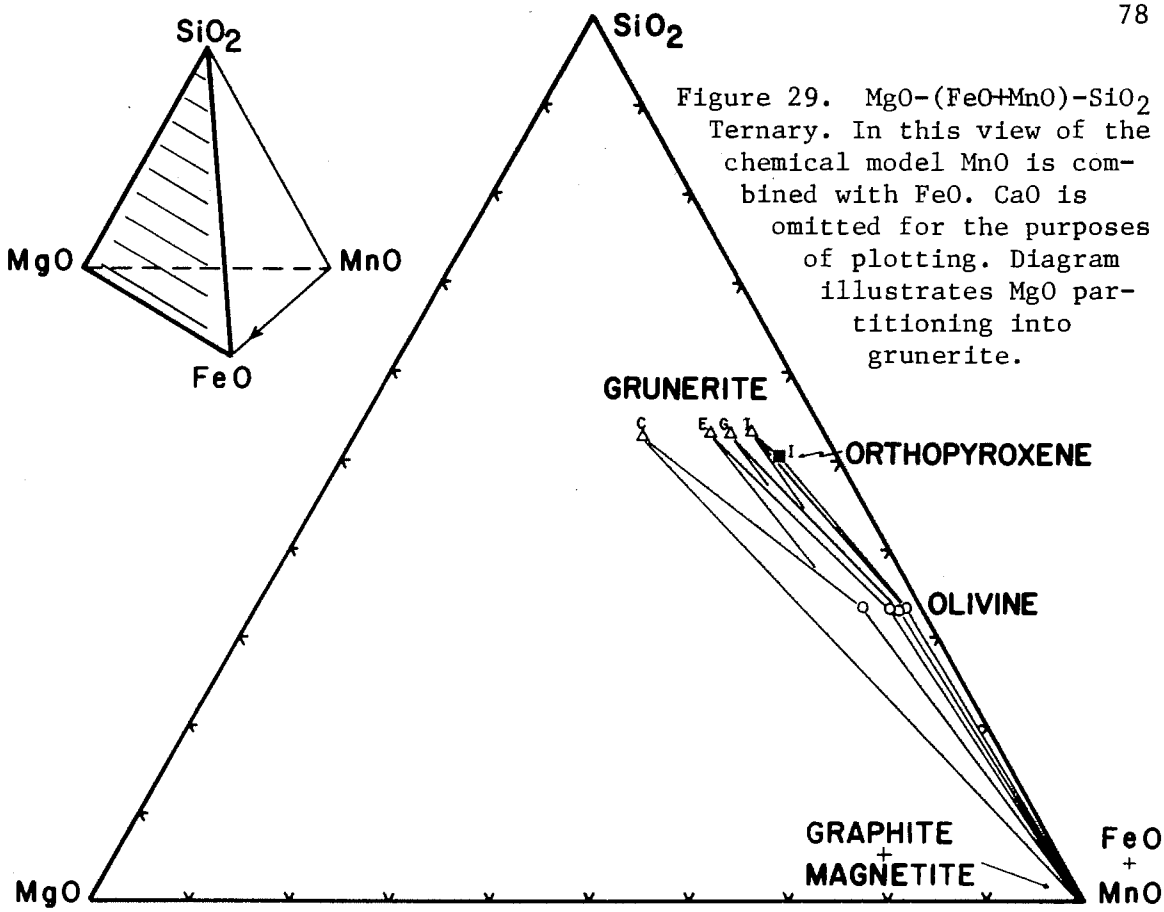

Figure 29. MgO-(FeO+MnO)-SiO_2 Ternary. In this view of the chemical model MnO is combined with FeO. CaO is omitted for the purposes of plotting. Diagram illustrates MgO partitioning into grunerite.

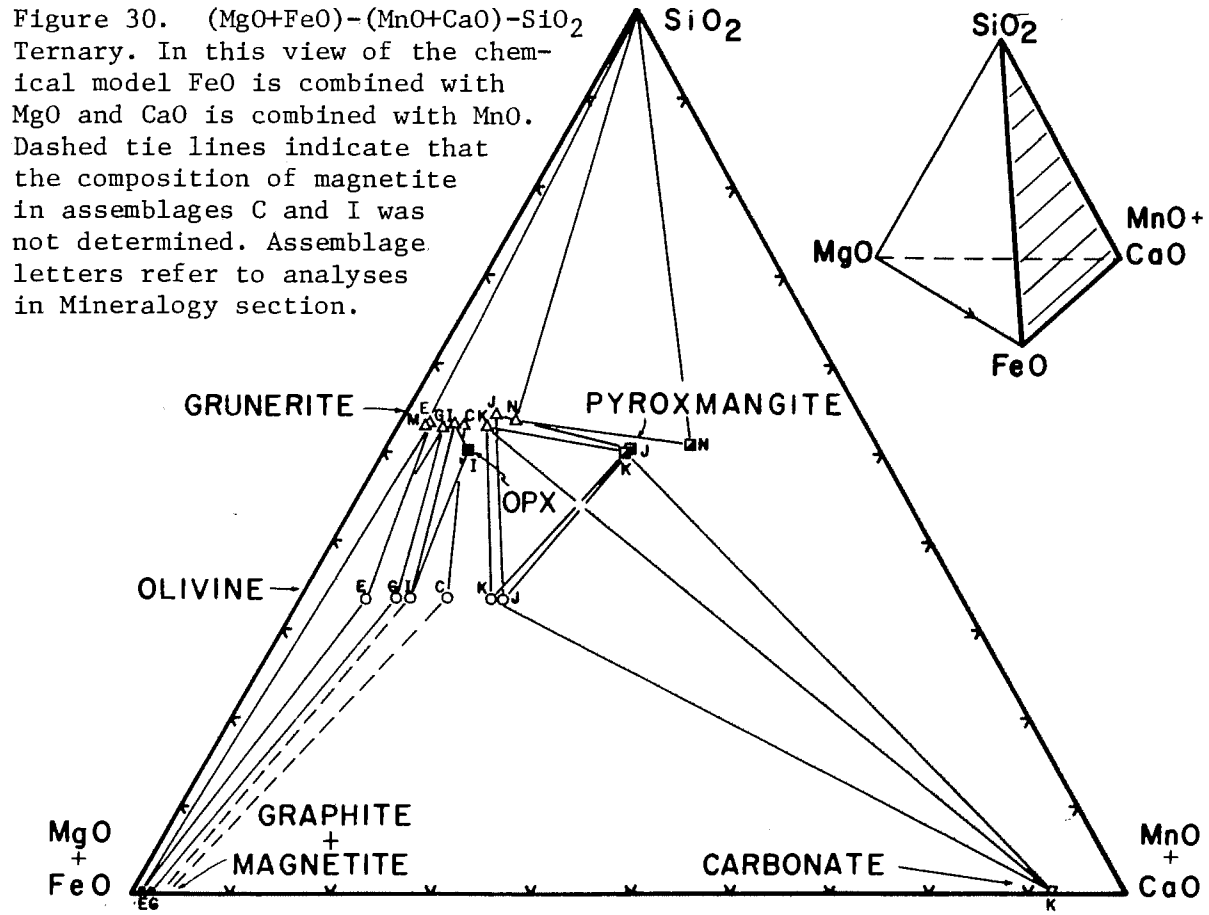

Figure 30. (MgO+FeO)-(MnO+CaO)-SiO_2 Ternary. In this view of the chemical model FeO is combined with MgO and CaO is combined with MnO. Dashed tie lines indicate that the composition of magnetite in assemblages C and I was not determined. Assemblage letters refer to analyses in Mineralogy section.

The absence of graphite probably indicates a higher degree of oxidation during metamorphism than was present in assemblages E and G. Pyroxmangite-bearing assemblages J and K exist stably in more manganese-rich silica-undersaturated chemical space in equilibrium with olivine and grunerite. Assemblage K also contains kutnahorite.

The mineral assemblage topologies in Figure 30 may be similar to those which exist on the $FeO-MnO-SiO_2$ plane of the chemical model in the absence of MgO and CaO. If the chemographic relationships illustrated in Figure 30 are representative of the $FeO-MnO-SiO_2$ plane, then the element fractionation patterns shown can be used for theoretical analysis of the metamorphism of any highly metamorphosed iron-manganese sediments. Another significant feature evident from Figure 30 is that olivine and quartz do not occur together in any assemblage. This is due to stability of grunerite and pyroxmangite which prohibit olivine-quartz assemblages.

$MgO-FeO-(MnO+CaO)-SiO_2$ Tetrahedron. To help visualize detailed phase relations, assemblages C, E, G, J, K, M and N are plotted in the tetrahedron $MgO-FeO-(MnO+CaO)-SiO_2$ (Figure 31). Approximate stability fields for olivine, pyroxmangite, and grunerite are indicated by the stippled pattern. Graphite-magnetite-olivine-grunerite tie planes for assemblages C, E and G are located near the left portion of the diagram. The olivine-pyroxmangite-grunerite tie plane, assemblage J, is situated in front of the olivine-pyroxmangite-grunerite-carbonate four phase volume assemblage K. Consequently the tie planes for assemblages J and K do not cross as appeared to be the case in Figures 27 and 30. The assemblages pyroxmangite-grunerite-quartz and grunerite-quartz are readily distinguished in the silica-saturated portion of the system. In the construction of Figure 31 it was assumed that the olivine field

Figure 31. MgO-FeO-$(MnO+CaO)$-SiO_2 Tetrahedron. Mineral assemblages plotted in the chemical model. Mineral fields for olivine, pyroxmangite and grunerite are indicated by the stippled pattern. Topologic relations for mineral assemblages are approximately correct.

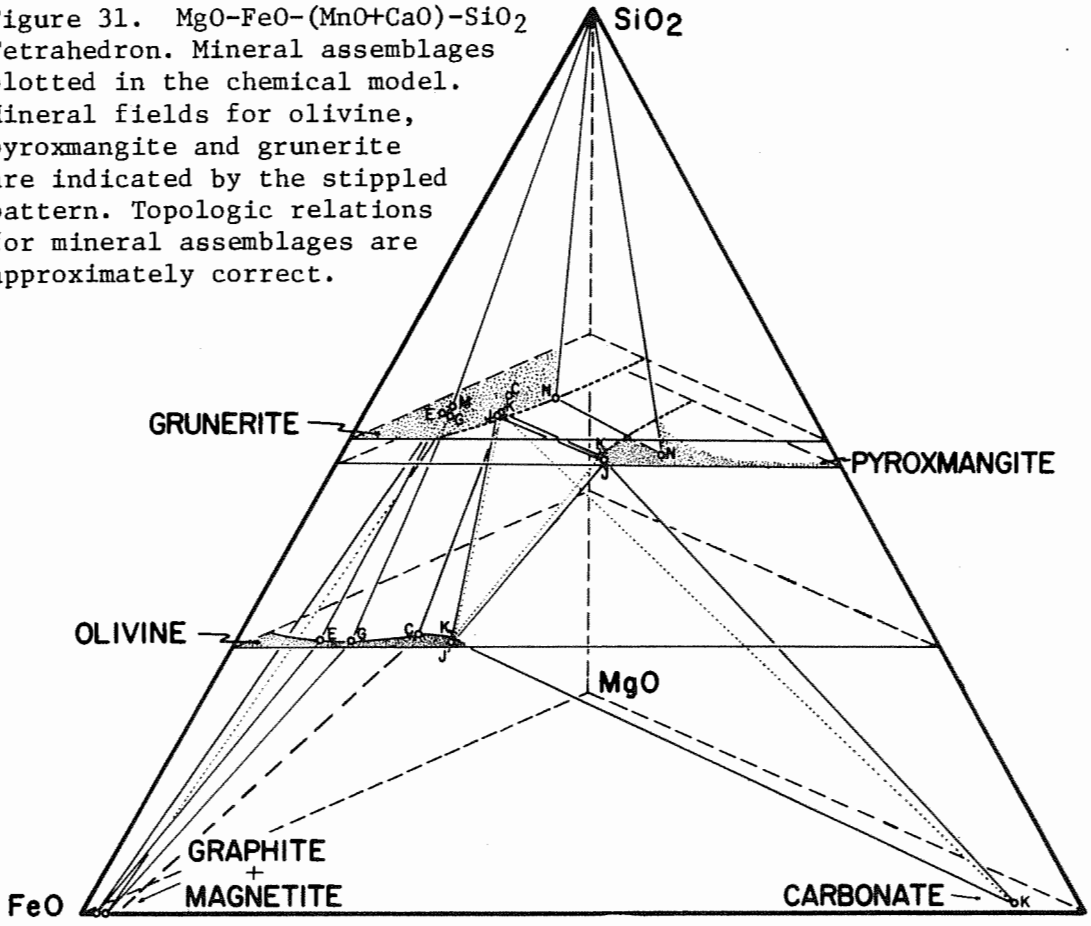

Figure 32. Olivine plane within the chemical model, 33.3 mole % SiO_2. Olivine field as determined by assemblages C, E, G, I and K is stippled. Tie lines connecting other phases pierce olivine plane at the points indicated.

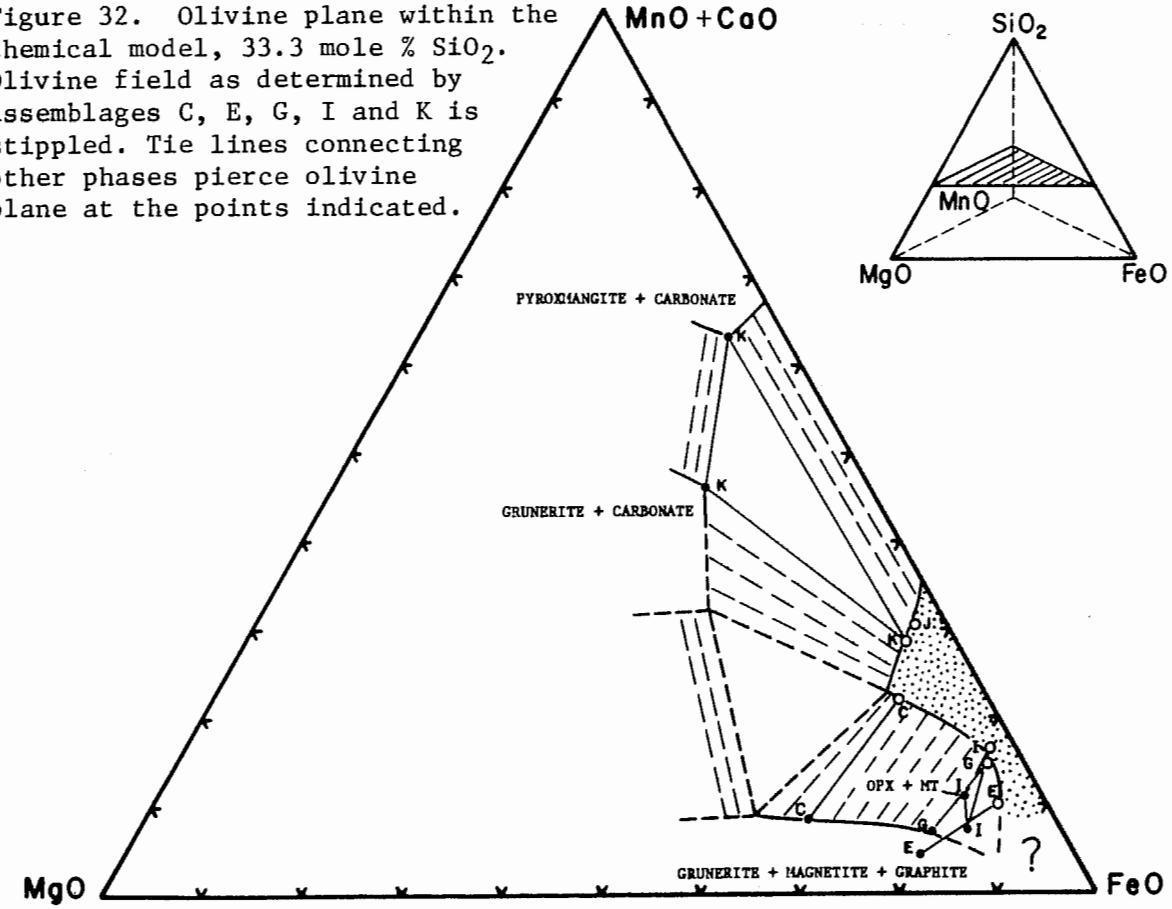

extends to the MgO-FeO join and that pure Fe fayalite is stable. The validity of this assumption is discussed below.

Olivine Plane. In order to consider the stability of fayalite, a two-dimensional section of the chemical model is illustrated (Figure 32) that corresponds to the olivine plane of the tetrahedron. Tie lines in assemblages C, E, G, I, J and K pierce the olivine plane (Figure 32). The geometric relationships of tie line piercing points in the olivine plane were calculated on the basis of MgO, FeO and (MnO+CaO) ratios for each mineral group assuming ideal SiO_2 values. Microprobe data are available for all phases except magnetite in assemblages C and I which was assumed to be Fe_3O_4.

The field of olivine in Figure 32 is situated close to the FeO-(MnO+CaO) join, and because Ca is trivial in these olivines, it is extremely close to the FeO-MnO join. Olivines in assemblages C, E, G, I and K must lie on the edge of the olivine field because they are in equilibrium with phases both above and below the plane. The approximate edge of the olivine field is defined by these points. Mineral fields in the olivine plane, defined by piercing points of tie lines, are also illustrated in Figure 32. These include two four-phase assemblages: K, olivine-pyroxmangite-grunerite-carbonate; and I, olivine-orthopyroxene-grunerite-magnetite. A third four-phase assemblage, olivine-grunerite-carbonate-graphite-magnetite, was not observed in the iron-rich rocks but may be inferred to exist in the chemical model on the basis of surrounding mineral topologies. Of particular interest to the question of fayalite stability is the two-phase field, grunerite-graphite-magnetite. If this field, limited by piercing points C, E, G and I, extends to the FeO-(MnO+CaO) join, it prohibits the stability of

fayalite, Fe_2SiO_4. On the other hand, if the olivine field, limited by olivine analyses C, E, G, I and K, extends to the MgO-FeO join, then fayalite is stable. No samples analyzed by the electron microprobe in this study were iron-rich enough to provide an answer to this question. However, the olivine field (Figure 32) appears to be expanding toward the MgO-FeO join, which may indicate fayalite stability at conditions of metamorphism.

The Chemical Relationship of Garnet and Ilmenite to Other Minerals in the Chemical Model

Garnet has been excluded from the chemical model because it is the only phase with substantial Al_2O_3. Thus, Al_2O_3 can be considered as an accessory inert component even though garnet is commonly an abundant phase. It is useful to consider the chemical relationships between garnet and coexisting mineral phases on the basis of MgO-FeO-(MnO+CaO) ratios. Grunerite occurs with garnet in virtually all of the analyzed assemblages and it is therefore an ideal mineral by which garnet chemistry may be related to mineral assemblages inside the chemical model. Figure 33 is a ternary plot that illustrates coexisting garnet-grunerite pairs in several different mineral assemblages (Table 2). Note that garnet-grunerite pairs from similar mineral assemblages tend to have a similar range of chemistry with respect to MgO-FeO-(MnO+CaO) ratios. Assemblages G, H, I and D form one such group and assemblages J and K form another. Garnet-grunerite tie pairs C and M cross these two groups, but occur in different mineral assemblages than those which they cross.

In a general way garnet compositions tend to monitor the bulk chemistry of assemblages within the chemical model. For example, garnet

Figure 33. Garnet-grunerite pairs plotted in terms of mole fraction MgO-FeO-(MnO+CaO).

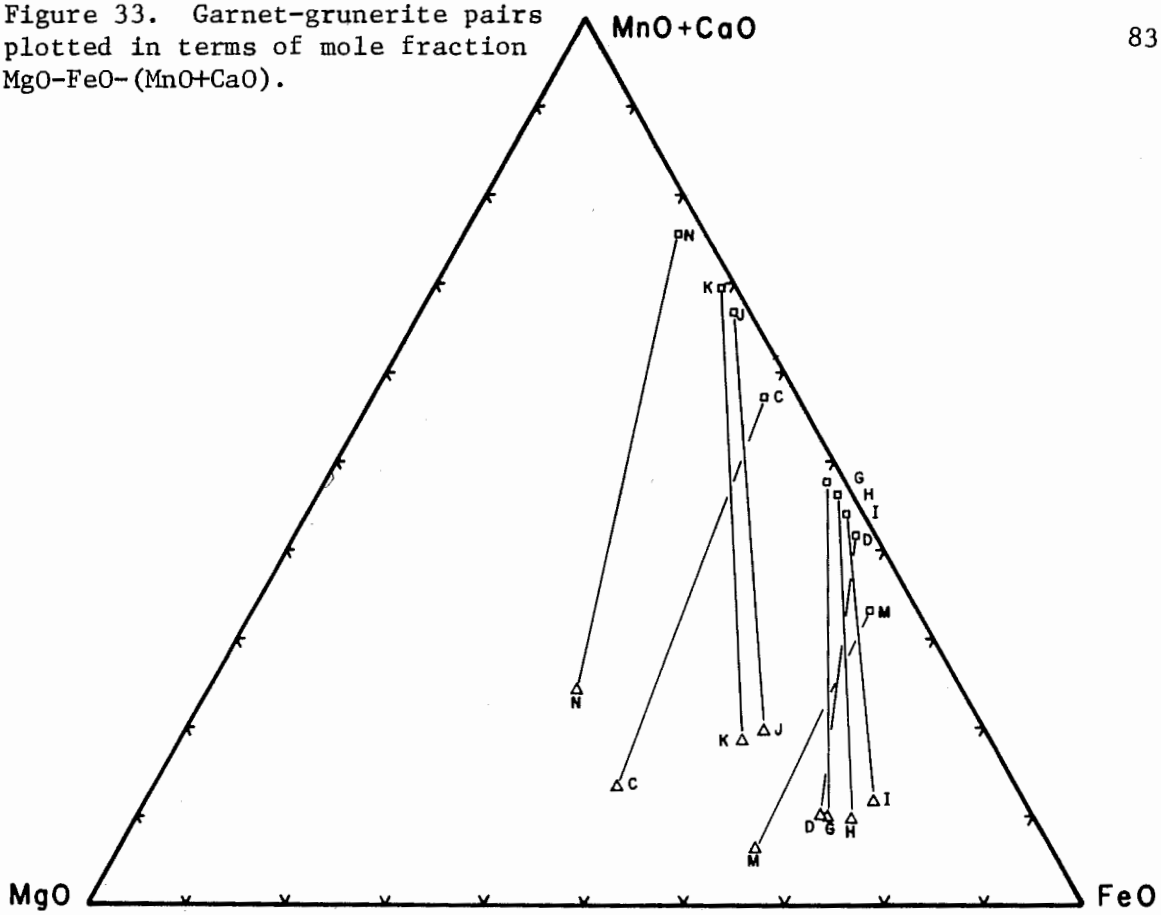

Figure 34. Ilmenite-grunerite pairs plotted in terms of mole fraction MgO-FeO-(MnO+CaO).

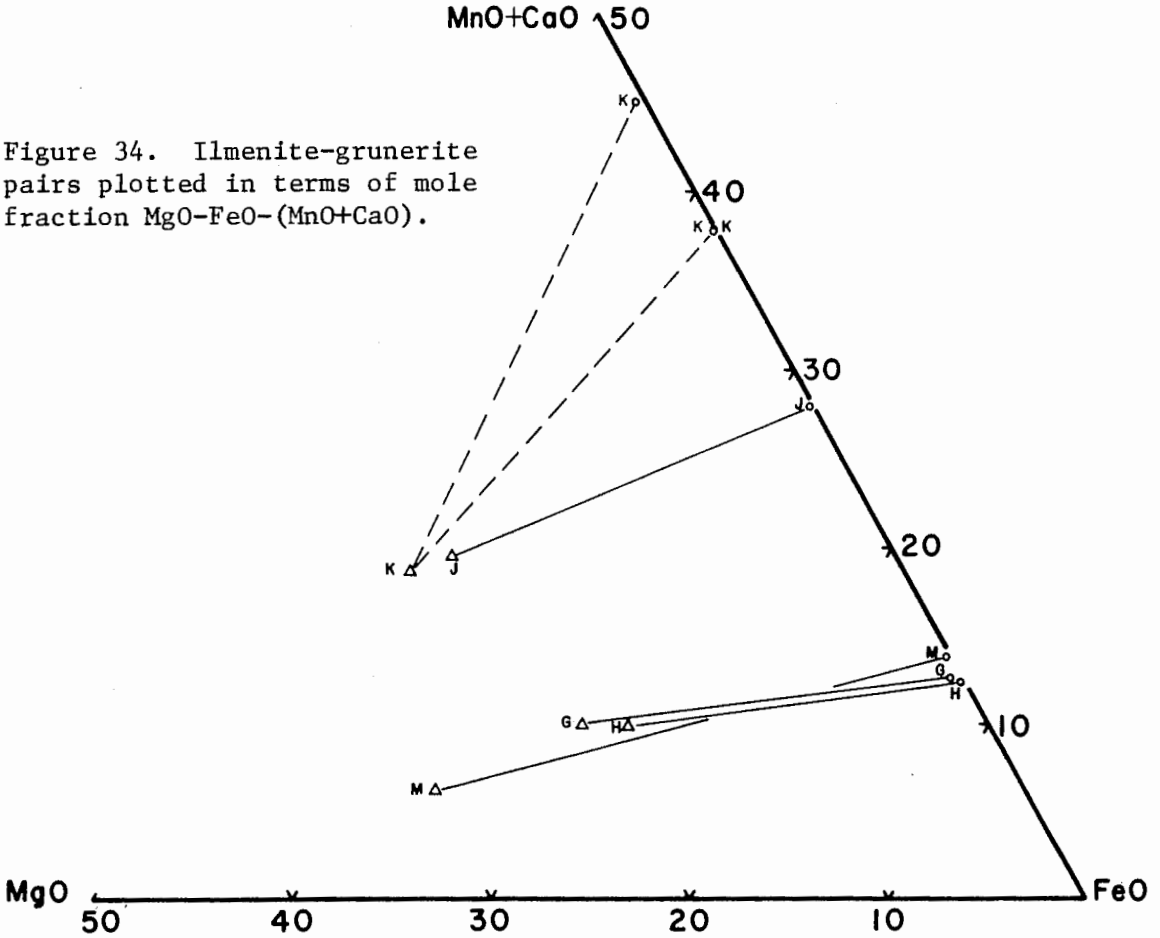

N is the most manganese-rich garnet and it is associated with the most manganese-rich grunerite and pyroxmangite analyzed in this study. By knowing the composition of the garnet in the iron-rich lithologies a qualitative estimate can be made of the composition of coexisting silicate and oxide minerals with respect to MgO-FeO-(MnO+CaO) ratios in similar mineral assemblages.

Ilmenite has been excluded from the chemical model because it is the only phase with substantial TiO_2. Thus TiO_2, like Al_2O_3, may be considered as an accessory inert component in the observed iron-rich mineral assemblages. Ilmenite-grunerite pairs are illustrated in Figure 34 on the basis of MgO-FeO-(MnO+CaO) ratios. Ilmenites lie extremely close to the FeO-MnO join with only minor solid solution toward MgO relative to grunerite. Ilmenite-grunerite pairs in assemblages G, H, J and M show approximately the same slope suggesting equilibration between the two minerals. Ilmenite analyses in assemblage K show variable Fe/Fe+Mn fractionations resulting in different tie line slopes. This indicates that complete equilibration was not achieved among the ilmenite grains analyzed.

METAMORPHIC PHASE EQUILIBRIA

Metamorphic equilibria are presented in this section that may have produced some of the mineral assemblages observed in the iron-rich lenses. Of particular interest are metamorphic equilibria directly associated with mineral assemblages in olivine-pyroxmangite granulite, olivine-magnetite granulite, and quartz-pyroxmangite gneiss. Minerals involved in metamorphic reactions include olivine, pyroxmangite, grunerite, graphite, magnetite, carbonate and quartz. As in the development of the chemical model, the minerals garnet, ilmenite, apatite, and pyrrhotite will not be considered because the components Al_2O_3, TiO_2, P_2O_5 and S, respectively, would have to be added to the system as accessory inert components.

The chemistry of mineral assemblages in the model Fe-C-O-H-MgO-(MnO+CaO)-SiO_2 was illustrated in Figures 27, 28, 29, 30, 31 and 32. In order to consider metamorphic equilibria that may have produced these assemblages, the chemical model must be simplified to include only the following components: Fe-C-O-H-MnO-SiO_2. These components are illustrated on a ternary diagram (Figure 35). Mineral assemblages from Figure 30 are plotted in terms of these components and are illustrated in Figure 35. Unlike Figure 30, Figure 35 does not include the components MgO and CaO, but mineral assemblages in both of these figures are topologically similar. Fe/Fe+Mn ratios for coexisting minerals in the observed assemblages (Figure 35) are magnetite > grunerite > olivine > orthopyroxene > pyroxmangite > carbonate.

One of the major problems associated with prograde metamorphic reactions in these rocks is that the precise chemical and mineralogical

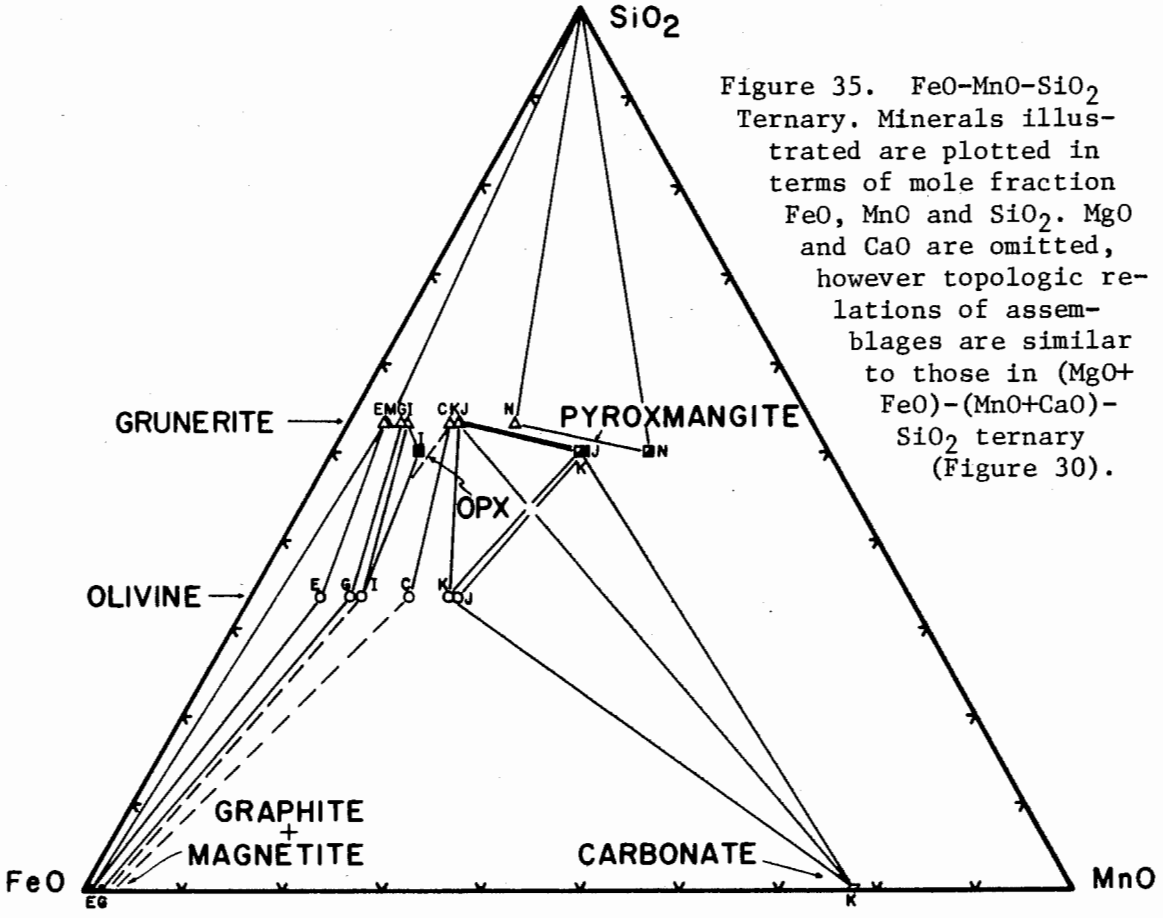

Figure 35. FeO-MnO-SiO_2 Ternary. Minerals illustrated are plotted in terms of mole fraction FeO, MnO and SiO_2. MgO and CaO are omitted, however topologic relations of assemblages are similar to those in (MgO+FeO)-(MnO+CaO)-SiO_2 ternary (Figure 30).

nature of the protolith is unknown. However, on the basis of metamorphic equilibria discussed below, the genesis of the Fe-Mn minerals is compatible with a protolith consisting of Fe-Mn carbonate and quartz with or without organic carbon. The presence of minor carbonate in the olivine-pyroxmangite granulite is in agreement with this. Such a rock would precipitate under reducing conditions, probably in a marine environment that is consistent with the surrounding metamorphosed black shales of the Littleton Formation. The source of Al for garnet in alkali-poor iron-rich rocks is problematical; however, chamosite or some high-Al clay such as kaolinite might have provided the necessary Al.

The phosphorus source for the apatite-rich beds in the olivine-magnetite granulite should also be taken into account, but integration of all the chemical and mineralogical data mentioned above would involve detailed consideration of aqueous geochemistry that is beyond the scope of this paper.

$T - X_{CO_2}/X_{H_2O} + X_{CO_2}$ plots were constructed for the system Fe-C-O-H-MnO-SiO_2 to investigate mineral reactions that may have produced the observed assemblages from siliceous Fe-Mn carbonate parent rocks during prograde metamorphism. In order to generate a $T - X_{CO_2}/X_{H_2O} + X_{CO_2}$ grid for the iron-rich lithologies, six assumptions were made. These are:

1) The partitioning of FeO and MnO among coexisting minerals (Figure 35), inferred from electron probe analysis of natural minerals containing the divalent cations MgO, FeO, MnO and CaO (Figure 30), is representative of partitioning in the simplified system Fe-C-O-H-MnO-SiO_2.

2) The partitioning of FeO and MnO noted above remains constant under geologically relevant metamorphic conditions.

3) Metamorphic equilibria on the pure Fe edge of the system Fe-C-O-H-MnO-SiO_2 involve the phases

Graphite	C
Magnetite	Fe_3O_4
Siderite	$FeCO_3$
Fayalite	Fe_2SiO_4
Grunerite	$Fe_7Si_8O_{22}(OH)_2$
Quartz	SiO_2

Metamorphic equilibria on the pure Mn edge of the system Fe-C-O-H-MnO-SiO_2 involve the phases

Graphite	C
Manganosite	MnO
Rhodochrosite	$MnCO_3$
Tephroite	Mn_2SiO_4
Mn-Pyroxmangite	$MnSiO_3$
Quartz	SiO_2

Slope calculations of model metamorphic equilibria within the system Fe-C-O-H-MnO-SiO_2 were based on fixed mineral compositions derived from Fe/Fe+Mn fractionations in Figure 35. These fixed compositions are listed below and illustrated in the caption of Plate 2.

Graphite	C
Magnetite	Fe_3O_4
Fe-Mn Carbonate	$FeMn_3(CO_3)_4$
Fe-Mn Olivine	$Fe_6Mn_4Si_5O_{20}$
Fe-Mn Pyroxmangite	$FeMnSi_2O_6$
Fe-Mn Grunerite	$Fe_6MnSi_8O_{22}(OH)_2$
Quartz	SiO_2

In reality, carbonate, olivine, pyroxmangite and grunerite exist as Fe-Mn solid solution series. It is assumed that the calculated metamorphic equilibria (Plates 1 and 2) based on fixed compositions are analogous to natural metamorphic equilibria which involve continuously changing mineral and fluid compositions.

4) A C-O-H gas phase is present during metamorphism and is in equilibrium with graphite and associated minerals in the rocks. In actuality, graphite is not present in all assemblages (Table 2), and therefore this assumption is not uniformly applicable.

5) $XCO_2/XH_2O + XCO_2$ is the ratio of the components CO_2 and H_2O in a C-O-H gas phase. In conjunction with an arbitrarily chosen total pressure and temperature, this ratio defines the exact composition of the C-O-H gas in equilibrium with graphite (French, 1966; Burt, 1972). Using the ratio $XCO_2/XH_2O + XCO_2$, CH_4-H_2 gas mixtures plot at -1.0 (Burt, 1972).

6) Extrapolation of experimentally determined equilibria at 2 Kbar (Plate 1) to metamorphic conditions of the Littleton Formation in the Mount Grace quadrangle, 6 Kbar (Robinson, 1966; Thompson et al., 1968), does not disrupt the relative sequence of metamorphic equilibria.

Although the assumptions presented above have not yet been substantiated by independent data, they form the basis of the T-X plots (Plates 1 and 2). Plate 1 illustrates experimentally determined equilibria in the pure Fe system, and the pure Mn system at 2 Kbar total pressure. Model reactions in the system Fe-C-O-H-MnO-SiO_2 are also illustrated. Experimentally determined equilibria are identified by the experimentalist's name and date of publication. Crosses with associated temperature

values indicate known reaction points. The location of IP-6 was determined by Peters (1973), but IP-1 and IP-5 were generated by Schreinemakers analysis and are not precisely defined in T - $X_{CO_2}/X_{H_2O} + X_{CO_2}$ space by experimental data. Ternary plots (Plate 1) in the presence of a CO_2-rich gas phase illustrate a prograde reaction sequence beginning at approximately 400°C for a hypothetical Fe-Mn carbonate-quartz rock. No hydrous minerals are present in this prograde sequence due to high $X_{CO_2}/X_{H_2O} + X_{CO_2}$. By contrast the mineral assemblages observed contain grunerite which suggests that $X_{CO_2}/X_{H_2O} + X_{CO_2}$ values were not high enough to prohibit grunerite formation during metamorphism. The stability field of pure Fe-Grunerite with respect to T and $X_{CO_2}/X_{H_2O} + X_{CO_2}$ (Plate 1) is limited by the following reactions:

$$\text{Fe-Grun} + 7\ CO_2 = 7\ \text{Sid} + 8\ \text{Qtz} + H_2O$$
$$6\ \text{Fe-Grun} + 7\ CO_2 = 7\ \text{Graph} + 14\ \text{Mt} + 48\ \text{Qtz} + 6\ H_2O$$
$$2\ \text{Fe-Grun} = 7\ \text{Fa} + 9\ \text{Qtz} + 2\ H_2O$$

The topologic relationship between the stability of fayalite and the stability of grunerite-magnetite-graphite was illustrated in the olivine plane (Figure 32). In terms of temperature and $X_{CO_2}/X_{H_2O} + X_{CO_2}$ in the pure Fe system, this relationship is shown in Plate 1 by the model reaction:

$$3\ \text{Graph} + 6\ \text{Mt} + 2\ \text{Fe Grun} = 16\ \text{Fa} + 2\ H_2O + 3\ CO_2.$$

For values of $X_{CO_2}/X_{H_2O} + X_{CO_2}$ greater than IP-5, fayalite stability is defined by the reaction:

$$\text{Graph} + 2\ \text{Mt} + 3\ \text{Qtz} = 3\ \text{Fa} + CO_2.$$

This reaction was experimentally determined at 2 Kbar by Eugster and Skippen (1968).

Plate 2 illustrates model equilibria in the system Fe-C-O-H-MnO-SiO_2 including details of grunerite stability. The stability of manganese-bearing grunerite extends beyond that of Fe-grunerite with respect to $X_{CO_2}/X_{H_2O} + X_{CO_2}$ and is bounded by univariant equilibria connecting invariant points 1, 2, 4, and 5.

All mineral assemblages (Figure 35) with the exception of the vein assemblage, I, are plotted in the appropriate ternary diagrams on Plate 2. These assemblages delineate the portion of T - $X_{CO_2}/X_{H_2O} + X_{CO_2}$ space in which the iron-rich units of the Littleton Formation were metamorphosed. The univariant equilibria (Plate 2) bounding the T-X space in which these assemblages (Figure 35) developed are:

2 Grun + 3 Carb = 2 Ol + 3 Pym + 2 H_2O + 12 CO_2
2 Grun + 4 Ol + 3 CO_2 = 3 Graph + 6Mt + 18 Pym + 2 H_2O
2 Grun + 18 Pym = 5 Ol + 27 Qtz + 2 H_2O

A sequence of ternary diagrams in Figures 36 and 37 illustrate model metamorphic reactions in the system Fe-C-O-H-MnO-SiO_2 that are thought to have produced olivine-magnetite-graphite-grunerite, quartz-pyroxmangite-grunerite-graphite, and olivine-pyroxmangite-grunerite-carbonate mineral assemblages from Fe-Mn carbonate-quartz parent rocks. Two possible T-X paths, V and W, are possible at low temperatures depending on the initial composition of the gas phase (Figure 36), but both T-X paths become indistinguishable at higher temperatures (Figure 37). Model reactions from Plate 2 for paths V and W are:

Path V. For values of $X_{CO_2}/X_{H_2O} + X_{CO_2}$ lower than IP-1.

[1] 7 Sid + 8 Qtz + H_2O = Fe-Grun + 7 CO_2
[2] 6 Sid = Graph + 2 Mt + 5 CO_2

Path W. For values of $X_{CO_2}/X_{H_2O} + X_{CO_2}$ higher than IP-1.

[2] 6 Sid = Graph + 2 Mt + 5 CO_2

[3] 17 Graph + 34 Mt + 144 Qtz + 6 Carb + 18 H_2O = 18 Grun + 41 CO_2

[4] 7 Graph + 14 Mt + 48 Qtz + 6 H_2O = 6 Fe-Grun + 7 CO_2

Paths V and W.

[5] 5 Carb + 2 Grun + 18 Qtz = 17 Pym + 20 CO_2 + 2 H_2O

[6] 3 Graph + 6Mt + 18 Carb + 10 Grun = 16 Ol + 10 H_2O +75 CO_2

[7] 2 Grun + 3 Carb = 2 Ol + 3 Pym + 2 H_2O + 12 CO_2

[8] 3 Graph + 6 Mt + 2 Fe-Grun = 16 Fa + 2 H_2O + 3 CO_2

[9] 2 Grun + 18 Pym = 5 Ol + 27 Qtz + 2 H_2O

Generalized bulk compositions for the olivine-magnetite-graphite-grunerite, quartz-pyroxmangite-grunerite-graphite and olivine-pyroxmangite-grunerite-carbonate assemblages are shown in Figures 36 and 37 and are labelled OM, QP and OP, respectively.

Composition OM, now consisting of olivine-magnetite-graphite-grunerite, may have been originally a combination of Fe-Mn carbonate and quartz. For path V (Figure 36), composition OM is converted from Fe-Mn carbonate-quartz to carbonate-grunerite by a continuous reaction:

Fe-Mn Carb + Qtz + H_2O = Fe-Mn Grun + CO_2 (Figure 36b)

that is analogous to reaction [1]. This proceeds continuously with increasing temperature until quartz is completely exhausted for composition OM leaving a carbonate-grunerite rock. Then Fe-Mn carbonate breaks down in a continuous reaction analogous to reaction [2]:

Fe-Mn Carb = Graph + Mt + CO_2

until carbonate is consumed leaving a rock composed of grunerite-

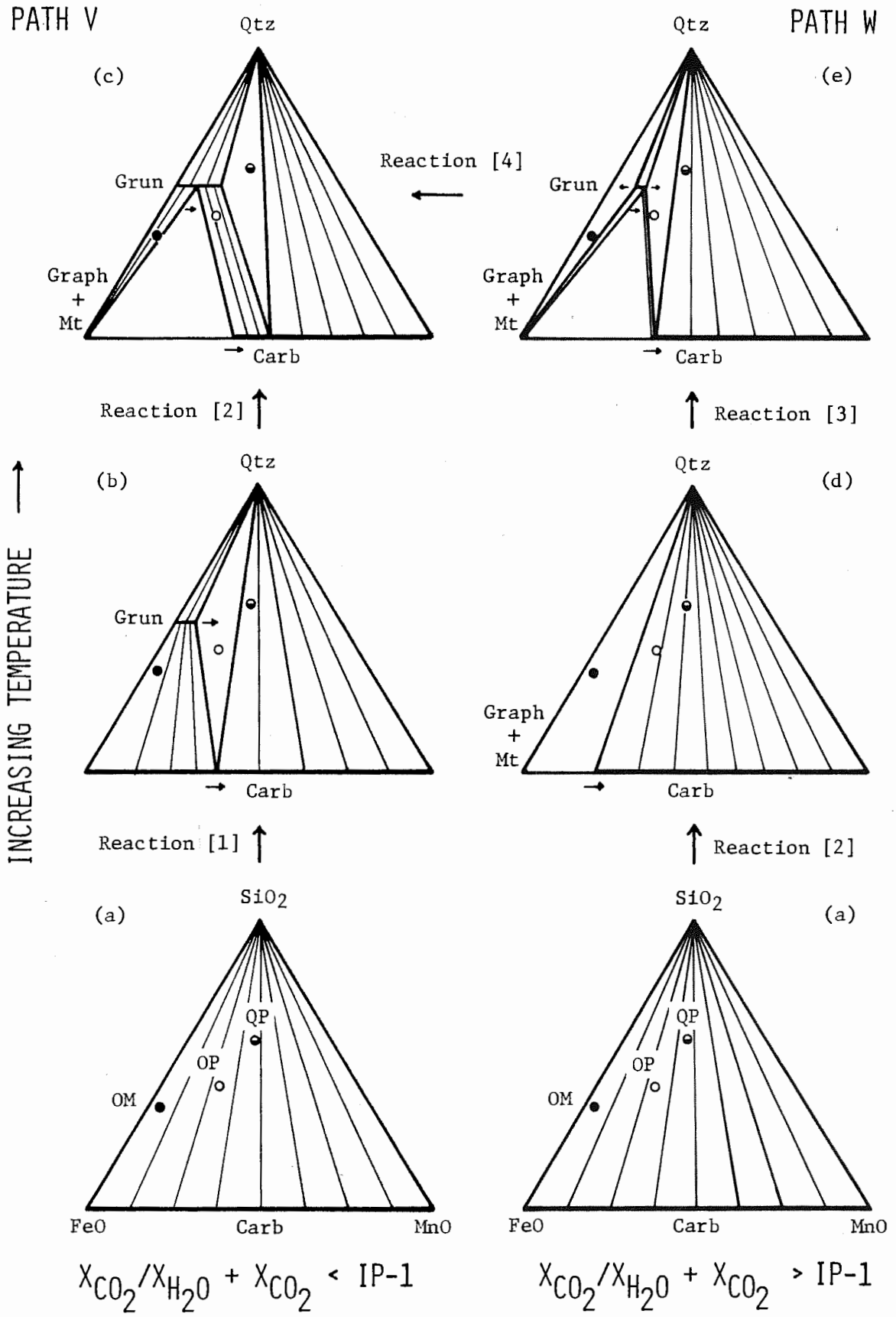

Figure 36. Composition diagrams in the system Fe-Mn-Si-C-O-H for several conditions of fixed P, T, and fluid composition showing progressive metamorphism of three carbonate-quartz protoliths. Small arrows indicate movement direction of three-phase fields (continuous reactions) with increasing temperature.

magnetite-graphite (Figure 36c). This sequence of reactions may have produced the commonly observed grunerite-magnetite intergrowths illustrated in Figures 8 and 9 from what were grunerite-carbonate intergrowths at lower metamorphic grade.

An alternate sequence of reactions (Figure 36, path W) could produce the grunerite-magnetite intergrowths from composition OM at $X_{CO_2}/X_{H_2O} + X_{CO_2}$ greater than IP-1. For path W, composition OM is initially converted from Fe-Mn carbonate-quartz to magnetite-graphite-carbonate-quartz by a continuous reaction:

$$\text{FeMn Carb} = \text{Graph} + \text{Mt} + CO_2$$

analogous to reaction [2] (Figure 36d). With increasing temperature Mn-bearing grunerite is produced by reaction [3] (Figure 36e) at which point all carbonate in composition OM is consumed and the rock consists of magnetite-graphite-grunerite quartz. In order to form Fe-Grunerite by reaction [4] the gas phase associated with path W must be depleted in $X_{CO_2}/X_{H_2O} + X_{CO_2}$ relative to its initial starting value. This could occur in nature if the volumetrically abundant surrounding pelitic schists underwent dehydration reactions, thereby increasing P_{H_2O} of the gas in equilibrium with the iron-rich assemblages. As a result of a decrease in $X_{CO_2}/X_{H_2O} + X_{CO_2}$ a continuous reaction:

$$\text{Graph} + \text{Mt} + \text{Qtz} + H_2O = \text{Fe-Mn Grun} + CO_2$$

would drive the grunerite composition toward pure Fe-Grunerite until all quartz in composition OM was consumed and the rock consisted of grunerite-magnetite-graphite. By this path grunerite-magnetite intergrowths could be derived from what were magnetite-graphite-quartz

intergrowths at lower metamorphic grade. It is not known whether grunerite-magnetite intergrowths were derived from grunerite-carbonate intergrowths as on path V or from magnetite-graphite-quartz intergrowths as on path W. The absence or scarcity of graphite in the natural intergrowths could result from graphite precipitation elsewhere in the rock or from an increase in fO_2 thereby oxidizing the graphite.

After the formation of Fe-grunerite path V cannot be distinguished from path W. Olivine is formed first by reaction [6] (Figure 37b) and the three-phase field magnetite-graphite-olivine-grunerite moves by continuous reaction toward iron-rich compositions with rising temperature until it intersects composition OM yielding the observed olivine-magnetite-graphite-grunerite assemblages D, E, G and H (Table 2).

Composition QP, now consisting of quartz-pyroxmangite-grunerite-graphite, may have been originally a combination of quartz, Fe-Mn carbonate, and organic carbon. For paths V and W composition QP is converted from quartz, Fe-Mn carbonate, and carbon to quartz, grunerite, Fe-Mn carbonate and graphite when the bulk composition is overtaken by the continuous reaction:

$$\text{Fe-Mn Carb} + \text{Qtz} + H_2O = \text{Fe-Mn Grun} + CO_2.$$

Pyroxmangite is produced by reaction [5] and composition QP lies within the three-phase field quartz-pyroxmangite-grunerite (Figure 37a). With increasing temperature this three-phase field shifts toward more iron-rich compositions so that composition QP, assemblage N (Figure 14), contains only minor grunerite. Because no magnetite occurs with graphite in the assemblage N, the graphite is not likely to be the result of the

Figure 37. Composition diagrams in the system Fe-Mn-Si-C-OH for several conditions of fixed P, T, and fluid composition. A continuation of Figure 36. Small arrows indicate movement direction of three-phase fields (continuous reactions) with increasing temperature.

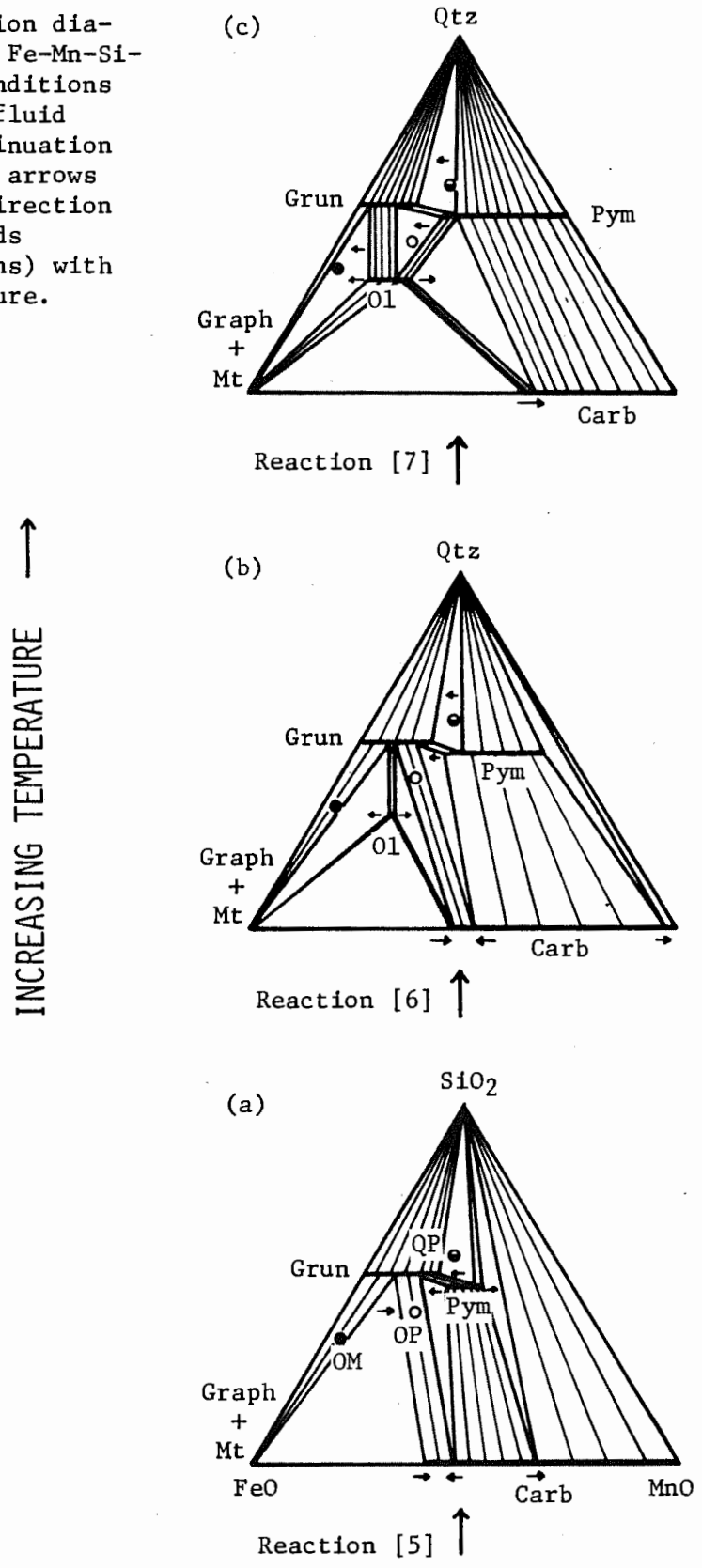

breakdown of carbonate, reaction [2]. Therefore, organic carbon is assumed to have been present in the parent rock.

Composition OP now consisting of olivine-pyroxmangite-grunerite may have been initially composed of Fe-Mn carbonate and quartz (Figure 36a). With increasing temperature it was converted to carbonate-grunerite-quartz by a continuous reaction:

$$\text{Fe-Mn Carb} + \text{Qtz} + H_2O = \text{Fe-Mn Grun} + CO_2$$

analogous to reaction [1] (Figure 36b or e) and then to carbonate-grunerite (Figure 36c) as quartz is exhausted for composition OP. Both pyroxmangite and olivine become stable phases in other bulk compositions by reactions [5] and [6] (Figure 37a and b) but composition OP remains in the grunerite-carbonate field. With increasing temperature the three-phase fields carbonate-olivine-grunerite and carbonate-pyroxmangite-grunerite (Figure 37b) continuously approach each other and decrease the width of the carbonate-grunerite field in which OP is situated. As the width of this field approaches zero, reaction [7]:

$$\text{Fe-Mn Carb} + \text{Grun} = \text{Ol} + \text{Pym} + H_2O + CO_2$$

is attained. This yields the observed olivine-pyroxmangite-grunerite assemblage, J (Figure 37c). Textural features (Figure 6) and electron microprobe data of mineral assemblage K, olivine-pyroxmangite-grunerite-carbonate, suggest that model reaction [7] has already taken place but that the Ca content of the carbonate permitted carbonate to persist as an additional phase. Thus a real reaction similar to model reaction [7] may have been in progress in the system $Fe\text{-}C\text{-}O\text{-}H\text{-}MnO\text{-}SiO_2+(MgO\text{-}CaO)$. In this continuous reaction olivine and pyroxmangite grow at the expense

of grunerite and carbonate. As the reaction continues grunerite and carbonate become progressively enriched in Mg and Ca, respectively.

If metamorphic equilibria illustrated in Plate 2 are correct, then model reaction [7] provides the absolute minimum T-X metamorphic conditions for the iron-rich units in the Littleton Formation. Graphical reasoning (Figure 32) was used above to suggest that pure Fe fayalite might have become stable had the bulk composition been appropriate, by the reaction [8]:

$$3\ \text{Graph} + 6\ \text{Mt} + 2\ \text{Fe Grun} = 16\ \text{Fa} + 2\ H_2O + 3CO_2.$$

With increasing temperature grunerite and pyroxmangite would be expected to react to produce olivine, quartz and H_2O. Since no olivine-quartz assemblages have been observed and grunerite-pyroxmangite assemblages occur in three different samples, the model reaction [9]:

$$2\ \text{Grun} + 18\ \text{Pym} = 5\ \text{Ol} + 27\ \text{Qtz} + 2\ H_2O$$

apparently was not achieved under the maximum temperature conditions to which the iron-rich units were subjected.

GENESIS OF ORTHOPYROXENE VEIN

Orthopyroxene, which occurs only in a vein (Figure 13) within olivine-magnetite granulite, was not included in the development of T-X plots discussed above, because orthopyroxene is probably not stable in the system Fe-C-O-H-MnO-SiO_2 except at very high pressure. Nevertheless, its occurrence is both mineralogically and texturally interesting. The restricted occurrence of orthopyroxene in sample A22H2 suggests either that metamorphic conditions in the vein were different than those in the host olivine-magnetite granulite or that the vein environment provided a unique bulk composition. A possible explanation for development of the vein is presented below.

Orthopyroxene stability is not to be expected in the system Fe-C-O-H-MnO-SiO_2 in the absence of Mg, due to crystal chemical considerations. However, by adding a modest amount of Mg to the Fe component, an orthopyroxene-producing reaction can be deduced in ternary diagrams with topologies like those of the model system (Figure 38a). This deduction is based on the reasonable observation that 1) Fe/Fe+Mn fractionations (Figure 35) are in the order: Magnetite > Grunerite > Olivine > Orthopyroxene > Pyroxmangite > Carbonate and 2) that pure Fe-Mg pyroxmangite is never stable. The reaction by which orthopyroxene would first appear in the chemical system would be:

Fe-Mg-Mn Grun + Fe-Mn-Mg Ol + Fe-Mn-Mg Pym = Fe-Mn-Mg Opx + H_2O.

This reaction could have been promoted by a low activity of H_2O associated with the vein and need not have affected the olivine-magnetite-graphite-grunerite mineral assemblages G and H (Table 2) in

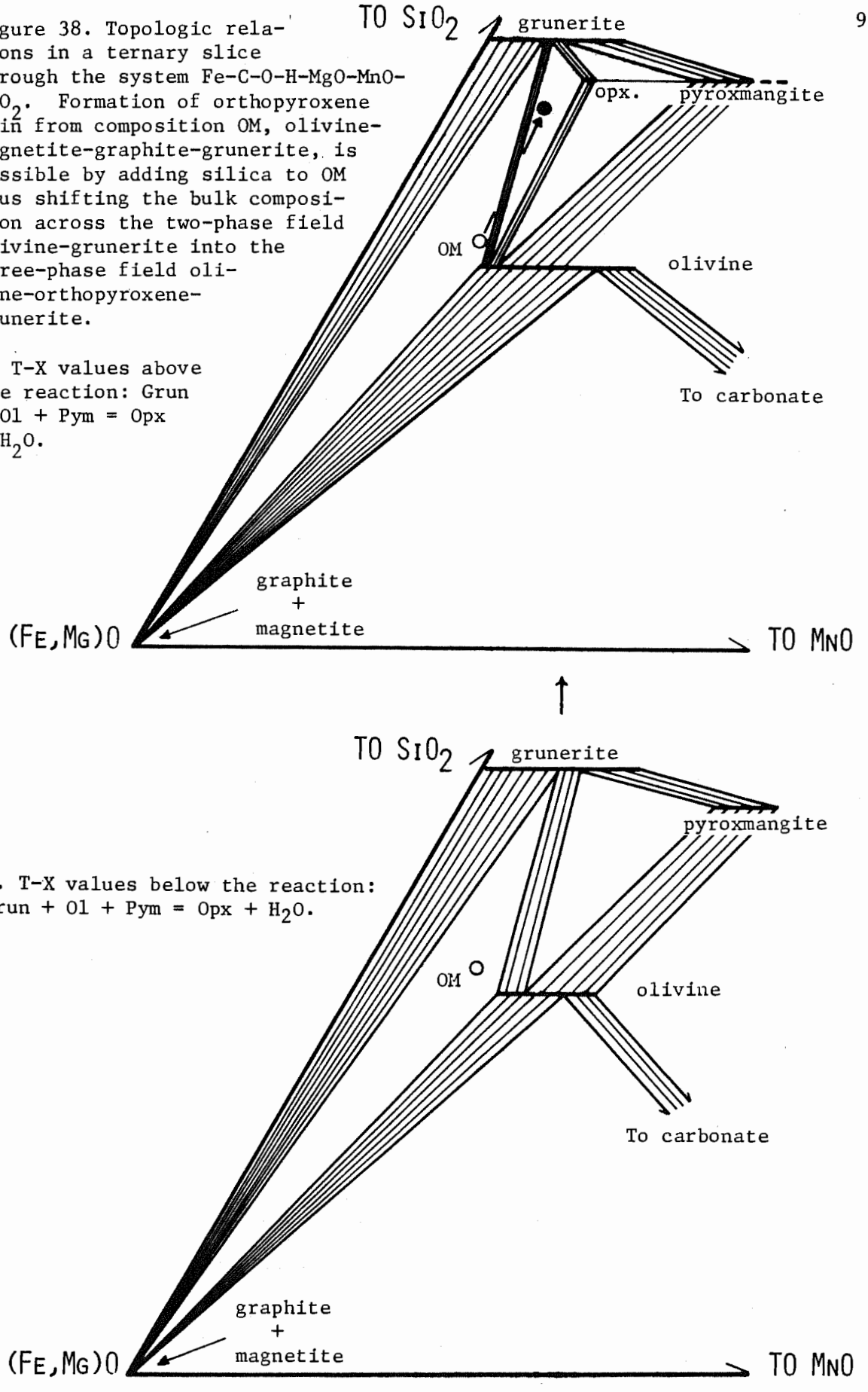

Figure 38. Topologic relations in a ternary slice through the system Fe-C-O-H-MgO-MnO-SiO_2. Formation of orthopyroxene vein from composition OM, olivine-magnetite-graphite-grunerite, is possible by adding silica to OM thus shifting the bulk composition across the two-phase field olivine-grunerite into the three-phase field olivine-orthopyroxene-grunerite.

B. T-X values above the reaction: Grun + Ol + Pym = Opx + H_2O.

A. T-X values below the reaction: Grun + Ol + Pym = Opx + H_2O.

the host granulite (Figure 38b, composition OM). However, if a hairline fracture developed during metamorphism within the host olivine-magnetite granulite, then solutions present during metamorphism could migrate toward the relatively low pressure regime of the fracture from adjacent more siliceous rocks. If the bulk composition of the olivine-magnetite granulite is enriched in SiO_2 by solutions entering the fracture, then the bulk composition could have shifted from OM (Figure 38b) toward SiO_2 across the thin two-phase field, olivine-grunerite,into the three-phase field olivine-orthopyroxene-grunerite. The following observations lend validity to this genetic scheme: 1) magnetite in the vein is greatly diminished relative to that in the host granulite (Table 1) and where present may persist metastably, 2) graphite is absent in the vein but present in the host olivine-magnetite granulite, 3) olivine in the vein is embayed by orthopyroxene and grunerite (Figure 13) and 4) olivine is less abundant and grunerite more abundant in the vein than in the host granulite (Table 1) which is consistent with topologic relations of Figure 38b.

The formation of the garnet wall rock (Figure 13) is unequivocally connected to the formation of the vein. Since Al_2O_3 is generally not considered a mobile constituent in metamorphic equilibria (Carmichael, 1969) it seems unlikely that sufficient Al_2O_3 was introduced from surrounding pelitic rocks to form the garnet wall rock. Moreover, the absence of alkali-bearing phases in the vein suggests that solution transport from the pelitic rocks was negligible. Silica-rich solutions in the vein are assumed to originate in adjacent iron-rich lithologies. A possible alternative explanation for the garnet wall rock could involve a chemical refining model. As solutions continually pass

through the fracture, the reaction(s) by which the vein assemblage formed continue further into the host granulite. If garnet, initially present in the olivine-magnetite host, goes into solution by the reactions which produce the vein assemblage (a reasonable assumption, since no primary garnet is associated with the vein or wall rock), the garnet could be concentrated by reprecipitation at the reaction front. Although the concept of chemical refining has been highly generalized with respect to its application for garnet wall rock formation, it provides a mechanism for answering two of the problems associated with the vein: 1) What is the source of Al in garnet from the vein? and 2) Why is garnet concentrated along the outer boundaries of the vein? By this mechanism Al is liberated from pre-existing garnet in the host and is concentrated at the reaction front.

PRESSURE, TEMPERATURE AND FLUID COMPOSITION DURING METAMORPHISM

Due to the unusual Fe-Mn chemistry of mineral assemblages discussed above, little quantitative information can be directly obtained as to the conditions of metamorphism. Kyanite and sillimanite-bearing assemblages in muscovite schists and surrounding rocks suggest peak metamorphic conditions of about 650°C and 6 Kbar (Robinson, 1966; Thompson et al., 1968). The temperature and pressure conditions at which the iron-rich rocks equilibrated are assumed to be equivalent to those in the surrounding rocks, but the composition of the hypothesized C-O-H gas might have differed significantly.

Figure 39 illustrates compositions of C-O-H gas in equilibrium with

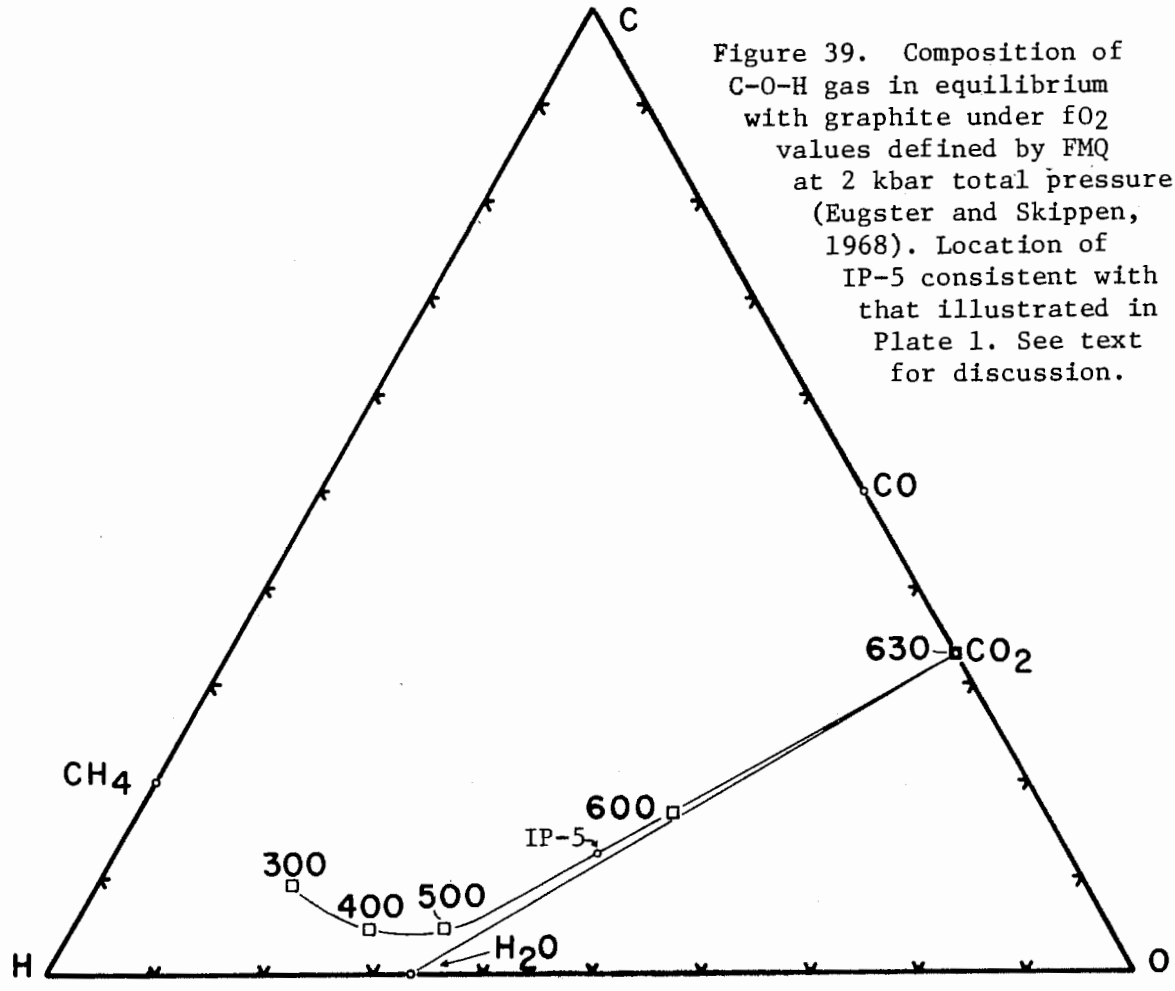

Figure 39. Composition of C-O-H gas in equilibrium with graphite under fO_2 values defined by FMQ at 2 kbar total pressure (Eugster and Skippen, 1968). Location of IP-5 consistent with that illustrated in Plate 1. See text for discussion.

graphite under fO_2 conditions defined by the FMQ buffer at 2 Kbar total pressure (Eugster and Skippen, 1968). The equilibrium between graphite, magnetite, quartz and fayalite is:

$$\text{Graph} + 2\ \text{Mt} + 3\ \text{Qtz} = 3\ \text{Fa} + CO_2 \quad \text{(Plates 1 and 2)}$$

and is metastable for $X_{CO_2}/X_{H_2O} + X_{CO_2}$ values less than IP-5. The T and $X_{CO_2}/X_{H_2O} + X_{CO_2}$ values of IP-5 are not known due to the absence of experimental data on grunerite stability, but in Plate 1 they are arbitrarily shown at 560°C and 0.25, respectively. T - X paths for mineral assemblages in the olivine-magnetite, quartz-pyroxmangite and olivine-pyroxmangite rocks discussed above suggest $X_{CO_2}/X_{H_2O} + X_{CO_2}$ values less than IP-5. This indicates that gas compositions for these rocks are reduced with respect to IP-5 as shown in Figure 39. Data obtained by French (1966) indicate that at constant T and fO_2, higher gas pressures favor a reduced gas phase. Thus a 6 Kbar gas phase composition for specific temperatures in Figure 39 should be richer in CH_4, H_2 and H_2O relative to those experimentally determined at 2 Kbar. Further, it is obvious that the increase in pressure would increase the temperature of IP-5. Evaluation of molar volumes for the reaction [4]:

$$7\ \text{Graph} + 14\ \text{Mt} + 48\ \text{Qtz} + 6\ H_2O = 6\ \text{Fe Grun} + 7\ CO_2$$

indicate that increased pressure would shift the reaction toward lower values of $X_{CO_2}/X_{H_2O} + X_{CO_2}$ and hence shift IP-5 in the same direction. Thus, although the absolute T - X position of IP-5 is unknown, the gas composition in equilibrium with the assemblages considered here must have lower $X_{CO_2}/X_{H_2O} + X_{CO_2}$ values than IP-5.

REFERENCES

BILLINGS, M. P. (1956) The geology of New Hampshire, Part II - bedrock geology. New Hampshire State Planning and Development Commission, 200 p.

BURT, D. M. (1972) The system Fe-Si-C-O-H: A model for metamorphosed iron formations. Carnegie Inst. Wash. Year Book, 71, 435-443.

CARMICHAEL, D. M. (1969) On the mechanism of prograde metamorphic reactions in quartz-bearing pelitic rocks. Contrib. Mineral. Petrol. 20, 244-267.

DAYHOFF, M. O., E. R. LIPPINCOTT AND R. V. ECK (1964) Thermodynamic equilibria in prebiological atmospheres. Science, 146, 1461-1464.

EMERSON, B. K. (1895) Mineralogical lexicon of Franklin, Hampshire and Hampden Counties, Massachusetts. U.S. Geol. Surv. Bull. 126.

EUGSTER, H. P. AND G. B. SKIPPEN (1968) Igneous and metamorphic reactions involving gas equilibria. In, P. H. Abelson, Ed., Researches in Geochemistry, 2. John Wiley and Sons, New York. 492-520.

FRENCH, B. M. (1966) Some geologic implications of equilibrium between graphite and a C-H-O gas at high temperatures and pressures. Rev. Geophysics, 4, 223-253.

_____(1968) Progressive contact metamorphism of the Biwabik iron-formation, Mesabi Range, Minnesota. Minn. Geol. Surv. Bull. 45, 102 p.

_____(1971) Stability relations of siderite ($FeCO_3$) in the system Fe-C-O. Am. J. Sci. 271, 37-78.

_____, AND H. P. EUGSTER (1965) Experimental control of oxygen fugacities by graphite gas equilibriums. J. Geophys. Res. 70, 1529-1539.

FRONDEL, C. AND L. H. BAUER (1955) Kutnahorite: a manganese dolomite, $CaMn(CO_3)_2$. Am. Mineral. 40, 748-760.

GUNDERSON, J. N. AND G. M. SCHWARTZ (1962) The geology of the metamorphosed Biwabik iron-formation, Eastern Mesabi district, Minnesota. Minn. Geol. Surv. Bull. 43, 139 p.

HADLEY, J. B. (1949) Bedrock geology of the Mount Grace quadrangle, Massachusetts. U.S. Geol. Surv. Geol. Quad. Map GQ-3.

HESS, H. H. (1952) Orthopyroxenes of the Bushveld Type, ion substitutions, and changes in unit cell dimensions. Am. J. Sci., Bowen Vol., 173-187.

HITCHCOCK, E. (1841) Final Report on the Geology of Massachusetts. J. S. and C. Adams, Amherst, Mass. and J. H. Butler, Northampton, Mass.

HUEBNER, J. S. (1969) Stability relations of rhodochrosite in the system manganese-carbon-oxygen. Am. Mineral. 54, 457-481.

JAFFE, H. W., W. O. J. GROENVELD MEYER AND D. H. SELCHOW (1961) Manganoan cummingtonite from Nsuta, Ghana. Am. Mineral. 46, 642-653.

KERRICK, D. M. (1974) Review of metamorphic mixed-volatile (H_2O-CO_2) equilibria. Am. Mineral. 59, 729-762.

KLEIN, C., JR. (1964) Cummingtonite-grunerite series: a chemical, optical and X-ray study. Am. Mineral. 49, 963-982.

_____(1973) Changes in mineral assemblages with metamorphism of some banded Precambrian iron formations. Econ. Geol. 68, 1075-1088.

PERUTZ, M. (1937) "Iron rhodonite" (from slag) and pyroxmangite and their relation to rhodonite. Mineral. Mag. 24, 573-576.

PETERS, T. (1971) Pyroxmangite: stability in H_2O-CO_2 mixtures at a total pressure of 2000 bars. Contrib. Mineral. and Petrol. 32, 267-273.

_____, H. SCHWANDER AND V. TROMMSDORFF (1973) Assemblages among tephroite, pyroxmangite, rhodochrosite, quartz: experimental data and occurences in the Rhetic Alps. Contrib. Mineral. and Petrol. 42, 325-332.

ROBINSON, P. (1963) Gneiss domes of the Orange area, Mass. and N. H. Ph.D. thesis, Harvard University.

_____(1966) Aluminum silicate polymorphs and Paleozoic erosion rates in central Massachusetts (abst.). Trans. Amer. Geophys. Union, 47, 424.

_____(1967) Gneiss domes and recumbent folds of the Orange area, west central Massachusetts. Guideb. New England Intercollegiate Geol. Conf., Amherst, Mass. 17-47.

_____,AND H. W. JAFFE (1969) Chemographic exploration of amphibole assemblages from central Massachusetts and southwestern New Hampshire. Mineral. Soc. Amer. Spec. Pap. 2, 251-274.

RUMBLE, D., III (1973) Fe-Ti oxide minerals from regionally metamorphosed quartzites of western New Hampshire. Contrib. Mineral. and Petrol. 42, 181-195.

THOMPSON, J. B. (1955) The thermodynamic basis for the mineral facies concept. Am. J. Sci. 253, 65-103.

_____(1957) Graphical analysis of mineral assemblages in pelitic schists. Am. Mineral. 42, 842-858.

_____(1972) Oxides and sulphides in regional metamorphism of pelitic schists. 24th Internat. Geol. Conf., 27-35.

_____,P. ROBINSON, T. N. CLIFFORD, AND N. J. TRASK (1968) Nappes and gneiss domes in west-central New England. In: E-an Zen, W. S. White, J. B. Hadley and J. B. Thompson, Jr., Eds., Studies of Appalachian Geology: Northern and Maritime. John Wiley and Sons, New York. 811-838.

TILLEY, C. E. (1936) Eulysites and related rock types from Loch Duich, Ross-shire. Mineral Mag. 24, 331-342.

ZEN, E-AN (1966) Construction of P-T diagrams for multicomponent systems after the method of Schreinemakers: a geometric approach. U.S. Geol. Surv. Bull. 1225, 56 p.

T-X PLOT FOR THE SYSTEM Fe-C-O-H-MnO-SiO_2

PLATE 1

——— Reactions in Fe-system

—— -- Reactions in Mn-system

— — — Reactions in Fe-Mn system

$P_{FLUID} = 2$ kbar

2/21/75

TEMPERATURE °C →

800

700

600

500

400

$MnO + CO_2 = Rh$

(1969) Huebner + 773

Qtz, Pym, Ol., Graph, Mt +, Manganosite

$3\,Fa + CO_2 = Graph + 2\,Mt + 3\,Qtz$

+600

$7\,Fa + 9\,Qtz + 2\,H_2O = 2\,FeGrun$

IP-5

$3\,Ol. + 9\,Qtz + CO_2 = Graph + 2\,Mt + 12\,Pym$

EITHER ORDER

(1973) Peters + 581

+550

$16\,Fa + 2\,H_2O + 3\,CO_2 = 3\,Graph + 6\,Mt + 2\,FeGrun$

$Te + CO_2 = Rh + Pym$

$2\,Ol. + 5\,CO_2 = Graph + 2\,Mt + Carb + 5\,Pym$

(1971) Peters + 508

+500

500

$Pym + CO_2 = Rh + Qtz$

$6\,Fe\,Grun + 7\,CO_2 = 7\,Graph + 14\,Mt + 48\,Qtz + 6\,H_2O$

+475

$9\,Pym + 13\,CO_2 = Graph + 2\,Mt + 18\,Qtz + 3\,Carb$

(1971) French + 465

$Graph + 2\,Mt + 5\,CO_2 = 6\,Sid$

+450

(1968) Eugster + Skippen + 650

Qtz, Pym, Ol., Graph, Mt +, Carb

Qtz, Pym, Ol., Graph, Mt +, Carbonate

(1973) Peters

$2\,Pym = Te + Qtz$

IP-6

IP-1

$Te + CO_2 = 2\,Rh + Qtz$

$Grun + 7CO_2 = 7\,Sid + 8\,Qtz + H_2O$

H_2O

$XCO_2 / XH_2O + XCO_2 \rightarrow$

CO_2

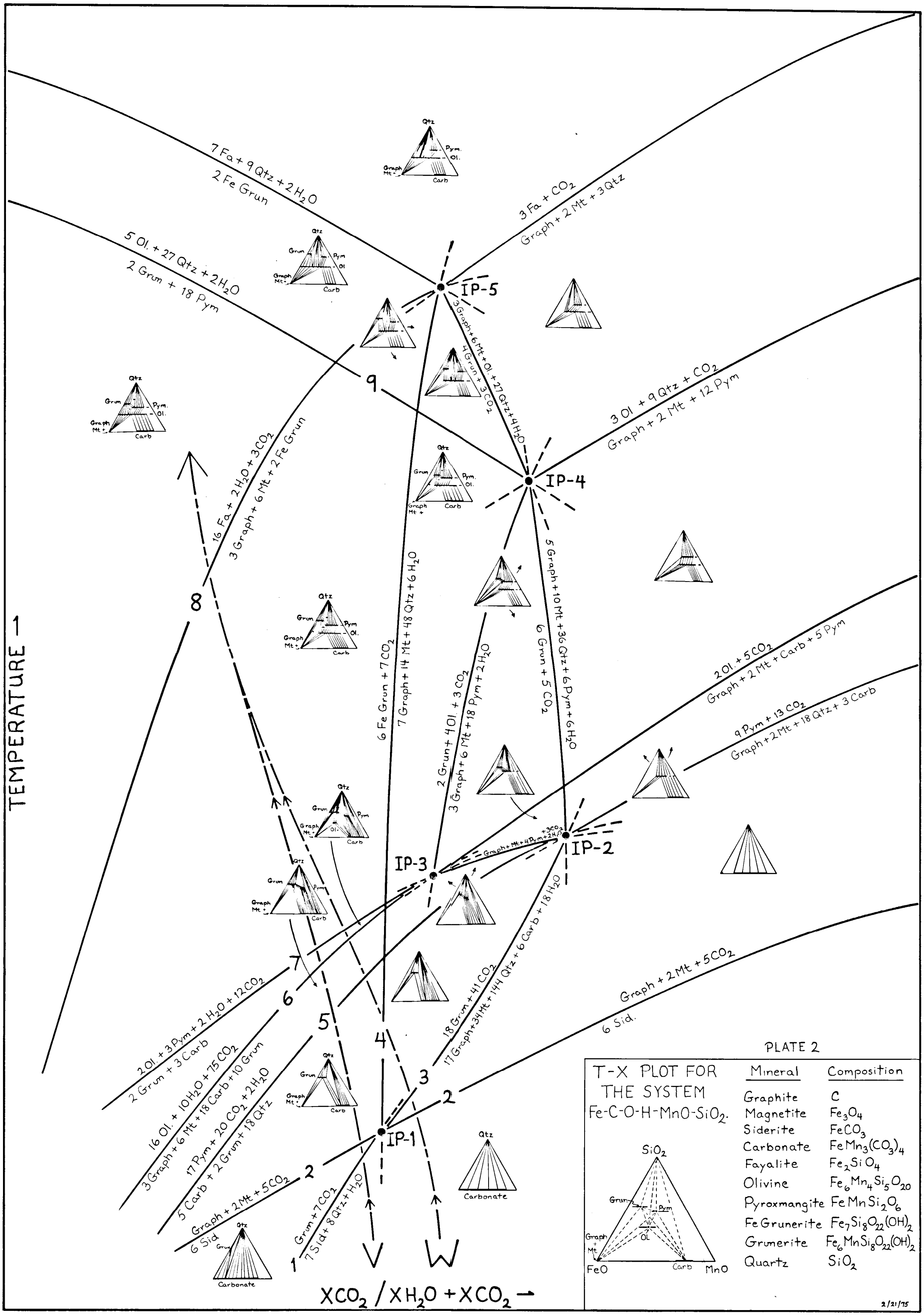

PLATE 2

T-X PLOT FOR THE SYSTEM Fe-C-O-H-MnO-SiO_2.

Mineral	Composition
Graphite	C
Magnetite	Fe_3O_4
Siderite	$FeCO_3$
Carbonate	$FeMn_3(CO_3)_4$
Fayalite	Fe_2SiO_4
Olivine	$Fe_6Mn_4Si_5O_{20}$
Pyroxmangite	$FeMnSi_2O_6$
Fe Grunerite	$Fe_7Si_8O_{22}(OH)_2$
Grunerite	$Fe_6MnSi_8O_{22}(OH)_2$
Quartz	SiO_2

2/21/75